Safety-Critical Control of Uncertain Nonlinear Systems via Control Barrier Functions

By

Yujie Wang

A dissertation submitted in partial fulfillment of
the requirements for the degree of
Doctor of Philosophy
(Mechanical Engineering)

at the
UNIVERSITY OF WISCONSIN-MADISON
2026

Date of final oral examination: 03/12/2026

The dissertation is approved by the following members of the Final Oral Committee:
Xiangru Xu, Assistant Professor, Mechanical Engineering
Dan Negrut, Professor, Mechanical Engineering
Lei Zhou, Assistant Professor, Mechanical Engineering
Wei Wang, Assistant Professor, Mechanical Engineering
Jeremy Coulson, Assistant Professor, Electrical & Computer Engineering

Acknowledgements

I would like to begin by expressing my deepest gratitude to my advisor, Xiangru Xu. His unwavering support and guidance have been fundamental to my growth throughout my Ph.D. journey. Over the course of this long and challenging path, he has consistently provided invaluable advice, insight, and encouragement, which have enabled me to grow and mature in all aspects of academic research.

I am sincerely grateful to all of my dissertation committee members for their insightful comments and thoughtful feedback. Their perspectives and suggestions significantly strengthened this work and broadened my understanding of the field.

I would like to thank my labmates in the Autonomous & Resilient Controls Lab. In particular, I am grateful to Yuhao Zhang, Hang Zhang, Tianxiao Ye, Jiarong Kang, Yanze Liu, and Sequoyah Walters for their many helpful discussions, technical insights, and camaraderie during my time in the lab.

I am deeply indebted to my parents for their unconditional love, which has been a constant source of strength throughout my academic journey.

Finally, I would like to thank all the teachers, colleagues, and friends who have helped, inspired, and supported me along the way. Their kindness and encouragement have made this journey both meaningful and memorable.

Contents

List of Figures

Abstract

Autonomous systems are increasingly deployed across a wide range of applications, including robotics, autonomous vehicles, and intelligent manufacturing, where they are required to operate reliably in complex, dynamic, and often unpredictable environments. As these systems interact more closely with humans and the physical surroundings, safety has become a fundamental design requirement rather than a secondary performance objective. Failures in autonomous system control can result in severe and irreversible consequences, making it essential to rigorously ensure safe operation under all admissible conditions. However, the safety guarantees are often compromised by uncertainties inherent in real-world control systems, including modeling errors, external disturbances, and imperfect measurements. These challenges highlight the need for systematic safe control methodologies capable of enforcing safety in the presence of uncertainties. This dissertation addresses this need by developing systematic and theoretically grounded safe control techniques that ensure rigorous safety guarantees under a wide range of uncertainties.

The first part of this dissertation aims to ensure safety for systems with unstructured uncertainties using disturbance observers (DOBs). A new immersion-and-invariance-based DOB is developed to estimate the unstructured uncertainties for generic nonlinear control-affine systems, avoiding restrictive assumptions commonly required by existing DOB designs. By integrating the proposed DOB with control barrier functions (CBFs), a DOB-CBF-based safe control method is developed, enabling real-time safety enforcement while explicitly estimating and compensating for uncertainties. Rigorous sufficient conditions are provided to guarantee safety, and numerical simulations demonstrate that the pro-

posed approach can substantially reduce conservatism compared with worst-case robust CBF methods.

The second part of this dissertation studies the adaptive safe control problem for control-affine systems with structured (parametric) uncertainties in both drift terms and control-input matrices. An adaptive CBF-based control method is proposed, in which online parameter adaptation is integrated with CBF constraints to ensure safety. By formulating the resulting control synthesis problem as a nonlinear program with an explicit closed-form solution, the proposed method ensures non-emptiness of the admissible control set and avoids singularities commonly encountered in adaptive CBF design. A data-driven technique is developed to tighten parameter bounds using data, thereby improving control performance while rigorously preserving safety guarantees.

The third part of this dissertation investigates safe control problems for systems with limited model information. A new proxy CBF framework is introduced for strict-feedback systems with unknown dynamics, combining barrier-based and Lyapunov-based safe control methods. The proposed approach employs a modular design procedure, decomposing the original system into a proxy subsystem and a virtual tracking subsystem that are controlled by the CBF-based and Lyapunov-based controllers, respectively. By integrating these separately designed controllers, the overall system's safety is ensured.

The final part of this dissertation develops a hierarchical control strategy for occlusion-free visual servoing of robotic manipulators in the presence of measurement uncertainties. The proposed architecture consists of two control layers operating at different update rates. The high-level control layer employs a model predictive controller with explicit uncertainty compensation to perform long-horizon planning at a lower update frequency, while the low-level control layer adopts a robust CBF-based controller that operates at a higher update frequency to reject measurement uncertainties and strictly enforce occlusion-avoidance constraints in continuous time. Extensive experiments on a Franka Research 3 manipulator demonstrate the effectiveness, robustness, and real-time implementability of the proposed method.

Chapter 1

Introduction

1.1 Motivation

Autonomous systems are intelligent machines that can perform tasks and make decisions without direct human oversight by perceiving their environment, processing data, and executing actions to achieve specific objectives. These systems integrate sensors, computation, and control algorithms to function independently in dynamic and often uncertain environments. Examples include drones, self-driving cars, medical robots, and automated manufacturing systems. In this context, safety refers to the system's ability to operate without causing harm to humans, the environment, or itself. It encompasses the prevention of hazardous behaviors, adherence to operational constraints, and the system's capacity to handle unforeseen situations gracefully. Ensuring safety in autonomous systems is especially critical, as they frequently interact with humans and other systems in complex, real-world scenarios where errors can lead to severe consequences.

The importance of safe control in autonomous systems cannot be overstated. Unlike conventional control systems, where performance degradation may simply reduce efficiency or accuracy, failures in autonomous systems can lead to irreversible harm, such as physical injury, environmental damage, or even loss of life. For instance, a minor misjudgment in the control logic of a self-driving car could result in serious traffic accidents [1], and a small error in robotic surgical systems could compromise patients' safety [2]. These high-stakes

environments demand that safety should be treated as a foundational aspect of the control design process. It is no longer sufficient to optimize for performance alone; instead, safety must be integrated into the control architecture.

Furthermore, autonomous systems are often deployed in environments that are unpredictable and continuously evolving, such as urban traffic, human-populated spaces, or remote medical settings. In these contexts, traditional considerations about stability and robustness may not adequately account for rare but critical events. This necessitates the development of formal methods and control techniques that can provide provable guarantees of safety. Embedding such mechanisms directly into the control loop ensures that safety constraints are never violated, even in the presence of incomplete information. Ultimately, as autonomous systems become more deeply integrated into society, prioritizing safe control is not only a technical challenge but also a moral responsibility to ensure that these technologies remain reliable, accountable, and aligned with human well-being.

Over the past decades, a large number of safe control strategies have been proposed in the literature, such as Model Predictive Control (MPC) [3], Barrier Lyapunov Functions (BLFs) [4], Prescribed Performance Control (PPC) [5] , Control barrier functions (CBFs) [6], and Reference Governors (RGs) [7]. Among these methods, CBFs, which ensure constraint satisfaction through set invariance for control-affine systems, have drawn increasing attention recently. By including the CBF condition in a convex quadratic program (QP), a CBF-QP-based controller is generated in real time and acts as a safety filter that modifies potentially unsafe control inputs in a minimally invasive fashion. This safety-filtering mechanism enables CBF-QP-based controllers to intervene only when safety is at risk, while otherwise preserving the behavior of the nominal controller. Compared with other safe control strategies, CBF methods offer several fundamental advantages, which contribute to the widespread adoption of CBFs in a variety of safety-critical applications, including robotic manipulation [8], autonomous driving [9], and UAV systems [10]:

- CBF methods do not impose strict structural requirements on the constraints adopted by Lyapunov-based safe control, such as BLFs and PPC, and do not require the ref-

erence trajectory to stay inside the constraints.

- For nonlinear control-affine systems, CBF-QP is more computationally efficient than MPC, which requires solving a nonlinear program online.
- CBF approaches decouple performance and safety: the control objective can be specified via a nominal controller or reference trajectory, while safety requirements are independently encoded through CBF constraints.

Despite the success of CBFs in practical applications, their safety guarantees may be compromised in the presence of uncertainties that are unavoidable in real-world systems. These challenges are further amplified when safe controllers are designed and validated in high-fidelity simulation environments before deployment to real-world systems. Advanced physics-based simulators, such as MuJoCo [11] and Project Chrono [12], are capable of capturing complex multibody dynamics, contact interactions, and actuation effects with high accuracy, and have become indispensable tools for system analysis, algorithm validation, and data generation. In particular, learning-based control methods, such as reinforcement learning algorithms, rely heavily on large-scale data collection and are typically trained and evaluated in simulation environments before being transferred to physical systems. However, in real-world scenarios, sensing and perception processes are inevitably subject to uncertainties arising from noise, delays, limited resolution, and imperfect state estimation. Moreover, discrepancies between simulated models and real-world systems, commonly referred to as the sim-to-real gap, introduce additional sources of uncertainty that can significantly degrade the reliability of safety guarantees when controllers are transferred from simulation to hardware.

As a result, safe control methods that rely on idealized dynamics or noise-free state information may exhibit satisfactory performance in simulations while failing to rigorously enforce safety constraints in real-world deployments. These observations highlight the critical need for safe control frameworks that explicitly account for sensing uncertainties and sim-to-real discrepancies, and that remain robust when safety-critical controllers are implemented beyond idealized simulation settings.

Technically, when safe controllers are designed based on nominal models and accurate state measurements, even mild model mismatches or state estimation error may lead to violations of safe constraints, thereby undermining the validity of the safety guarantees. In autonomous systems, uncertainties arise from multiple sources and affect safety in fundamentally different ways:

- **Unstructured uncertainties**: Unmodeled dynamics and possibly time-varying exogenous inputs with unknown structure that directly perturb system trajectories, potentially driving the system outside the safe set.
- **Structured uncertainties**: Uncertainties with known structure but unknown or time-varying parameters that can compromise safety guarantees.
- **Measurement uncertainties**: Errors in state measurements or state estimation arising from noisy or delayed sensors, which compromise the reliability of feedback signals used for safety enforcement and may result in safety violation.
- **Unknown dynamics**: The system dynamics is partially or entirely unavailable, which can invalidate model-based control methods, including CBFs.

These heterogeneous uncertainty sources pose distinct challenges to safe control design. Therefore, developing systematic safe control techniques that explicitly account for and mitigate the effects of diverse uncertainties is essential for ensuring safety in autonomous systems. To address these challenges, this dissertation develops robust and adaptive CBF-based safe control techniques for uncertain systems, providing systematic methods to ensure constraint satisfaction despite imperfect model knowledge and state estimation.

1.2 Related Work

1.2.1 Constrained Control For Safety Assurance

Over the past decades, numerous constrained control strategies have been proposed to enforce safety constraints for control systems, such as MPC [3], [13], BLFs [4], [14], PPC [5],

[15], and RGs [7]. MPC uses the dynamic model to predict future behavior and optimizes control actions over a receding time horizon while satisfying constraints. Although MPC enables optimal decision-making and constraint satisfaction simultaneously, it is computationally expensive for nonlinear systems, especially when multiple nonconvex constraints are taken into account. BLF/PPC employs a Lyapunov-like function or defines a transformed error signal whose values tend to infinity at the boundary of the safe set, and a control law is designed to ensure the boundedness of the Lyapunov function. These methods can ensure stability and constraint satisfaction simultaneously, while they impose strict structural requirements on the constraints (i.e., the constraints are usually functions of time rather than states) and require the reference trajectory to stay inside the constraints. RG modifies the reference command of a well-designed closed-loop system to guarantee constraint satisfaction. The main advantage of RG is that it can avoid compromising the system performance because it only modifies the command when necessary. Nevertheless, RG mainly works for discrete systems and results in a non-convex optimization program for nonlinear systems. Moreover, RG needs to compute the maximum output admissible set, which could be challenging in practice.

1.2.2 Robust CBF Approaches & Disturbance Observers

To ensure safety under disturbances and uncertainties, a large number of robust CBF approaches have been proposed in the literature [16], [17], [18], [19], [20], [21], [22], [23], [24], [25]. In general, existing robust CBF approaches can be categorized into two classes. The first class adopts a worst-case perspective [16], [17], [18], [19], in which safety is enforced against all admissible disturbances and uncertainties within prescribed bounds. While these methods provide strong robustness properties, they can lead to overly conservative control behavior and degraded performance [26]. The second class aims to reduce conservatism by explicitly estimating and attenuating the effects of disturbances and uncertainties using state feedback [20], [21], [22], [23], [24], [25]. Instead of considering the worst-cases, these approaches incorporate online disturbance/uncertainty estimation into

the CBF condition, thereby enabling less conservative control performance.

Disturbance Observers (DOBs) [27], which is one of the most popular disturbance estimation approaches, aim to estimate the external disturbances by using identified dynamics and measurable states of plants and have been widely employed in applications such as robotics, automotive, and power electronics [27], [28], [29]. Compared with other robust control schemes, DOB-based control has two main advantages: (i) the DOB can be designed independently and added to a baseline controller to improve its robustness and disturbance attenuation capability; (ii) in the presence of disturbances/uncertainties, the nominal performance of the baseline controller can be recovered by the DOB-based controller [27], [29], [30]. Recently, several studies have integrated DOBs into CBF frameworks to improve control performance while preserving safety guarantees [20], [21], [22], [23]. The simulation and experimental studies show the superiority of the DOB-CBF-based methods over worst-case-based robust CBF approaches.

However, the design of DOBs is non-trivial and highly problem-specific. Specifically, designing a DOB requires the existence of two functions that can ensure the asymptotic stability of the error dynamics and the satisfaction of a PDE simultaneously [27]. Fulfilling these two requirements is challenging, and existing methods rely on relatively strong assumptions, e.g., the disturbance relative degree is uniformly well-defined [31], [32]. A systematic and computationally feasible method for constructing DOBs for generic nonlinear control-affine systems is still lacking.

1.2.3 Adaptive CBF-QP-based Approaches

Adaptive control aims to achieve stabilization or desired tracking performance for uncertain dynamic systems through an adaptive law, and has been extensively studied in the past decades [33], [34], [35], [36], [37]. Most adaptive control strategies are based on uncertainty parameterization and the certainty equivalence principle, which means that the estimated parameters are used as if they are the true parameters in the feedback control design. For uncertain nonlinear systems in some canonical forms, many adaptive control

design techniques have been developed using feedback linearization [38], [39], backstepping [35], [40], or averaging [41], [42]. A summary of the fundamental theoretical concepts and technical issues involved in multivariable adaptive control is documented in [43], and a historical overview of adaptive control and its intersection with learning is provided in [44].

Inspired by the idea of adaptive control Lyapunov functions (aCLFs) [45], the adaptive CBF (aCBF) approach, which estimates the unknown parameters online to guarantee the safety of control affine systems with parametric uncertainties via a QP-based safe controller, is first proposed in [46]. In contrast to the aCLF-based stabilizing controller design, the aCBF-based safe control design is more challenging partially because the forward invariance of a predefined safe set must be ensured for all time and aCBFs do not have the positive definiteness property possessed by aCLFs. Following the pioneering work of [46], various aCBF-based control methods are developed in the literature [47], [48], [49], [50], [51], [52], [53], [54] and applied to several practical scenarios, such as adaptive cruise control [46], aircraft control [47], control of wing rock motion [52], and control of unicycle vehicles [54].

However, most of these works only take into account parametric uncertainties in the drift terms, not the control-input matrix. In practice, uncertainties in the control-input matrix is pretty common, such as robotic systems that have error in their mass and inertia parameters [55]. This issue has received relatively limited attention in the robust CBF literature until only very recently. In [53], a filtering-based concurrent learning algorithm in the CBF framework is proposed to design safe controllers for single-input-single-output systems with unknown control coefficients; the estimated parameter converges to the true value exponentially, but system safety is not guaranteed before the convergence of the parameter adaptations. In [54], a zeroing CBF-based adaptive control algorithm is proposed to solve the funnel control problem for systems with parametrically uncertain control-input matrices, which can achieve tracking of a reference trajectory within a pre-defined funnel; however, this method may fail in singular configurations. Despite these early con-

tributions, the aCBF-based control design for systems with parametric uncertainties in the control-input matrix terms is still an open field and merits further investigation.

1.2.4 Safe Control Under Measurement Uncertainties

Most existing results using CBFs rely on accurate state information, which is hard to obtain in practice. For example, in the absence of velocity sensors, the angular velocities of robot manipulators cannot be obtained exactly; even when the manipulator is equipped with velocity sensors, the velocity signals are usually contaminated by noise. Recently, various methods have been proposed to address this issue [18], [56], [57], [58], [59], [60]. [18] employs robust CBF and fixed-time control Lyapunov functions to guaranty the stability and safety of the system in the presence of additive disturbance and state estimation error. In [56], a function mapping from outputs to states is learned via supervised learning techniques, and the controller is designed under the assumption that for any given output value, all possible state estimation error is bounded by a known constant. [57] proposes a controller synthesis approach involving feedback from pixels, which does not require feature extraction, object detection, or state estimation. [58] develops a method that trains classifiers for sensor-based control problems, bypassing the state estimation step. [59] proposes a QP-based controller with an unscented Kalman filter which is capable of attenuating the effects of state disturbances and measurement noises. [60] develops an observer-based safe control approach that integrates the estimation error quantified observer and adaptive CBFs.

1.2.5 Multi-rate Safe Control

Nowadays, control of complex cyber-physical systems is commonly structured in a hierarchical framework [61], [62], [63], [64], [65], [66], [67], [68], [69], where the control design and decision making are divided into different control layers with varying fidelity and complexity. Multi-rate control [67], [68], [69], a prominent example of hierarchical control, is a control strategy in which different layers of a system operate at distinct sampling or up-

date rates. This approach is especially valuable in modern autonomous and cyber-physical systems, where sensing, planning, and actuation inherently occur on different time scales. For instance, low-level control tasks such as motor actuation and sensor feedback processing often demand millisecond-level updates to ensure responsiveness and stability. In contrast, high-level decision-making processes, such as trajectory planning, optimization-based control (e.g., MPC), or learning algorithms, are computationally expensive and therefore operate at slower update rates. By decoupling these rates, multi-rate control allows the system to maintain real-time responsiveness at the low level while accommodating complex computation at the high level. This decoupling leads to improved overall system performance, better utilization of computational resources, and greater scalability and modularity in system design.

Recently, there are several works that employ multi-rate control framework for ensuring safety [66], [67], [69], [70]. In [70], a multi-rate control architecture is proposed for safety-critical systems that combines a low-frequency MPC planner with a high-frequency CBF-based safety controller and provides sufficient conditions for constraint satisfaction under time-scale separation. By modeling the system as a hybrid piecewise nonlinear system, the approach enables convex optimization-based control and demonstrates improved safety and performance through simulation. [67] develops a hierarchical multi-rate control architecture for autonomous systems operating in partially observable environments, combining high-level decision-making based on temporal logic specifications with low-level safety enforcement. A high-level policy updates the constraints and cost of an MPC planner, whose reference trajectory is tracked by a high-frequency CBF-based controller, to ensure constraint satisfaction. In [66], a multi-rate control scheme is designed for a nonlinear system using a linearized model by integrating MPC and CLFs. Bézier curves are utilized to ensure constraint satisfaction by constructing continuous trajectories from sequences of discrete points that satisfy the given constraints. A comprehensive survey of multi-rate control is presented in [69].

1.3 Summary of Contributions

This dissertation is organized to present four major research contributions and is structured as follows (see Figure 1.1).

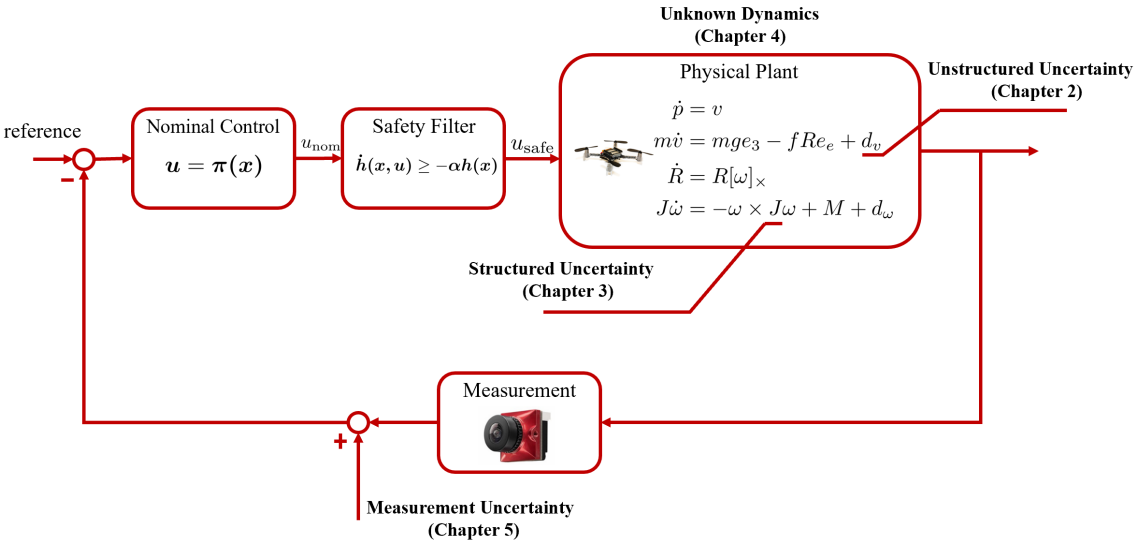

Figure 1.1: Illustration of the structure of this dissertation.

Chapter 2 presents a novel immersion-and-invariance (I&I)-based DOB design approach and corresponding DOB-CBF-QP-based safe control design method for systems with unstructured uncertainties. Inspired by the I&I technique [71], we propose a systematic approach for designing DOB for general nonlinear control-affine systems without imposing the strong assumptions adopted by existing DOB design methods, such as the solvability of a partial differential equation (PDE). Furthermore, a filter-based DOB-CBF-QP safe control design approach is developed for control-affine systems with disturbances, where a filter is designed to obtain an alternative disturbance estimation signal with a known derivative, and sufficient conditions are provided to ensure the safety of the disturbed system.

Chapter 3 focuses on safe control design for systems with structured (parametric) uncertainties in both drift terms and control-input matrices. A new adaptive CBF approach, which combines CBFs and adaptive laws, is developed to generate a safe controller through

a nonlinear program with an explicitly given closed-form solution. The proposed approach verifies the non-emptiness of the admissible control set independently of online parameter estimations, which can ensure that the safe controller is singularity-free. A data-driven algorithm is also developed to improve the performance of the proposed controller by tightening the bounds of the unknown parameters.

Chapter 4 investigates the CBF-based safe control design problem for strict-feedback systems with limited model information (unknown dynamics). We develop a novel proxy CBF scheme that integrates barrier-based and Lyapunov-based safe control strategies. The proposed method employs a modular design procedure, decomposing the original system into a proxy subsystem and a virtual tracking subsystem that are controlled by the CBF-based and Lyapunov-based controllers, respectively. By integrating these separately designed controllers, the overall system's safety is ensured in the presence of limited model information.

Chapter 5 develops an occlusion-free multi-rate visual servoing control framework for robotic manipulators in the presence of measurement uncertainties. This framework integrates a high-level MPC with a low-level CBF-based controller, where occlusion-avoidance constraints are reformulated into differentiable convex constraints. In this architecture, the high-level MPC incorporates state estimation techniques to mitigate the impact of measurement uncertainties during long-horizon planning, while the low-level controller employs robust CBF methods to strictly enforce occlusion avoidance in continuous time. Hardware experiments on a Franka Research 3 manipulator validate the real-time implementability and strict occlusion avoidance of the proposed approach.

Finally, Chapter 6 summarizes the main contributions and key findings of this dissertation. The chapter concludes with a discussion of potential directions for future research and highlights open problems that motivate further development of CBF-based safe control approaches.

1.4 Notations

For a positive integer n, denote $[n] = \{1, 2, \cdots, n\}$ and $[0, n] = \{0, 1, 2, \cdots, n\}$. For a column vector $x \in \mathbb{R}^n$ or a row vector $x \in \mathbb{R}^{1\times n}$, let x_i denote its i-th entry and $\|x\|$ its 2-norm, $\|x\|_Q = \sqrt{x^\top Q x}$ where Q is a positive definite matrix, and $x \geq 0$ implies $x_i \geq 0$ for any $i \in [n]$. Define $\mathbb{R}_{\geq 0} = \{x \in \mathbb{R} : x \geq 0\}$. Denote by I_n the $n \times n$ identity matrix and by $\mathbf{1}_n$ the n-dimensional column vector with all entries equal to 1. For a matrix $A \in \mathbb{R}^{n\times m}$, let A_{ij} denote its (i, j)-th entry, $\|A\|$ its Frobenius norm, and $\lambda_{\max}(A)$ and $\lambda_{\min}(A)$ denote the maximal and minimal eigenvalues of A, respectively, if A is a square matrix. Denote $\mathrm{diag}(a_1, a_2, \cdots, a_n) \in \mathbb{R}^{n\times n}$ as the diagonal matrix with entries $a_1, a_2, \cdots, a_n \in \mathbb{R}$, and $\mathrm{blkdiag}(A_1, A_2, \cdots, A_n)$ as the block-diagonal matrix with diagonal blocks $A_1, A_2, \cdots, A_n$, which need not be square. For a scalar function $h : \mathbb{R}^n \to \mathbb{R}$ with respect to $x \in \mathbb{R}^n$, the gradient $\frac{\partial h}{\partial x} \in \mathbb{R}^{n\times 1}$ is considered a row vector. For a vector-valued function $f : \mathbb{R}^n \to \mathbb{R}^m$ with respect to $x \in \mathbb{R}^n$, $f^{(i)}$ represented its i-th derivative, and $\frac{\partial f}{\partial x}$ denotes its Jacobian matrix, whose (i, j)-th entry is $\frac{\partial f_i}{\partial x_j}$. Given n points $p_1, p_2, \cdots, p_n \in \mathbb{R}^m$, their convex hull is defined as

$$\mathrm{conv}(p_1, \cdots, p_n) = \left\{ \sum_{i=1}^{n} \lambda_i p_i : \lambda_i \geq 0, \sum_{i=1}^{n} \lambda_i = 1 \right\}.$$

Denote the set of intervals on $\mathbb{R}$ by $\mathbb{IR}$, the set of n-dimensional interval vectors by $\mathbb{IR}^n$, and the set of $n \times m$-dimensional interval matrices by $\mathbb{IR}^{n\times m}$. The definition of interval operations, e.g., addition, substraction, multiplication, etc., follows those in [72]. Given two vectors $x, y \in \mathbb{R}^n$ and $x \leq y$, $[x, y] = [[x_1, y_1] \ \cdots \ [x_n, y_n]]^\top \in \mathbb{IR}^n$ represents an interval vector.

Chapter 2

DOB-CBF-based Safe Control for Systems With Unstructured Uncertainties

2.1 Introduction

This chapter focuses on developing robust safe controllers for generic systems with unstructured uncertainties. Recently, various robust CBF approaches have been proposed for systems with model uncertainties and external disturbances [16], [17], [18], [19]; however, most of these robust CBF methods consider the worst-case of uncertainties, resulting in overly conservative control behaviors. To improve control performance while rigorously ensuring safety, several works integrate DOBs, which can estimate disturbances and uncertainties by using model information and state measurements, into the CBF-QP framework [20], [23], [26], [73]. Compared with worst-case-based robust CBF methods, DOB-CBF-QP-based control has two main advantages: (i) DOBs can be designed independently and added to a nominal CBF-QP-based controller to improve its robustness and disturbance attenuation capability; (ii) in the presence of disturbances/uncertainties, the nominal performance of the CBF-QP-based controller can be recovered by using DOBs [27], [29],

[30].

Nevertheless, the design of DOBs is non-trivial and highly problem-specific. Specifically, designing a DOB requires the existence of two functions that can ensure the asymptotic stability of the error dynamics and the satisfaction of a PDE simultaneously (more details will be given in the Section 2.2.2) [27]. Fulfilling these two requirements is challenging, and existing methods rely on relatively strong assumptions, e.g., the solvability of a PDE or the disturbance relative degree is uniformly well-defined [31], [32]. A systematic and computationally tractable method for constructing DOBs for generic nonlinear control-affine systems is still lacking.

To address the aforementioned DOB design challenge, we develop a systematic DOB design method and incorporate it into the CBF-QP framework. The main contributions of this chapter are summarized as follows.

- Inspired by the I&I technique [37], [71], [74], we propose a systematic approach for designing I&I-based Disturbance Observer (IIDOB) for general nonlinear control-affine systems without imposing the strong assumptions adopted by existing DOB design methods. By approximately solving the PDE and compensating for the approximation error, the proposed IIDOB ensures that the disturbance estimation error is globally Uniformly Ultimately Bounded (UUB).

- Based on the proposed IIDOB, we develop a filter-based IIDOB-CBF-QP safe control design approach for control-affine systems with disturbances. We design a filter to obtain an alternative disturbance estimation signal with a known derivative and provide sufficient conditions that ensure the safety of the disturbed system.

An illustration of the proposed IIDOB-CBF-QP method is presented in Figure 2.1.

This chapter is adapted from previously published work in [26], [75].

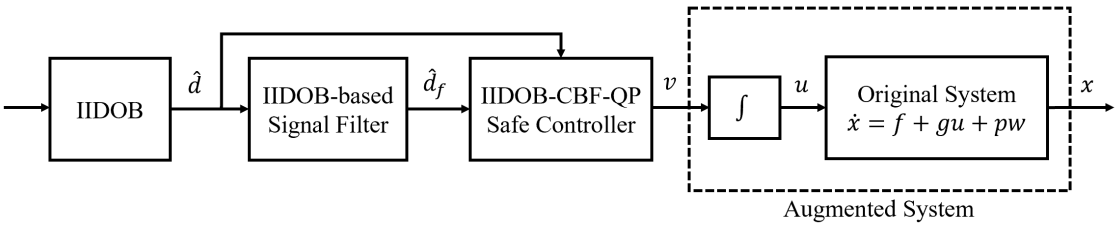

Figure 2.1: Configuration of the proposed IIDOB-CBF-QP method.

2.2 Preliminaries and Problem Formulation

2.2.1 Control Barrier Functions

Consider the following control-affine system:

$$\dot{x} = f(x) + g(x)u, \tag{2.1}$$

where $x \in \mathbb{R}^n$ is the state, $u \in U \subset \mathbb{R}^m$ is the control input, $l : \mathbb{R}^n \to \mathbb{R}^k$ is the output measurement, $f : \mathbb{R}^n \to \mathbb{R}^n$ and $g : \mathbb{R}^n \to \mathbb{R}^{n\times m}$ are locally Lipchitz continuous functions. A set $\mathcal{S}$ is called forward controlled invariant with respect to system (2.1) if for every $x_0 \in \mathcal{S}$, there exists a control signal $u(t)$ such that $x(t; t_0, x_0) \in \mathcal{S}$ for all $t \geq t_0$, where $x(t; t_0, x_0)$ denotes the solution of (2.1) at time t with initial condition $x_0 \in \mathbb{R}^n$ at time t_0.

Consider system (2.1) and a set $\mathcal{C} \subset \mathbb{R}^n$ defined by

$$\mathcal{C} = \{x \in \mathbb{R}^n : h(x) \geq 0\} \tag{2.2}$$

for a continuously differentiable function $h : \mathbb{R}^n \to \mathbb{R}$. The function h is called a (zeroing) CBF if there exists a constant $\gamma > 0$ such that

$$\sup_{u\in U} [L_f h(x) + L_g h(x)u + \gamma h(x)] \geq 0 \tag{2.3}$$

where $L_f h(x) = \frac{\partial h}{\partial x} f(x)$ and $L_g h(x) = \frac{\partial h}{\partial x} g(x)$ are Lie derivatives [76]. Given a CBF h,

the set of all control values that satisfy (2.3) for all $x \in \mathbb{R}^n$ is defined as

$$K_{\text{zcbf}}(x) = \{u \in U : L_f h(x) + L_g h(x) u + \gamma h(x) \geq 0\}. \tag{2.4}$$

It was proven in [76] that any Lipschitz continuous controller $u(x) \in K_{\text{zcbf}}(x)$ for every $x \in \mathbb{R}^n$ will guarantee the forward invariance of $\mathcal{C}$. The provably safe control law is obtained by solving the following convex QP online:

$$\begin{aligned} u(x) = \arg\min_{u} \ & \|u - u_d(x)\|^2 \\ \text{s.t.} \quad & L_f h(x) + L_g h(x) u \geq -\gamma h(x), \end{aligned} \tag{2.5}$$

where $u_d(x)$ is the desired control law which is potentially unsafe. Note that the CBF condition (i.e., the constraint of the CBF-QP (2.5)) is affine on u for any nonlinear control-affine system, which makes the CBF-QP convex.

2.2.2 Disturbance Observers

Consider the following control-affine system with disturbances:

$$\dot{x} = f(x) + g(x)u + p(x)w(t) \tag{2.6}$$

where $x \in \mathbb{R}^n$ is the state, $u \in \mathbb{R}^m$ is the control input, $w : \mathbb{R}_{\geq 0} \to \mathbb{R}^l$ is the disturbance, and $f : \mathbb{R}^n \to \mathbb{R}^n$, $g : \mathbb{R}^n \to \mathbb{R}^{n \times m}$, and $p : \mathbb{R}^n \to \mathbb{R}^{n \times l}$ are known functions. The DOB design aims to estimate $w(t)$ using the state measurement $x(t)$. A standard assumption for DOB is given first.

Assumption 2.1 The disturbance $w(t)$ and its derivative $\dot{w}(t)$ are bounded by known positive constants, i.e., $\|w(t)\| \leq \omega_0$ and $\|\dot{w}(t)\| \leq \omega_1, \forall t > 0$ where $\omega_0 > 0$ and $\omega_1 > 0$.

As shown in [27], [32], the DOB for system (2.6) has the following structure:

$$\hat{w} = z + q(x), \tag{2.7a}$$

$$\dot{z} = -l(x)p(x)z - l(x)[f(x) + g(x)u + p(x)q(x)], \tag{2.7b}$$

where $\hat{w}$ is the disturbance estimation, $z \in \mathbb{R}^l$ is the internal state of the DOB. The function $l(x)$, known as the DOB gain, and the function $q(x)$ should be designed such that [27]

$$\frac{\partial q(x)}{\partial x} = l(x), \tag{2.8}$$

and the error dynamics is globally asymptotically stable for any $x \in \mathbb{R}^n$:

$$\dot{e}_w + l(x)p(x)e_w = 0, \tag{2.9}$$

where $e_w = w - \hat{w}$ is the disturbance estimation error. It can be proved [27] that the disturbance estimation error of DOB (2.7) is globally UUB.

Nevertheless, designing l and q is a challenging and highly case-specific task in general [27]. Several methods have been proposed based on relatively strong assumptions. If p has full column rank for any $x \in \mathbb{R}^n$, then one can select q by solving the PDE $\frac{\partial q}{\partial x} = p^\dagger$, where $p^\dagger$ denotes the left inverse of p [28]; however, when $n > 1$, this PDE is generally unsolvable and even when solvable, its closed-form solution is hard to obtain. If the disturbance relative degree is uniformly well-defined with respect to an output function $s(x)$, an approach for designing q is proposed in [31], [32]; however selecting such a function s is challenging and its existence is not guaranteed (e.g., there may exist $x^* \in \mathbb{R}^n$ such that $p(x^*) = 0$). A practically useful approach involves treating pw as the total disturbance and assuming that $\frac{\mathrm{d}}{\mathrm{d}t}(pw)$ is bounded [77], [78]; however, this assumption is rather restrictive because $\frac{\mathrm{d}}{\mathrm{d}t}(pw)$ explicitly relies on u and x.

2.2.3 Problem Formulation

Consider system (2.6) and the safe set defined in (2.2), where h is a sufficiently smooth function. Recall that g_j denotes the j-th column of g for $j \in [m]$, and p_i denotes the i-th column of p for $i \in [l]$. System (2.6) is said to have a vector Input Relative Degree

(IRD) $\mathcal{I} = (\sigma_1, \sigma_2, \cdots, \sigma_m)$ at a given point $x_0 \in \mathbb{R}^n$ if $L_{g_j} L_f^k h(x) = 0$ for any $k \in [\sigma_j - 2]$, $j \in [m]$, and for all x in a neighborhood of x_0, and $L_{g_j} L_f^{\sigma_j - 1} h(x_0) \neq 0$ holds for any $j \in [m]$ [79, Remark 5.1.1]. Similarly, system (2.6) is said to have a vector Disturbance Relative Degree (DRD) $\mathcal{D} = (\nu_1, \nu_2, \cdots, \nu_l)$ at a given point $x_0 \in \mathbb{R}^n$ if $L_{p_j} L_f^k h(x) = 0$ for any $k \in [\nu_j - 2]$, $j \in [l]$, and for all x in a neighborhood of x_0, and $L_{p_j} L_f^{\nu_j - 1} h(x_0) \neq 0$ holds for any $j \in [l]$ [80]. Note that because system (2.6) is multiple-input-single-output with h as the output, the definitions of vector IRD and vector DRD above are slight modifications of those given in [79], [80].

In this dissertation, with a slight abuse of notation, we will call $r_I = \min \mathcal{I}$ and $r_D = \min \mathcal{D}$ as the minimum IRD and the minimum DRD of system (2.6) with respect to function h at a given point $x_0 \in \mathbb{R}^n$, respectively; that is, r_I (or r_D) denotes the number of times h has to be differentiated to have at least one component of u (or w) explicitly appearing.

The first problem investigated in this chapter is to design a disturbance estimation law to estimate the total disturbance

$$d(x, t) = p(x)w(t). \tag{2.10}$$

Problem 2.1 *Consider system* (2.6) *with* $f, g \in C^1$ *and* $p \in C^2$ *and suppose Assumption 2.1 holds. Design a DOB-based estimation law to estimate the total disturbance* d *online.*

Using the DOB-based estimation of the total disturbance, the second problem investigated in this chapter is to design a feedback control law such that system (2.6) is safe.

Problem 2.2 *Consider system* (2.6) *with* $f, g \in C^1$ *and* $p \in C^2$ *and the safe set* $\mathcal{C}$ *defined in* (2.2)*. Suppose that Assumption 2.1 holds and* $r_I = r_D$ *for system* (2.6) *with respect to* h*. Given the DOB developed via solving Problem 2.1, design a feedback control law such that system* (2.6) *is safe, i.e.,* $h(x(t)) \geq 0$ *for any* $t > 0$ *provided* $h(x(0)) > 0$*.*

In this dissertation, we aim to estimate the total disturbance d rather than the disturbance w for two main reasons: first, since no assumption is imposed on p except for

$p \in C^2$, the disturbance w may not be uniquely determined in general; second, Problem 2 can be solved by using the information of d only.

2.3 Immersion-and-invariance-based Disturbance Observer

Inspired by the I&I technique [37], [71], [74], we propose an IIDOB design approach to solve Problem 2.1 in this section.

First, we augment system (2.6) with an additional integrator:

$$\dot{x} = f(x) + g(x)u + p(x)w(t), \tag{2.11a}$$

$$\dot{u} = v, \tag{2.11b}$$

where v denotes the auxiliary control input to be designed, and u is considered as a state variable of the augmented system. As will be shown in this section and next section, the auxiliary control input v will be used in the design of IIDOB, and it will be generated from solving the IIDOB-CBF-QP. The control input u for the original system (2.6) will be obtained through integrating v.

Define a time-varying set

$$\mathcal{M}(t) = \{(x, \hat{x}, u) \in \mathbb{R}^n \times \mathbb{R}^n \times \mathbb{R}^m : \xi(t) + \beta(\hat{x}, x, u) - p(x)w(t) = 0\}, \tag{2.12}$$

where $\hat{x}$ denotes the state estimation and ξ, β are known functions that will be all specified later. Define

$$\hat{d} = \xi + \beta \tag{2.13}$$

as the estimated total disturbance, and the disturbance estimation error as

$$e_d = \hat{d} - d. \tag{2.14}$$

It is clearly that if the system trajectories are restricted to $\mathcal{M}(t)$, the disturbance estima-

tion is accurate. We also define

$$z = \frac{\xi + \beta - d}{r}, \tag{2.15}$$

where r is the scaling factor governed by an adaptive law yet to be designed. It is clear that $e_d = rz$. Our IIDOB design will render e_d globally UUB [81, Definition 4.6] by guaranteeing that z is globally UUB and r remains bounded. Note that $\dot{z}$, the time derivative of z, can be expressed as

$$\dot{z} = -\frac{\dot{r}}{r}z + \frac{1}{r}\left(\dot{\xi} + \frac{\partial \beta}{\partial x}(f+gu+pw) + \frac{\partial \beta}{\partial u}v + \frac{\partial \beta}{\partial \hat{x}}\dot{\hat{x}} - p\dot{w} - \sum_{i=1}^{l}\frac{\partial p_i}{\partial x}(f+gu+pw)w_i\right), \tag{2.16}$$

where p_i denotes the i-th column of p, $i \in [l]$. Define

$$\psi(x,u) = \frac{\eta}{2}\left[\|p\|^2 + \sum_{i=1}^{l}\left(\left\|\frac{\partial p_i}{\partial x}(f+gu)\right\|^2 + \left\|\frac{\partial p_i}{\partial x}p\right\|^2\right)\right] + \gamma, \tag{2.17}$$

where $\gamma, \eta > 0$ are tuning parameters and γ denotes the observer gain.

If $\delta(x,u) \in \mathbb{R}^n$ is a solution to the following PDE:

$$\frac{\partial \delta}{\partial x} = \psi I_n, \tag{2.18}$$

then the DOB design becomes straightforward by following [71]. Specifically, one can design the total disturbance estimation as $\hat{d} = \xi + \delta$, where ξ is governed by

$$\dot{\xi} = -\frac{\partial \delta}{\partial x}(f + gu + \xi + \delta) - \frac{\partial \delta}{\partial u}v. \tag{2.19}$$

Invoking (2.11) and (2.14), one can see

$$\dot{e}_d = -\psi e_d - p\dot{w} - \sum_{i=1}^{l}\frac{\partial p_i}{\partial x}(f + gu + pw)w_i. \tag{2.20}$$

By selecting a candidate Lyapunov function $V = \frac{1}{2}e_d^\top e_d$, one can easily verify that

$$\begin{aligned}\dot{V} &= e_d^\top \left(-\psi e_d - p\dot{w} - \sum_{i=1}^{l} \frac{\partial p_i}{\partial x}(f + gu + pw)w_i \right) \\ &\leq -\psi \|e_d\|^2 + \omega_1 \|p\| \|e_d\| + \sum_{i=1}^{l} \omega_0 \left\| \frac{\partial p_i}{\partial x}(f + gu) \right\| \|e_d\| + \sum_{i=1}^{l} \omega_0^2 \left\| \frac{\partial p_i}{\partial x} p \right\| \|e_d\| \\ &\leq -\gamma \|e_d\|^2 + \frac{1}{2\eta}(\omega_1^2 + l\omega_0^2 + l\omega_0^4), \end{aligned} \tag{2.21}$$

which indicates that e_d is globally UUB. However, when $n > 1$, solving (2.18) is extremely challenging in principle, and even a solution to (2.18) may not exist [74]. To tackle this issue, we will follow [74] to first "approximately solve" (2.18) and then use $\dot{r}$ to compensate for the approximation error.

Recall that $f, g \in C^1$ and $p \in C^2$. Then, $\psi \in C^1$, and it is easy to verify that there exist continuous functions $\delta_{ij} : \mathbb{R}^n \times \mathbb{R}^n \times \mathbb{R}^m \to \mathbb{R}$, $i, j \in [n]$, such that [82], [83]:

$$\psi(\hat{x}_1, \cdots, \hat{x}_{i-1}, x_i, \hat{x}_{i+1}, \cdots, \hat{x}_n, u) - \psi(x, u) = -\sum_{j=1}^{n} \delta_{ij}(x, \hat{x}, u) e_j, \tag{2.22}$$

where

$$e = \hat{x} - x \tag{2.23}$$

and e_j denotes the j-th entry of e. The following theorem shows that our IIDOB design ensures the disturbance estimation error e_d is globally UUB.

Theorem 2.1 *Consider system* (2.11) *where* $f, g \in C^1$ *and* $p \in C^2$*, and suppose Assumption 2.1 holds. If the disturbance estimation law* $\hat{d}$ *is designed as:*

$$\hat{d} = \xi + \beta, \tag{2.24a}$$

$$\Lambda = (k_1 + k_2 r^2) I_n + \frac{cr^2}{2} \mathrm{diag}[\|\Delta_1\|^2, \cdots, \|\Delta_n\|^2], \tag{2.24b}$$

$$\beta = \begin{bmatrix} \int_0^{x_1} \psi(\tau, \hat{x}_2, \hat{x}_3, \cdots, \hat{x}_n, u)\mathrm{d}\tau \\ \int_0^{x_2} \psi(\hat{x}_1, \tau, \hat{x}_3, \cdots, \hat{x}_n, u)\mathrm{d}\tau \\ \vdots \\ \int_0^{x_n} \psi(\hat{x}_1, \hat{x}_2, \cdots, \hat{x}_{n-1}, \tau, u)\mathrm{d}\tau \end{bmatrix}, \tag{2.24c}$$

$$\dot{\hat{x}} = f + gu + \hat{d} - \Lambda e, \tag{2.24d}$$

$$\dot{\xi} = -\frac{\partial \beta}{\partial x}(f + gu + \hat{d}) - \frac{\partial \beta}{\partial u} v - \frac{\partial \beta}{\partial \hat{x}} \dot{\hat{x}}, \tag{2.24e}$$

$$\dot{r} = -\theta(r-1) + \frac{cr}{2} \sum_{j=1}^{n} e_j^2 \|\Delta_j\|^2, \ r(0) > 1, \tag{2.24f}$$

where ψ is defined in (2.17)*, e is defined in* (2.23)*, $\gamma, c, \theta > 0$ are positive constants satisfying $\gamma > \frac{n}{2c} + \theta$, $\Delta_j = diag[\delta_{1j}, \delta_{2j}, \cdots, \delta_{nj}] \in \mathbb{R}^{n \times n}$ with δ_{ij} defined in* (2.22) *for $i, j \in [n]$, and $k_1, k_2 > 0$ are positive constants satisfying $k_2 > \frac{1}{4\gamma - 2n/c - 4\theta}$, then e_d is globally UUB.*

Proof *Recall that $e_d = rz$. To prove that e_d is globally UUB, we will first show z is globally UUB, and then r is bounded.*

Substituting (2.24e) *into* (2.16) *yields*

$$\dot{z} = -\frac{\dot{r}}{r} z - \frac{\partial \beta}{\partial x} z - \frac{1}{r} \left(p\dot{w} + \sum_{i=1}^{l} \frac{\partial p_i}{\partial x} (f + gu + pw) w_i \right). \tag{2.25}$$

Recall that $\psi \in C^1$. According to the fundamental theorem of calculus, one can see that

$$\frac{\partial \beta}{\partial x} = \mathrm{diag}[\psi(x_1, \hat{x}_2, \cdots, \hat{x}_n, u), \psi(\hat{x}_1, x_2, \hat{x}_3, \cdots, \hat{x}_n, u), \cdots, \psi(\hat{x}_1, \hat{x}_2, \cdots, \hat{x}_{n-1}, x_n, u)]. \tag{2.26}$$

Define $e_\psi = \left\| \psi(x,u) I_n - \frac{\partial \beta}{\partial x} \right\|$ as the "approximation error" induced by approximately solving (2.18) *using β designed in* (2.24c)*. Intuitively, from* (2.26) *one can see that if $\hat{x}$ is very close to x, e_ψ would be negligible. Note that the influence of e_ψ will be eliminated by $\dot{r}$ as shown in the following analysis.*

Then, substituting (2.22) *into* (2.26) *yields*

$$\frac{\partial \beta}{\partial x} = \psi(x,u) I_n - \sum_{j=1}^{n} \Delta_j e_j, \tag{2.27}$$

and substituting (2.17) *and* (2.27) *into* (2.25) *yields*

$$\begin{aligned}\dot{z} = &-\frac{\dot{r}}{r} z - \gamma z - \frac{\eta}{2}\left[\sum_{i=1}^{l}\left(\left\|\frac{\partial p_i}{\partial x}(f+gu)\right\|^2 + \left\|\frac{\partial p_i}{\partial x} p\right\|^2\right) + \|p\|^2\right] z + \sum_{j=1}^{n} \Delta_j e_j z \\ &+\frac{1}{r}\left(-p\dot{w} - \sum_{i=1}^{l} \frac{\partial p_i}{\partial x}(f+gu+pw) w_i\right).\end{aligned} \tag{2.28}$$

From (2.24f) *one can easily verify that* $r \geq 1$ *for any* $t > 0$ *because the set* $\{r : r \geq 1\}$ *is invariant. Substituting* (2.24f) *into* (2.28) *gives*

$$\begin{aligned}\dot{z} = &-\frac{c}{2}\sum_{j=1}^{n} e_j^2 \|\Delta_j\|^2 z - \left[\frac{\eta}{2}\sum_{i=1}^{l}\left(\left\|\frac{\partial p_i}{\partial x}(f+gu)\right\|^2 + \left\|\frac{\partial p_i}{\partial x} p\right\|^2\right) + \frac{\eta}{2}\|p\|^2 - \sum_{j=1}^{n} \Delta_j e_j\right] z \\ &+\frac{1}{r}\left(-p\dot{w} - \sum_{i=1}^{l} \frac{\partial p_i}{\partial x}(f+gu) w_i - \sum_{i=1}^{l} \frac{\partial p_i}{\partial x} p w w_i\right) - \gamma z + \theta \frac{r-1}{r} z.\end{aligned} \tag{2.29}$$

Meanwhile, subtracting (2.11) *from* (2.24d) *yields*

$$\dot{e} = \hat{d} - d - \Lambda e = rz - \Lambda e. \tag{2.30}$$

Next, we prove that z *is globally UUB. Define a candidate Lyapunov function as*

$$V = \frac{1}{2} z^\top z, \tag{2.31}$$

whose time derivative is

$$\begin{aligned}\dot{V} \overset{(2.29)}{=} &-\gamma\|z\|^2 + z^\top \sum_{j=1}^{n} \Delta_j e_j z - \frac{\eta}{2}\left[\sum_{i=1}^{l}\left(\left\|\frac{\partial p_i}{\partial x}(f+gu)\right\|^2 + \left\|\frac{\partial p_i}{\partial x} p\right\|^2\right) + \|p\|^2\right]\|z\|^2 \\ &+\theta\frac{r-1}{r}\|z\|^2 - \frac{c}{2}\sum_{j=1}^{n} e_j^2 \|\Delta_j\|^2 \|z\|^2 + \frac{z^\top}{r}\left(-p\dot{w} - \sum_{i=1}^{l} \frac{\partial p_i}{\partial x}(f+gu+pw) w_i\right)\end{aligned}$$

$$
\begin{aligned}
&\leq \theta\frac{r-1}{r}\|z\|^2+\sum_{j=1}^{n}\|\Delta_j\|\|e_j\|\|z\|^2-\frac{\eta}{2}\left[\sum_{i=1}^{l}\left(\left\|\frac{\partial p_i}{\partial x}(f+gu)\right\|^2+\left\|\frac{\partial p_i}{\partial x}p\right\|^2\right)+\|p\|^2\right]\|z\|^2\\
&\quad+\frac{\|z\|}{r}\left(\|p\|\omega_1+\sum_{i=1}^{l}\left\|\frac{\partial p_i}{\partial x}(f+gu)\right\|\omega_0+\sum_{i=1}^{l}\left\|\frac{\partial p_i}{\partial x}p\right\|\omega_0^2\right)-\frac{c}{2}\sum_{j=1}^{n}e_j^2\|\Delta_j\|^2\|z\|^2\\
&\quad-\gamma\|z\|^2\\
&\leq -\left(\gamma-\theta-\frac{n}{2c}\right)\|z\|^2+\frac{1}{2\eta r^2}(\omega_1^2+l\omega_0^2+l\omega_0^4)\\
&\leq -\kappa\|z\|^2+\omega, \qquad (2.32)
\end{aligned}
$$

where

$$\kappa=\gamma-\frac{n}{2c}-\theta>0, \qquad (2.33a)$$

$$\omega=\frac{1}{2\eta}(\omega_1^2+l\omega_0^2+l\omega_0^4)>0, \qquad (2.33b)$$

the first and second inequality arise from Cauchy-Schwarz inequality, and the last inequality comes from the fact that $r\geq 1$. *Therefore, one can see that*

$$\|z\|\leq\sqrt{\|z(0)\|^2e^{-2\kappa t}+\frac{\omega}{\kappa}}=\varrho_z(t), \qquad (2.34)$$

which indicates that z *is UUB. Note that selecting a larger* κ *will result in a smaller final bound of* $\|z\|$. *However, the convergence of* $\|z\|$ *does not imply the convergence of* e_d *unless* r *is bounded. To show the boundedness of* r, *we construct an augmented candidate Lyapunov function* W *as*

$$W=V+\frac{1}{2}e^\top e+\frac{1}{2}r^2, \qquad (2.35)$$

whose time derivative satisfies

$$
\begin{aligned}
\dot{W}&\overset{(2.30)}{\leq} -\kappa\|z\|^2+\omega-e^\top\Lambda e+e^\top rz-\theta r(r-1)+\frac{cr^2}{2}\sum_{j=1}^{n}e_j^2\|\Delta_j\|^2\\
&\overset{(2.24b)}{=} -\kappa\|z\|^2+\omega-k_1\|e\|^2-k_2r^2\|e\|^2-\theta r(r-1)+e^\top rz
\end{aligned}
$$

$$
\begin{aligned}
&\leq -\kappa\|z\|^2+\omega-k_1\|e\|^2-k_2r^2\|e\|^2+k_2r^2\|e\|^2+\frac{1}{4k_2}\|z\|^2-\frac{\theta}{2}r^2+\frac{\theta}{2}\\
&= -\left(\kappa-\frac{1}{4k_2}\right)\|z\|^2-k_1\|e\|^2-\frac{\theta}{2}r^2+\left(\frac{\theta}{2}+\omega\right)\\
&\leq -\chi W+\left(\frac{\theta}{2}+\omega\right), \qquad (2.36)
\end{aligned}
$$

where $\chi=\min\left\{2\kappa-\frac{1}{2k_2},2k_1,\theta\right\}$. *From* (2.36) *we have*

$$
r\leq\sqrt{2W(0)e^{-\chi t}+\frac{\theta+2\omega}{\chi}}=\varrho_r(t). \qquad (2.37)
$$

Recall that $e_d=rz$. *From* (2.34) *and* (2.37), *it is easy to conclude that* e_d *is globally UUB. This completes the proof.* □

Remark 2.1 *From* (2.34) *and* (2.37), *one can see that* $\lim_{t\to\infty}\|e_d(t)\|\leq\sqrt{\frac{\omega(\theta+2\omega)}{\kappa\chi}}$, *implying that the ultimate bound of* e_d *can be made arbitrarily small by appropriately choosing the tuning parameters* γ,θ,c,k_1,k_2 *in the IIDOB design. In practice, the selection of these parameters should reflect a trade-off between reducing the ultimate disturbance estimation error and achieving a desired transient performance.*

Remark 2.2 *From* (2.24c) *one can see that* β *is obtained via calculating an (indefinite) integral, whose explicit form is hard to obtain in general. In practice, a numerical integration can be adopted to compute* β. *Moreover, since* $\psi\in C^1$, $\frac{\partial\beta}{\partial\hat{x}}$ *can be computed using the Leibniz integral rule [84] as* $\left(\frac{\partial\beta}{\partial\hat{x}}\right)_{ij}=\int_0^{x_i}\frac{\partial}{\partial\hat{x}_j}\psi(\hat{x}_1,\cdots,\hat{x}_{i-1},\tau,\hat{x}_{i+1},\cdots,\hat{x}_n)\mathrm{d}\tau$, *where* $\left(\frac{\partial\beta}{\partial\hat{x}}\right)_{ij}$ *denotes the* ij*-th entry of* $\frac{\partial\beta}{\partial\hat{x}}$.

Before the end of this section, we show the design of an IIDOB-based tracking controller, which could be used as a nominal controller in the IIDOB-CBF-QP in Section 2.4. Note that $\dot{\hat{d}}$ can be expressed as

$$
\dot{\hat{d}}=\dot{\xi}+\frac{\partial\beta}{\partial x}\dot{x}+\frac{\partial\beta}{\partial\hat{x}}\dot{\hat{x}}+\frac{\partial\beta}{\partial u}v\overset{(2.24)}{=}-r\frac{\partial\beta}{\partial x}z. \qquad (2.38)
$$

The following proposition presents an IIDOB-based tracking control law provided the right

inverse of g exists.

Proposition 2.1 *Consider system* (2.11) *and suppose that all conditions of Theorem 2.1 hold such that the IIDOB shown in* (2.24) *exists. Suppose that* κ *defined in* (2.33a) *is greater than* 1*, and the right inverse of* g *exists for any* $x \in \mathbb{R}^n$*. Given a reference trajectory* $x_d(t)$ *where* $x_d(t)$ *and* $\dot{x}_d(t)$ *are bounded,* $\forall t \geq 0$*, if the control law is designed as*

$$u_d = -g^\dagger \left(f + \left(\alpha_1 + \frac{1}{2} r^2 \right) e_x + \hat{d} - \dot{x}_d \right), \tag{2.39a}$$

$$v = -\alpha_2 e_u + \mathcal{G}_1 - g^\top e_x - \frac{\|\mathcal{G}_2\|^2}{2} e_u, \tag{2.39b}$$

where $e_x = x - x_d$*,* $e_u = u - u_d$*,* $g^\dagger$ *is the right inverse of* g*,* $\mathcal{G}_1 = \frac{\partial u_d}{\partial t} + \frac{\partial u_d}{\partial x}(f + gu + \hat{d}) + \frac{\partial u_d}{\partial r}\dot{r}$*,* $\alpha_1, \alpha_2 > 0$ *are positive constants, and* $\mathcal{G}_2 = r\left(\frac{\partial u_d}{\partial \hat{d}} \frac{\partial \beta}{\partial x} + \frac{\partial u_d}{\partial x} \right)$*, then the tracking error* e_x *is globally UUB.*

Proof *Define*

$$V_1 = \frac{1}{2} e_x^\top e_x + \frac{1}{2} z^\top z \tag{2.40}$$

as a candidate Lyapunov function where z *is defined in* (2.15)*. Note that*

$$\begin{aligned} \dot{V}_1 &\overset{(2.32)}{\leq} e_x^\top (f + gu + pw - \dot{x}_d) - \kappa \|z\|^2 + \omega \\ &\overset{(2.39a)}{\leq} -\left(\alpha_1 + \frac{1}{2} r^2 \right) \|e_x\|^2 - r e_x^\top z + e_x^\top g e_u - \kappa \|z\|^2 + \omega \\ &\leq -\alpha_1 \|e_x\|^2 - \left(\kappa - \frac{1}{2} \right) \|z\|^2 + e_x^\top g e_u + \omega \end{aligned} \tag{2.41}$$

where ω *is defined in* (2.33b)*. Since* u_d *is a function of* $x, r, \hat{d}$ *and* t*, its derivative is*

$$\dot{u}_d = \frac{\partial u_d}{\partial t} + \frac{\partial u_d}{\partial x}(f + gu + \hat{d}) + \frac{\partial u_d}{\partial r}\dot{r} - r\left(\frac{\partial u_d}{\partial \hat{d}} \frac{\partial \beta}{\partial x} + \frac{\partial u_d}{\partial x} \right) z = \mathcal{G}_1 - \mathcal{G}_2 z. \tag{2.42}$$

Then, we define

$$V_2 = V_1 + \frac{1}{2} e_u^\top e_u \tag{2.43}$$

as an augmented Lyapunov function candidate, whose derivative satisfies

$$\begin{aligned}
\dot{V}_2 &\overset{(2.38)}{\leq} \dot{V}_1 + e_u^\top (v - \mathcal{G}_1 + \mathcal{G}_2 z) \\
&\leq -\alpha_1 \|e_x\|^2 - (\kappa - 1)\|z\|^2 + e_u^\top g^\top e_x + e_u^\top (v - \mathcal{G}_1) + \frac{\|e_u\|^2 \|\mathcal{G}_2\|^2}{2} + \omega \\
&\overset{(2.39b)}{\leq} -\alpha_1 \|e_x\|^2 - (\kappa - 1)\|z\|^2 - \alpha_2 \|e_u\|^2 + \omega,
\end{aligned} \tag{2.44}$$

which implies

$$\dot{V}_2 \leq -\vartheta V_2 + \omega \tag{2.45}$$

with $\vartheta = \min\{2\alpha_1, 2\kappa - 2, 2\alpha_2\}$. *Hence, one can see that* $\|e_x\| \leq \sqrt{2V_2(0)e^{-\vartheta t} + \frac{2\omega}{\vartheta}}$, *indicating* e_x *is globally UUB. This completes the proof.* □

When g has no full row rank, an IIDOB-based tracking controller similar to Proposition 2.1 can still be designed by following the backstepping technique [35], provided some control Lyapunov function conditions hold.

Remark 2.3 *The dynamic surface control [85] or command filter [86] technique can be adopted to bypass the tedious calculation of partial derivatives of* u_d. *For example, the idea of the dynamic surface control is to let* u_d *defined in* (2.39a) *pass a low-pass filter* $\epsilon \dot{u}_d^f = -u_d^f + u_d$, *where* u_d^f *is the filtered signal and* ϵ *is a small time constant. Then, one can replace* u_d *with* u_d^f *and use* $\dot{u}_d^f$ *directly in the design of* v, *instead of computing partial derivatives of* u_d.

2.4 Disturbance Observer-based Control Barrier Functions

In this section, we will present an IIDOB-CBF-QP-based safe control design method to solve Problem 2.2. We will design a safe controller v based on the augmented system shown in (2.11) that is used for the IIDOB design in the preceding section. Two issues need to be addressed in this design: (i) The time derivative of $\hat{d}$ is indispensable in control design and it depends on z, which is unknown since z relies on w, as shown in (2.38); however, considering the worst-case of $\dot{\hat{d}}$ may lead to unnecessary conservatism. (ii) The minimum DRD of system (2.11) is lower than its minimum IRD (i.e., d appears prior to v when one differentiates h), which makes the direct decoupling of the disturbance from the system difficult even if the disturbance is precisely estimated [87].

We address the first challenge by designing a filter to obtain an alternative disturbance estimation signal whose derivative is known. Specifically, given an IIDOB shown in (2.24), we design the following filter:

$$\dot{\hat{d}}_f = -\left(T_1 + T_2 r^2 \left\|\frac{\partial \beta}{\partial x}\right\|^2\right)(\hat{d}_f - \hat{d}), \tag{2.46}$$

where $\hat{d}_f$ denotes the filtered disturbance estimation with $\hat{d}_f(0) = \hat{d}(0)$, r is governed by (2.24f), β is given in (2.24c), and $T_1, T_2 > 0$ are tuning parameters. The filter shown in (2.46) is a modified low-pass filter by adding an additional term $-T_2 r^2 \left\|\frac{\partial \beta}{\partial x}\right\|^2 (\hat{d}_f - \hat{d})$ whose usefulness will be clear from the proof of Lemma 1. From (2.46) one can see that the derivative of $\hat{d}_f$ is completely known. Define the filtering error e_f as

$$e_f = \hat{d}_f - \hat{d}. \tag{2.47}$$

The following result shows that $\hat{d}_f$ is close to $\hat{d}$ in the sense that e_f is bounded by a known time-varying function whose ultimate bound can be arbitrarily small by choosing appropriate parameters.

Lemma 2.1 *Consider the augmented system* (2.11)*, the IIDOB as shown in* (2.24)*, and*

the filter given in (2.46). *If Assumption 2.1 holds and* $T_2 > \frac{1}{4\kappa}$, *where* κ *is defined in* (2.33a), *then the filtering error* e_f *satisfies*

$$\|e_f(t)\| \leq \sqrt{\left(\|z(0)\|^2 - \frac{2\omega}{\zeta}\right) e^{-\zeta t} + \frac{2\omega}{\zeta}} = \varrho_f(t) \tag{2.48}$$

for any $t \geq 0$, *where* $\zeta = \min\{2T_1, 2\kappa - \frac{1}{2T_2}\}$ *and* ω *is defined in* (2.33b).

Proof *Substituting* (2.38) *into* (2.46) *gives*

$$\dot{e}_f = -T_1 e_f - T_2 r^2 \left\|\frac{\partial \beta}{\partial x}\right\|^2 e_f + r\frac{\partial \beta}{\partial x} z. \tag{2.49}$$

Construct a candidate Lyapunov function V_f *as*

$$V_f = \frac{1}{2} e_f^\top e_f + \frac{1}{2} z^\top z, \tag{2.50}$$

whose derivative satisfies

$$\begin{aligned}
\dot{V}_f &\overset{(2.32)}{\leq} -T_1\|e_f\|^2 - T_2 r^2 \left\|\frac{\partial \beta}{\partial x}\right\|^2 \|e_f\|^2 + r e_f^\top \frac{\partial \beta}{\partial x} z - \kappa\|z\|^2 + \omega \\
&\leq -T_1\|e_f\|^2 - T_2 r^2 \left\|\frac{\partial \beta}{\partial x}\right\|^2 \|e_f\|^2 + r\left\|\frac{\partial \beta}{\partial x}\right\| \|e_f\|\|z\| - \kappa\|z\|^2 + \omega \\
&\leq -T_1\|e_f\|^2 - \left(\kappa - \frac{1}{4T_2}\right)\|z\|^2 + \omega \\
&\leq -\zeta V_f + \omega,
\end{aligned} \tag{2.51}$$

where the second inequality comes from Cauchy-Schwarz inequality. Note that $V_f(0) = \frac{1}{2}\|z(0)\|^2$ *because* $\hat{d}_f(0) = \hat{d}(0)$. *It is standard to obtain* (2.48) *from* (2.51). □

Next, we will present the safe controller design. Consider system (2.6) and the safe set $\mathcal{C}$ defined in (2.2). Suppose that $r_I = r_D = \iota \geq 1$ for system (2.6) with respect to h; clearly, because of (2.11b), $r_D < r_I$ for the augmented system (2.11). To address the

second issue above, we define a set of functions $h_0, h_1, \ldots, h_\iota$ as

$$h_0(x) = h, \tag{2.52a}$$

$$h_i(x) = \left(\frac{\mathrm{d}}{\mathrm{d}t} + \lambda_{i-1}\right) \circ h_{i-1},\ i \in [\iota - 1], \tag{2.52b}$$

$$h_\iota(x, u, r, \hat{d}_f) = \frac{\partial h_{\iota-1}}{\partial x}(f + gu + \hat{d}_f) - \frac{(1 + r^2)\left\|\frac{\partial h_{\iota-1}}{\partial x}\right\|^2}{2\tilde{\rho}(\zeta - \lambda_{\iota-1})} - \tilde{\rho}\omega + \lambda_{\iota-1}h_{\iota-1}, \tag{2.52c}$$

where $\tilde{\rho} > 0, \lambda_i > 0$ $(i = 0, 1, \cdots, \iota - 1)$ are tuning parameters, and $\omega > 0$ is the constant defined in (2.33b). Based on the IIDOB shown in (2.24), the filter given in (2.46), and the notations above, the following result provides a safe controller v that ensures the forward invariance of $\mathcal{C}$ for system (2.6).

Theorem 2.2 *Consider system* (2.6) *and the safe set* $\mathcal{C}$ *defined in* (2.2). *Suppose that all conditions of Theorem 2.1 hold such that the IIDOB shown in* (2.24) *exists. Suppose that* $r_I = r_D = \iota \geq 1$ *for system* (2.6) *with respect to* h, *and there exist positive constants* ρ, $\tilde{\rho}$, *and* $\lambda_i (i = 0, 1, \cdots, \iota)$ *such that* $\lambda_\iota < 2\kappa$, $\lambda_{\iota-1} < \zeta$, $h_i(x(0)) > 0$ *for* $i = 0, \cdots, \iota - 2$, $h_{\iota-1}(x(0)) - \tilde{\rho}V_f(e_f(0), z(0)) > 0$, *and* $h_\iota(x(0), u(0), r(0), \hat{d}_f(0)) - \frac{\rho}{2}\|z(0)\|^2 > 0$, *where* κ, ζ, *and* V_f *are defined in* (2.33a), (2.48), *and* (2.50), *respectively. If* $\sup_{v \in \mathbb{R}^m}[\psi_0 + \psi_1 v] \geq 0$ *holds for any* $u \in \mathbb{R}^m$, $r \in [1, \varrho_r]$, $\|\hat{d}\| \leq \|p\|\omega_0 + \varrho_d$, $\|\hat{d}_f\| \leq \|p\|\omega_0 + \varrho_d + \varrho_f$, $\|e_f\| \leq \varrho_f$, $x \in \mathcal{C}$, *and* $t \geq 0$, *where* $\varrho_d = \varrho_z\varrho_r$ *with* ϱ_z *and* ϱ_r *defined in* (2.34) *and* (2.37), *respectively,* ϱ_f *is defined in* (2.48), *and*

$$\psi_0 = \frac{\partial h_\iota}{\partial x}(f + gu + \hat{d}) + \frac{\partial h_\iota}{\partial r}\dot{r} + \frac{\partial h_\iota}{\partial \hat{d}_f}\dot{\hat{d}}_f - \frac{r^2\left\|\frac{\partial h_\iota}{\partial x}\right\|^2}{\rho(4\kappa - 2\lambda_\iota)} - \rho\omega + \lambda_\iota h_\iota, \tag{2.53a}$$

$$\psi_1 = \frac{\partial h_\iota}{\partial u}, \tag{2.53b}$$

with $\dot{r}$, $\dot{\hat{d}}_f$, *and* h_ι *defined in* (2.24f), (2.46), *and* (2.52c), *respectively, then any Lipschitz controller* $v \in K_{BF} = \{\mathfrak{v} \in \mathbb{R}^m : \psi_0 + \psi_1\mathfrak{v} \geq 0\}$ *will ensure* $h \geq 0$ *for all* $t \geq 0$.

Proof *Define* $H_1(x,u,r,\hat{d}_f,z)=h_\iota-\frac{\rho}{2}z^\top z$, *where* h_ι *is given in* (2.52c). *Since*

$$\begin{aligned}\dot{H}_1 &\overset{(2.32)}{\geq} \frac{\partial h_\iota}{\partial x}(f+gu+pw)+\frac{\partial h_\iota}{\partial u}v+\frac{\partial h_\iota}{\partial r}\dot{r}+\frac{\partial h_\iota}{\partial \hat{d}_f}\dot{\hat{d}}_f+\rho\kappa\|z\|^2-\rho\omega\\ &= \frac{\partial h_\iota}{\partial x}(f+gu+\hat{d})+\frac{\partial h_\iota}{\partial u}v+\frac{\partial h_\iota}{\partial r}\dot{r}+\frac{1}{2}\rho\lambda_\iota\|z\|^2-\rho\omega+\frac{\partial h_\iota}{\partial \hat{d}_f}\dot{\hat{d}}_f-r\frac{\partial h_\iota}{\partial x}z+\rho\left(\kappa-\frac{\lambda_\iota}{2}\right)\|z\|^2\\ &\geq \frac{\partial h_\iota}{\partial x}(f+gu+\hat{d})+\frac{\partial h_\iota}{\partial r}\dot{r}+\frac{\partial h_\iota}{\partial \hat{d}_f}\dot{\hat{d}}_f-\frac{r^2\left\|\frac{\partial h_\iota}{\partial x}\right\|^2}{\rho(4\kappa-2\lambda_\iota)}+\frac{1}{2}\rho\lambda_\iota\|z\|^2+\frac{\partial h_\iota}{\partial u}v-\rho\omega\\ &= \psi_0+\psi_1 v-\lambda_\iota H_1, \end{aligned}\tag{2.54}$$

any $v\in K_{BF}$ *will result in* $\dot{H}_1\geq-\lambda_\iota\bar{H}_1$. *Noting that* $h_\iota(x(0),u(0),r(0),\hat{d}_f(0))-\frac{\rho}{2}\|z(0)\|^2>0 \implies H_1(x(0),u(0),r(0),\hat{d}_f(0),z(0))>0$, *we can conclude that* $H_1\geq 0$, *which implies that* $h_\iota\geq 0$, *for any* $t\geq 0$.

Define another function as $H_2(x,z,e_f)=h_{\iota-1}-\tilde{\rho}V_f$ *where* V_f *is given in* (2.50). *Note that*

$$\begin{aligned}\dot{H}_2+\lambda_{\iota-1}H_2 &\overset{(2.51)}{\geq} \frac{\partial h_{\iota-1}}{\partial x}(f+gu+\hat{d}_f)-r\frac{\partial h_{\iota-1}}{\partial x}z-\frac{\partial h_{\iota-1}}{\partial x}e_f+\frac{(\zeta-\lambda_{\iota-1})\tilde{\rho}}{2}(\|z\|^2+\|e_f\|^2)\\ &\quad -\tilde{\rho}\omega+\lambda_{\iota-1}h_{\iota-1}\\ &\geq \frac{\partial h_{\iota-1}}{\partial x}(f+gu+\hat{d}_f)-\frac{(1+r^2)\left\|\frac{\partial h_{\iota-1}}{\partial x}\right\|^2}{2\tilde{\rho}(\zeta-\lambda_{\iota-1})}-\tilde{\rho}\omega+\lambda_{\iota-1}h_{\iota-1}\\ &= h_\iota\geq 0. \end{aligned}\tag{2.55}$$

Since $h_{\iota-1}(x(0))-\tilde{\rho}V_f(e_f(0),z(0))>0 \implies H_2(x(0),z(0),e_f(0))>0$, *we have* $H_2\geq 0$, *which implies that* $h_{\iota-1}\geq 0$ *for all* $t\geq 0$. *According to* (2.52b), *one can conclude that* $h_i\geq 0 \implies h_{i-1}\geq 0$ *for any* $i\in[\iota-1]$ *because* $h_i(x(0))>0$, $i=0,1,\cdots,\iota-2$ *[88]. Therefore, one can see* $h\geq 0$ *for all* $t\geq 0$. *This completes the proof.* □

The safe controller v proposed in Theorem 2.2 can be obtained by solving the following convex IIDOB-CBF-QP:

$$\begin{aligned}\min_{v}\quad & \|v-v_d\|^2\\ \text{s.t.}\quad & \psi_0+\psi_1 v\geq 0,\end{aligned}\tag{2.56}$$

where ψ_0, ψ_1 are given in (2.53) and v_d is any given nominal control law that is potentially unsafe (e.g., the IIDOB-based tracking controller given in Proposition 2.1).

2.5 Numerical Simulations

In this section, two simulation examples are presented to demonstrate the effectiveness of the proposed IIDOB and IIDOB-CBF-QP-based controller.

Example 2.1 *Consider the following system:*

$$\begin{bmatrix} \dot{x}_1 \\ \dot{x}_2 \end{bmatrix} = \underbrace{\begin{bmatrix} x_2 \\ x_1 x_2 \end{bmatrix}}_{f(x)} + \underbrace{\begin{bmatrix} 1 & 0 \\ 0 & 1+\sin^2(x_1) \end{bmatrix}}_{g(x)} \begin{bmatrix} u_1 \\ u_2 \end{bmatrix} + \underbrace{\begin{bmatrix} x_1 \\ x_2 \end{bmatrix}}_{p(x)} w(t), \tag{2.57}$$

where $x = [x_1\ x_2]^\top$ is the state, $u = [u_1\ u_2]^\top$ is the control input, and w is the disturbance. It is easy to verify that f, g, p are smooth functions. In the simulation, we choose the disturbance as $w = 5\sin(t)+2\cos(2t)+4\sin(3t)+3\cos(4t)$, which implies that Assumption 2.1 holds with $\omega_0 = 8, \omega_1 = 26$. We select the initial condition as $x_1(0) = x_2(0) = -0.5$, and the reference trajectory of x is $x_d(t) = [x_{1d}(t)\ x_{2d}(t)]^\top$, where $x_{1d}(t) = 2\sin(t)$ and $x_{2d}(t) = 2\cos(t)$.

We choose parameters $\gamma = 100$, $k_1 = k_2 = 10$, $\theta = 10$, $c = 0.5$, and $\alpha_1 = \alpha_2 = 50$ in Theorem 2.1 and Proposition 2.1. It is easy to verify that all conditions of Theorem 2.1 hold so that the IIDOB is designed as shown in (2.24)*. We design a tracking controller for* (2.57) *using the dynamic surface technique in [85] with the filter parameter $\epsilon = 0.001$ (see Remark 2.3). As shown in Figure 2.2, the disturbance estimation of the proposed IIDOB is accurate and the tracking performance is satisfactory.*

Next, we consider two safety sets $\mathcal{C}_1 = \{x \in \mathbb{R}^2 : x_1 + 1 \geq 0\}$ and $\mathcal{C}_2 = \{x \in \mathbb{R}^2 : 1 - x_2 \geq 0\}$, which aim to keep $x_1 \geq -1$ and $x_2 \leq 1$. Define $h_1 = x_1 + 1$ and $h_2 = 1 - x_2$. One can easily verify that the minimum IRD and the minimum DRD of system (2.57) *with respect to h_1, h_2 are both 1, i.e., $r_I = r_D = 1$. We choose parameters $\rho = \tilde{\rho} = 1$, $\lambda_0 = \lambda_1 = 50, T_1 = 50, T_2 = 1$ in Theorem 2.2, and let other parameters the same as above.*

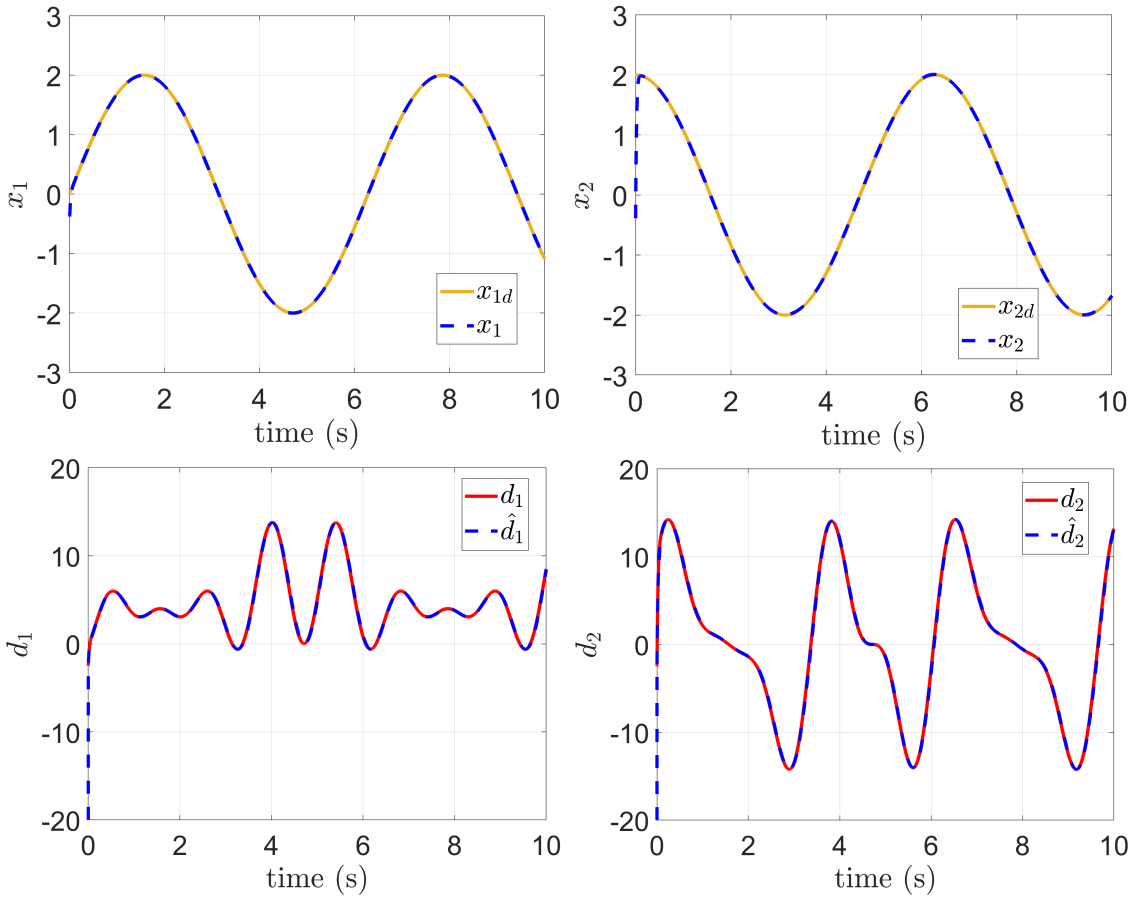

Figure 2.2: Simulation results of the proposed IIDOB and IIDOB-based tracking controller for system (2.57).

We also choose the nominal controller as the tracking controller designed above. One can verify that all conditions of Theorem 2.2 are satisfied, so that the IIDOB-CBF-QP-based controller (2.56) *can ensure* $h_1 \geq 0$ *and* $h_2 \geq 0$ *for all* $t \geq 0$*. Indeed, as shown in Figure 2.3, trajectories of* x_1 *(or* x_2*) always remain within the safety set* $\mathcal{C}_1$ *(or* $\mathcal{C}_2$*).*

We also compare the tracking performance of the proposed controller (2.56) *with the robust CBF approach proposed in [16]. As shown in Figure 2.3, although the robust CBF controller can always ensure safety, its tracking performance of the reference trajectories inside the safe region is not as good as our proposed controller* (2.56)*.*

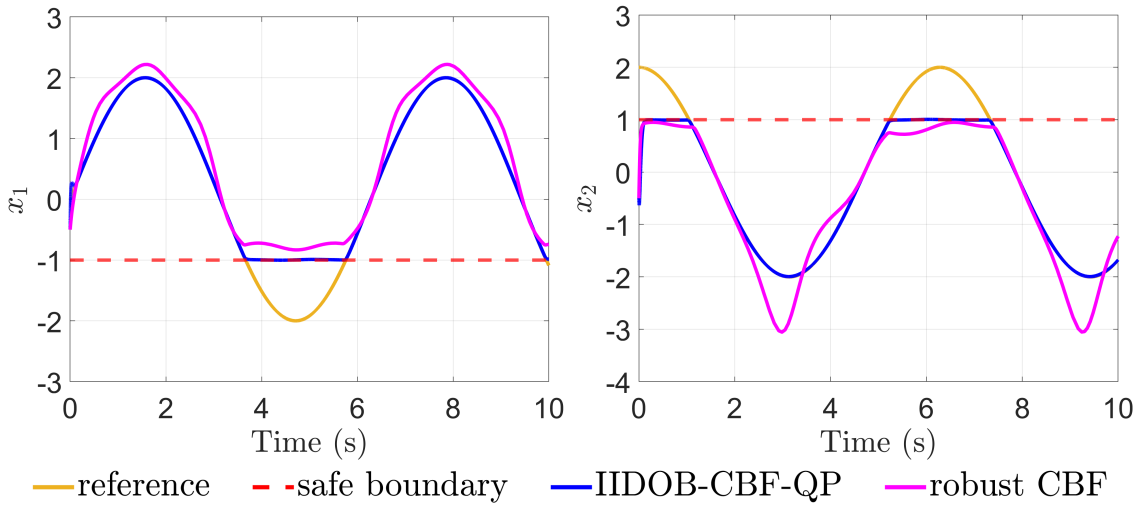

Figure 2.3: Simulation results of the IIDOB-CBF-QP-based controller (2.56) and the robust CBF-based controller proposed in [16].

Example 2.2 *Consider a two-linked planar robot manipulator:*

$$M(q)\ddot{q} + C(q,\dot{q})\dot{q} + G(q) = \tau + J^\top(q)F_d(t), \tag{2.58}$$

where $q = [q_1 \ q_2]^\top$ *is the joint angle,* $\dot{q} = [\dot{q}_1 \ \dot{q}_2]^\top$ *is the joint angular velocity,* $\tau \in \mathbb{R}^2$ *is the control input,* F_d *is the external disturbance satisfying Assumption 2.1, and* $M \in \mathbb{R}^{2\times 2}, C \in \mathbb{R}^{2\times 2}, G \in \mathbb{R}^2$, *and* $J \in \mathbb{R}^{2\times 2}$ *denote the inertia matrix, the Coriolis/centripetal matrix, the gravity term, and the Jacobian, respectively.*

It can be seen (2.58) *can be expressed in the form of* (2.6) *with* $x = [q_1 \ q_2 \ \dot{q}_1 \ \dot{q}_2]^\top$, $f = [\dot{q}^\top \ -(C+G)^\top M^{-\top}]^\top$, $g = [0_{2\times 2} \ M^{-\top}]^\top$, *and* $p = [0_{2\times 2} \ JM^{-\top}]^\top$. *It is obvious that* f, g, p *are smooth functions. The expression of* M, C, G *and physical parameters are chosen the same as those in [89]. Note that the Jacobian* J *is singular when* $q_2 = 0$ *such that it is impossible to uniquely recover* F_d *even if* $\ddot{q}$ *is available. The reference trajectory of* q *is* $q_d = [q_{1d}(t) \ q_{2d}(t)]^\top$, *where* $q_{1d}(t) = q_{2d}(t) = 2\sin(t)$; *the nominal controller is designed by following Proposition 2.1; the disturbance is selected as* $F_d = [d_1 \ d_2]^\top$ *with* $d_1 = d_2 = 5\sin(t) + 2\cos(2t) + 4\sin(3t) + 3\cos(4t)$ *such that Assumption 2.1 holds with* $\omega_0 = 11, \omega_1 = 37$; *four CBFs are selected as* $h_1 = q_1 + 1$, $h_2 = -q_1 + 1.5$, $h_3 = q_2 + 1.2$, *and* $h_4 = -q_2 + 1$, *which aim to ensure* $-1 \le q_1 \le 1.5$ *and* $-1.2 \le q_2 \le 1$. *It can be verified*

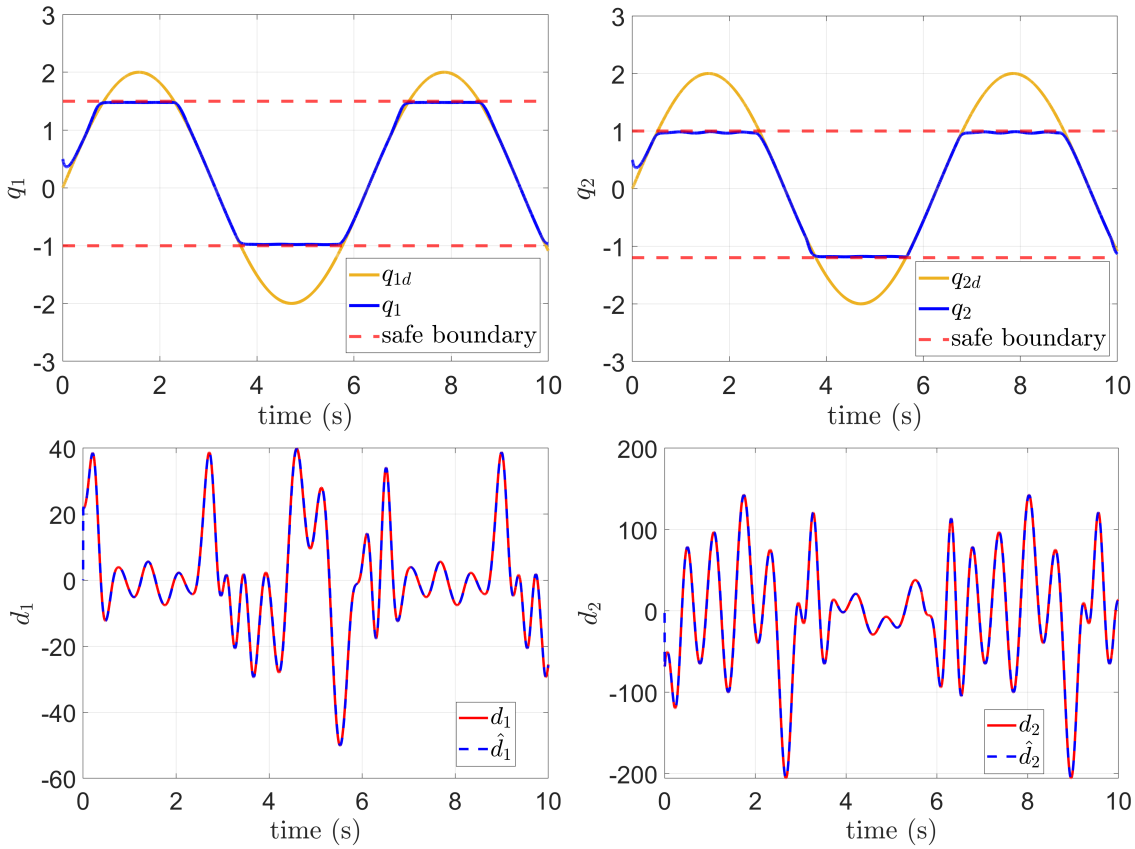

Figure 2.4: Simulation results of the proposed IIDOB-CBF-QP-based safe control for the two-linked planer robot (2.58).

that the minimum IRD and the minimum DRD of system (2.58) *with respect to* h_i, $i \in [4]$, *are 2, i.e.,* $r_I = r_D = 2$. *We select the control parameters as* $\gamma = 250, c = 5, \theta = 50, k_1 = k_2 = 20, \alpha_1 = \alpha_2 = 50, \rho = \tilde{\rho} = 1, \lambda_0 = 25, \lambda_1 = 30, \lambda_2 = 50, T_1 = 250, T_2 = 1$ *in Theorem 2.1 and 2.2.*

The simulation results are presented in Figure 2.4. One can observe that the disturbance is precisely estimated by the proposed IIDOB (2.24), *and the IIDOB-CBF-QP-based controller* (2.56) *can ensure the safety because the trajectories of* q_1, q_2 *remain within the safety sets.*

2.6 Chapter Summary and Future Directions

This chapter introduces a systematic approach for designing DOBs for general nonlinear control-affine systems without imposing restrictive assumptions employed by existing DOB design strategies. Based on that, a filter-based IIDOB-CBF-QP safe control design method is proposed. The numerical simulation results demonstrate the estimation accuracy achieved by the IIDOB and the superior performance of the proposed safe controller compared to the worst-case-based robust CBF methods.

The IIDOB design relies on the calculation of the integrands in (2.24c), which can be computationally expensive, especially for high-dimensional systems. This computational burden may limit the scalability and practical applicability of the proposed IIDOB. Therefore, it would be highly desirable to develop alternative DOB design approaches that avoid explicit computation of these integrands, thereby significantly reducing online computational complexity while preserving the disturbance estimation performance and theoretical guarantees. One possible way is to extend or adapt the constructive method proposed in [90].

Another limitation of the proposed IIDOB-CBF-QP framework is that, for system (2.6), the IRD is required to be equal to the DRD. While this assumption holds for certain classes of systems, many practical systems exhibit disturbances with a lower DRD. Consequently, the current IIDOB-CBF-QP formulation cannot be directly applied to such systems. An important direction for future research is extending the IIDOB-CBF-QP framework to accommodate systems with lower DRD, by developing new disturbance estimation and compensation mechanisms that remain compatible with the CBF-QP framework.

Chapter 3

Adaptive CBF-based Control for Systems With Structured Uncertainties

3.1 Introduction

In Chapter 2, an IIDOB-CBF-QP-based safe control approach is developed for systems with unstructured disturbances/uncertainties. Although this method can ensure safety and result in non-conservative control performance, the design of IIDOB and corresponding safe controller relies on the bounds of the uncertainty's derivatives, making it difficult to handle structured (parametric) uncertainties whose derivatives are generally unbounded. Inspired by the idea of adaptive control Lyapunov functions [45], various adaptive CBF (aCBF) approaches are developed in the literature [47], [48], [49], [50], [51], [52], [53], [54], [60], [91] to ensure safety under parametric uncertainties using the online estimation of the unknown parameters. However, most of these works only take into account parametric uncertainties in the drift terms, not the control-input matrix, while uncertainties in the control-input matrix is pretty common in practice, such as robotic systems that have error in their mass and inertia parameters [55].

Consider a control-affine system $\dot{x} = f(x)+g(x)u$ where f, g include parametric uncertainties (e.g., f and g are identified by universal approximators such as neural networks). The main challenge of stabilizing such a system using adaptive controllers arises from the so-called "loss of controllability" problem; that is, although the system is controllable, the identification model may lose its controllability at some points in time, owing to parameter adaptations [5], [36]. The same issue could happen in the aCBF-based control design, which will result in the emptiness of the admissible safe control set and therefore, the infeasibility of the QP. The singularity-free aCBF-based safe control is not sufficiently explored in the literature, though relevant stabilizing adaptive control schemes have been proposed in [5], [35], [36], [92]. To bridge this gap, in this chapter, we propose a new aCBF-based control design method. The main contributions of this chapter are summarized as follows.

- A singularity-free aCBF-based controller is developed for systems with parametric uncertainties in both f and g. The safety constraint (i.e., the CBF condition) of the proposed method only relies on the nominal values of the unknown parameters and thus, the non-emptiness of the admissible safe control set can be verified independent of the online parameter estimation process. The safe control is obtained by solving a nonlinear program (NLP), which has a closed-form solution.

- A data-driven approach is proposed to reduce the potential conservatism of the proposed controller by tightening the parameter bounds.

The effectiveness of the proposed control strategy is demonstrated by numerical simulations. Main results of this chapter are shown in Figure 3.1.

This chapter is adapted from previously published work in [93].

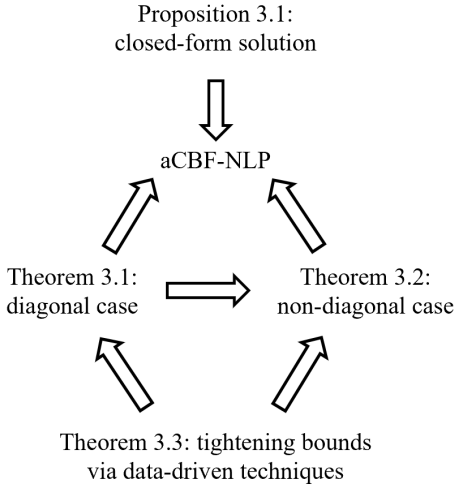

Figure 3.1: Main results of Chapter 3.

3.2 Problem Formulation

Consider the following control-affine system:

$$\begin{bmatrix} \dot{x}_1 \\ \dot{x}_2 \end{bmatrix} = f(x) + f_u(x) + \begin{bmatrix} \mathbf{0}_m \\ f_\theta(x) \end{bmatrix} + \begin{bmatrix} \mathbf{0}_{m\times n} \\ g(x) + g_\lambda(x) \end{bmatrix} u, \tag{3.1}$$

where $x = [x_1^\top \ x_2^\top]^\top$ is the state with $x_1 \in \mathbb{R}^m$ and $x_2 \in \mathbb{R}^n$, $u \in \mathbb{R}^n$ is the control input, $f : \mathbb{R}^{m+n} \to \mathbb{R}^{m+n}$ and $g : \mathbb{R}^{m+n} \to \mathbb{R}^{n\times n}$ are known Lipschitz functions, $f_u : \mathbb{R}^{m+n} \to \mathbb{R}^{m+n}$ is an unknown Lipschitz function, and $f_\theta : \mathbb{R}^{m+n} \to \mathbb{R}^n$ and $g_\lambda : \mathbb{R}^{m+n} \to \mathbb{R}^{n\times n}$ are parametric uncertainties. We assume that f_θ, g, and g_λ have the following forms:

$$f_\theta(x) = \begin{bmatrix} \theta_1^\top \varphi_1(x), & \theta_2^\top \varphi_2(x), & \cdots, & \theta_n^\top \varphi_n(x) \end{bmatrix}^\top, \tag{3.2a}$$

$$g(x) = \operatorname{diag}(g_1(x), g_2(x), \cdots, g_n(x)), \tag{3.2b}$$

$$g_\lambda(x) = \operatorname{diag}(\lambda_1^\top \psi_1(x), \lambda_2^\top \psi_2(x), \cdots, \lambda_n^\top \psi_n(x)), \tag{3.2c}$$

where $g_i : \mathbb{R}^{m+n} \to \mathbb{R}$ is a known function, $\theta_i \in \mathbb{R}^{p_i}$ and $\lambda_i \in \mathbb{R}^{q_i}$ are unknown parameters, and $\varphi_i : \mathbb{R}^{m+n} \to \mathbb{R}^{p_i}$ and $\psi_i : \mathbb{R}^{m+n} \to \mathbb{R}^{q_i}$ are known functions (regressors) with p_i, q_i

appropriate positive integers and $i \in [n]$. Define a safe set $\mathcal{C} \subset \mathbb{R}^{m+n}$ as

$$\mathcal{C} = \{x : h(x) \geq 0\}, \tag{3.3}$$

where $h : \mathbb{R}^{m+n} \to \mathbb{R}$ is a continuously differentiable function. We also make the following two assumptions on the boundedness of the unknown function f_u and the unknown parameters θ_i, λ_i.

Assumption 3.1 There exist known functions $\underline{f}_u(x)$, $\overline{f}_u(x) : \mathbb{R}^{m+n} \to \mathbb{R}^{m+n}$ *such that* $\underline{f}_u(x) \leq f_u(x) \leq \overline{f}_u(x)$.

Assumption 3.2 For every $i \in [n]$, *there exist known vectors* $\overline{\theta}_i, \underline{\theta}_i \in \mathbb{R}^{p_i}$ *and* $\overline{\lambda}_i, \underline{\lambda}_i \in \mathbb{R}^{q_i}$ *such that* $\underline{\theta}_i \leq \theta_i \leq \overline{\theta}_i$ *and* $\underline{\lambda}_i \leq \lambda_i \leq \overline{\lambda}_i$.

Remark 3.1 *In the adaptive stabilizing control design problem, bounds for the unknown parameters as given in Assumption 3.2 are not necessarily required to be known since the asymptotic stability of the closed-loop system can be proven using Barbalat's lemma when the derivative of the Lyapunov function is negative semi-definite [81]. Because CBFs do not have the favourable positive definiteness property as Lyapunov functions, the CBF-based safe control design is more challenging. Although an aCBF-based control approach is proposed in [46] without assuming boundedness of the unknown parameters, its performance is conservative as the system only operates in a subset of the original safety set. In [47], a robust aCBF-based controller is developed under the assumption that is similar to Assumption 3.2, i.e., the unknown parameters and the parameter estimation error both belong to known closed convex sets; however, the system model considered there does not include the parametric uncertainty* g_λ *in the control-input matrix.*

The main problem that will be investigated in this paper is stated as follows.

Problem 3.1 *Consider the system* (3.1) *with* f_θ, g, *and* g_λ *given in* (3.2) *and the safe set defined in* (3.3) *where* h *has a relative degree 1. Suppose that Assumptions 3.1 and 3.2 hold. Design a feedback controller* u *such that the closed-loop system is always safe, i.e.,* $h(x(t)) \geq 0$ *for all* $t \geq 0$.

We will propose an aCBF-NLP-based method for solving Problem 3.1 in Section 3.3. Moreover, although we only consider the CBF h with a relative degree 1 in this work, our results can be easily extended to the higher relative degree cases by using techniques in [88], [94], [95].

3.3 Adaptive Control Barrier Function-based Safe Control

3.3.1 aCBF-NLP-based Control Design

In this subsection, an aCBF-NLP-based control design method is proposed to solve Problem 3.1. Recall that f_θ, g, g_λ have the forms given in (3.2) where $\theta_i \in \mathbb{R}^{p_i}$ and $\lambda_i \in \mathbb{R}^{q_i}$ are unknown parameters. We choose arbitrary values $\theta_i^0 \in \mathbb{R}^{p_i}$ and $\lambda_i^0 \in \mathbb{R}^{q_i}$ satisfying $\underline{\theta}_i \leq \theta_i^0 \leq \overline{\theta}_i$ and $\underline{\lambda}_i \leq \lambda_i^0 \leq \overline{\lambda}_i$ as the nominal values for θ_i and λ_i, respectively. Furthermore, we define

$$\mu_i \triangleq \|\theta_i - \theta_i^0\|, \quad \nu_i \triangleq \|\lambda_i - \lambda_i^0\|, \quad \forall i \in [n]. \tag{3.4}$$

According to Assumption 3.2 and the definition of 2-norm, it can be seen

$$\mu_i \leq \bar{\mu}_i \triangleq \sqrt{\sum_{j=1}^{p_i} \max\{((\overline{\theta}_i)_j - (\theta_i^0)_j)^2, ((\underline{\theta}_i)_j - (\theta_i^0)_j)^2\}}, \tag{3.5a}$$

$$\nu_i \leq \bar{\nu}_i \triangleq \sqrt{\sum_{j=1}^{q_i} \max\{((\overline{\lambda}_i)_j - (\lambda_i^0)_j)^2, ((\underline{\lambda}_i)_j - (\lambda_i^0)_j)^2\}}, \tag{3.5b}$$

where $(\overline{\theta}_i)_j$, $(\underline{\theta}_i)_j$, $(\overline{\lambda}_i)_j$, $(\underline{\lambda}_i)_j$ denote the j-th entry of $\overline{\theta}_i$, $\underline{\theta}_i$, $\overline{\lambda}_i$, $\underline{\lambda}_i$, respectively. Note that in this subsection the adaptive laws are used to estimate parameters μ_i and ν_i, which are scalars, rather than parameters θ_i and λ_i, which are vectors.

In the adaptive stabilizing control design problem considered in [92], assumptions are imposed to ensure that the system is uniformly strongly controllable, such that the loss of controllability problem can be avoided. Analogous to [92, Assumption 1], the following assumption assumes that each diagonal entry of $g(x) + g_\lambda(x)$ is away from zero.

Assumption 3.3 For any $i \in [n]$ and any $x \in \mathcal{C}$, there exists a positive constant $b_i > 0$ such that $g_i(x) + \lambda_i^\top \psi_i(x)$, i.e., the i-th diagonal entry of $g(x) + g_\lambda(x)$, satisfies $|g_i(x) + \lambda_i^\top \psi_i(x)| \geq b_i$ and its sign is known. Without loss of generality, we assume that $g_i(x) + \lambda_i^\top \psi_i(x) > 0$ for any $i \in [n]$.

The following theorem shows an aCBF-based controller that ensures the safety of system (2.11b).

Theorem 3.1 *Consider the system* (3.1) *with f_θ, g, g_λ specified in* (3.2) *and the safe set $\mathcal{C}$ defined in* (3.3)*. Suppose that*

(i) Assumptions 3.1, 3.2 and 3.3 hold;

(ii) There exist positive constants $\gamma, \epsilon_1, \epsilon_2, \gamma_i^\theta, \gamma_i^\lambda > 0$ where $i \in [n]$, such that the following set is non-empty:

$$K_{BF}(x) \triangleq \{\mathfrak{u} \in \mathbb{R}^n \mid \Psi_0(x) + \Psi_1(x)\mathfrak{u} \geq 0\}, \ \forall x \in \mathcal{C}, \tag{3.6}$$

where

$$\Psi_0(x) = \mathcal{M} + \sum_{i=1}^{n} h_{x_2,i}\theta_i^{0\top}\varphi_i - n(\epsilon_1 + \epsilon_2) + \gamma\left[h - \sum_{i=1}^{n}\left(\frac{\bar{\mu}_i^2}{2\gamma_i^\theta} + \frac{\bar{\nu}_i^2}{2\gamma_i^\lambda}\right)\right], \tag{3.7a}$$

$$\Psi_1(x) = [h_{x_2,1}^2(g_1 + \lambda_1^{0\top}\psi_1), h_{x_2,2}^2(g_2 + \lambda_2^{0\top}\psi_2), \cdots, h_{x_2,n}^2(g_n + \lambda_n^{0\top}\psi_n)], \tag{3.7b}$$

$\mathcal{M} = h_x f + \sum_{j=1}^{m+n} \min\{h_{x,j}\underline{f}_{u,j}, h_{x,j}\overline{f}_{u,j}\}$, $h_x = \frac{\partial h}{\partial x}$, $h_{x_2} = \frac{\partial h}{\partial x_2}$, *and* $h_{x,i}$, $h_{x_2,i}$, $\underline{f}_{u,i}$, $\overline{f}_{u,i}$ *denotes the i-th entry of* h_x, h_{x_2}, $\underline{f}_u$, $\overline{f}_u$, $i \in [n]$, *respectively;*

(iii) For any $i \in [n]$, $\hat{\mu}_i$ and $\hat{\nu}_i$ are estimated parameters governed by the following adaptive laws:

$$\dot{\hat{\mu}}_i = -\gamma\hat{\mu}_i + \gamma_i^\theta |h_{x_2,i}| \|\varphi_i\|, \tag{3.8a}$$

$$\dot{\hat{\nu}}_i = -\gamma\hat{\nu}_i + \gamma_i^\lambda h_{x_2,i}^2 |u_{0,i}| \|\psi_i\|, \tag{3.8b}$$

where $\hat{\mu}_i(0) > 0, \hat{\nu}_i(0) > 0$ and $u_0 = [u_{0,1}, \cdots, u_{0,n}]^\top$ is a Lipschitz function satisfying $u_0 \in K_{BF}(x)$;

(iv) The following inequality holds:

$$h(x(0)) \geq \sum_{i=1}^{n} \left(\frac{\hat{\mu}_i(0)^2 + \bar{\mu}_i^2}{2\gamma_i^\theta} + \frac{\hat{\nu}_i(0)^2 + \bar{\nu}_i^2}{2\gamma_i^\lambda} \right). \tag{3.9}$$

Then, the control input $u = h_{x_2}^\top \odot s(u_0) \in \mathbb{R}^n$*, where* $\odot$ *represents the Hadamard product (element-wise product) [96], will make* $h(x(t)) \geq 0$ *for any* $t > 0$*, where* $s(u_0) \triangleq [s_1(u_{0,1}), s_2(u_{0,2}), \cdots, s_n(u_{0,n})]^\top$ *and*

$$s_i(u_{0,i}) \triangleq u_{0,i} + \frac{\kappa_{1,i}}{b_i} + \frac{\kappa_{2,i}^2 u_{0,i}^2}{b_i(\kappa_{2,i}|h_{x_2,i}||u_{0,i}| + \epsilon_2)}, \tag{3.10}$$

with $\kappa_{1,i} = \frac{\hat{\mu}_i^2 \|\varphi_i\|^2}{\hat{\mu}_i \|\varphi_i\| |h_{x_2,i}| + \epsilon_1}$*,* $\kappa_{2,i} = \hat{\nu}_i \|\psi_i\| |h_{x_2,i}|$*,* $i \in [n]$*.*

Proof *From* (3.8)*,* $\dot{\hat{\mu}}_i \geq -\gamma \hat{\mu}_i, \dot{\hat{\nu}}_i \geq -\gamma \hat{\nu}_i$ *hold. Since* $\hat{\mu}_i(0) > 0, \hat{\nu}_i(0) > 0$*, it is easy to see that* $\hat{\mu}_i(t) \geq 0$ *and* $\hat{\nu}_i(t) \geq 0$ *for any* $t > 0$ *by the Comparison Lemma [81, Lemma 2.5]. Define a new candidate CBF* $\bar{h}$ *as*

$$\bar{h}(x,t) = h(x) - \sum_{i=1}^{n} \left(\frac{\tilde{\mu}_i^2}{2\gamma_i^\theta} + \frac{\tilde{\nu}_i^2}{2\gamma_i^\lambda} \right), \tag{3.11}$$

where $\tilde{\mu}_i = \mu_i - \hat{\mu}_i$ *and* $\tilde{\nu}_i = \nu_i - \hat{\nu}_i$*. It can be seen that*

$$\begin{aligned} \bar{h}(x(0),0) &= h(x(0)) - \sum_{i=1}^{n} \left(\frac{(\mu_i - \hat{\mu}_i(0))^2}{2\gamma_i^\theta} + \frac{(\nu_i - \hat{\nu}_i(0))^2}{2\gamma_i^\lambda} \right) \\ &\geq h(x(0)) - \sum_{i=1}^{n} \left(\frac{\mu_i^2 + \hat{\mu}_i^2(0)}{2\gamma_i^\theta} + \frac{\nu_i^2 + \hat{\nu}_i^2(0)}{2\gamma_i^\lambda} \right) \\ &\geq h(x(0)) - \sum_{i=1}^{n} \left(\frac{\bar{\mu}_i^2 + \hat{\mu}_i^2(0)}{2\gamma_i^\theta} + \frac{\bar{\nu}_i^2 + \hat{\nu}_i^2(0)}{2\gamma_i^\lambda} \right) \geq 0, \end{aligned} \tag{3.12}$$

where the first inequality comes from the fact that $\mu_i, \nu_i, \hat{\mu}_i(0), \hat{\nu}_i(0) \geq 0$*, the second one arises from the definitions of* $\bar{\mu}_i, \bar{\nu}_i$*, and the last one holds because of condition (iv).*

We claim that $\dot{\bar{h}} \geq -\gamma \bar{h}$ *where* $\dot{\bar{h}}$ *is the time derivative of* $\bar{h}$*. Indeed, one can see*

$$\dot{\bar{h}} = h_x(f + f_u) + \sum_{i=1}^{n} \left(h_{x_2,i}(\theta_i^\top \varphi_i + (g_i + \lambda_i^\top \psi_i)u_i) + \frac{\tilde{\mu}_i \dot{\hat{\mu}}_i}{\gamma_i^\theta} + \frac{\tilde{\nu}_i \dot{\hat{\nu}}_i}{\gamma_i^\lambda} \right)$$

$$\geq \mathcal{M} + \sum_{i=1}^{n} \left(h_{x_2,i}(\theta_i^\top \varphi_i + (g_i + \lambda_i^\top \psi_i)u_i) + \frac{\tilde{\mu}_i \dot{\hat{\mu}}_i}{\gamma_i^\theta} + \frac{\tilde{\nu}_i \dot{\hat{\nu}}_i}{\gamma_i^\lambda} \right). \tag{3.13}$$

Substituting (3.10) *into the inequality above and recalling Assumption 3.3, we have*

$$\begin{aligned}
\dot{\bar{h}} &\geq \mathcal{M} + \sum_{i=1}^{n} \left(h_{x_2,i}\theta_i^\top \varphi_i + \frac{\tilde{\mu}_i \dot{\hat{\mu}}_i}{\gamma_i^\theta} + \frac{\tilde{\nu}_i \dot{\hat{\nu}}_i}{\gamma_i^\lambda} \right) + \sum_{i=1}^{n} h_{x_2,i}^2 \left((g_i + \lambda_i^\top \psi_i)u_{0,i} + \kappa_{1,i} + \frac{\kappa_{2,i}^2 u_{0,i}^2}{\kappa_{2,i}|h_{x_2,i}||u_{0,i}| + \epsilon_2} \right) \\
&\geq \sum_{i=1}^{n} (h_{x_2,i}\theta_i^{0\top} \varphi_i + h_{x_2,i}^2 (g_i + \lambda_i^{0\top} \psi_i)u_{0,i}) + \sum_{i=1}^{n} (h_{x_2,i}(\theta_i - \theta_i^0)^\top \varphi_i + h_{x_2,i}^2 (\lambda_i - \lambda_i^0)^\top \psi_i u_{0,i}) \\
&\quad + \mathcal{M} + \sum_{i=1}^{n} \left(\frac{\tilde{\mu}_i \dot{\hat{\mu}}_i}{\gamma_i^\theta} + \frac{\tilde{\nu}_i \dot{\hat{\nu}}_i}{\gamma_i^\lambda} + h_{x_2,i}^2 \left(\kappa_{1,i} + \frac{\kappa_{2,i}^2 u_{0,i}^2}{\kappa_{2,i}|h_{x_2,i}||u_{0,i}| + \epsilon_2} \right) \right) \\
&\geq \Psi_0 + \Psi_1 u_0 + n(\epsilon_1 + \epsilon_2) - \gamma \left[h - \sum_{i=1}^{n} \left(\frac{\bar{\mu}_i^2}{2\gamma_i^\theta} + \frac{\bar{\nu}_i^2}{2\gamma_i^\lambda} \right) \right] + \sum_{i=1}^{n} \left(\frac{\tilde{\mu}_i \dot{\hat{\mu}}_i}{\gamma_i^\theta} + \frac{\tilde{\nu}_i \dot{\hat{\nu}}_i}{\gamma_i^\lambda} \right) \\
&\quad + \sum_{i=1}^{n} \left(-\mu_i \|\varphi_i\| |h_{x_2,i}| + \kappa_{1,i} h_{x_2,i}^2 - \nu_i \|\psi_i\| |u_{0,i}| h_{x_2,i}^2 + \frac{\kappa_{2,i}^2 u_{0,i}^2 h_{x_2,i}^2}{\kappa_{2,i}|h_{x_2,i}||u_{0,i}| + \epsilon_2} \right),
\end{aligned} \tag{3.14}$$

where the third inequality arises from Cauchy–Schwarz inequality. It is easy to check that $-\hat{\mu}_i \|\varphi_i\| |h_{x_2,i}| + \kappa_{1,i} h_{x_2,i}^2 = -\frac{\hat{\mu}_i \|\varphi_i\| |h_{x_2,i}| \epsilon_1}{\hat{\mu}_i \|\varphi_i\| |h_{x_2,i}| + \epsilon_1} \geq -\epsilon_1$ *and* $-\hat{\nu}_i \|\psi_i\| |u_{0,i}| h_{x_2,i}^2 + \frac{\kappa_{2,i}^2 u_{0,i}^2 h_{x_2,i}^2}{\kappa_{2,i}|h_{x_2,i}||u_{0,i}| + \epsilon_2} = -\frac{\kappa_{2,i}|h_{x_2,i}||u_{0,i}|\epsilon_2}{\kappa_{2,i}|h_{x_2,i}||u_{0,i}| + \epsilon_2} \geq -\epsilon_2$*; furthermore,* $\Psi_0 + \Psi_1 u_0 \geq 0$ *because* $u_0 \in K_{BF}$*. Based on these two facts and recalling that* $\mu_i = \tilde{\mu}_i + \hat{\mu}$, $\nu_i = \tilde{\nu}_i + \hat{\nu}_i$, *one can see that* (3.14) *can be expressed as*

$$\dot{\bar{h}} \geq \sum_{i=1}^{n} \left(\tilde{\mu}_i \left(\frac{1}{\gamma_i^\theta} \dot{\hat{\mu}}_i - \|\varphi_i\| |h_{x_2,i}| \right) + \tilde{\nu}_i \left(\frac{1}{\gamma_i^\lambda} \dot{\hat{\nu}}_i - \|\psi_i\| |u_{0,i}| h_{x_2,i}^2 \right) \right) - \gamma \left[h - \sum_{i=1}^{n} \left(\frac{\bar{\mu}_i^2}{2\gamma_i^\theta} + \frac{\bar{\nu}_i^2}{2\gamma_i^\lambda} \right) \right]. \tag{3.15}$$

Substituting (3.8) *into the inequality above yields*

$$\dot{\bar{h}} \geq -\gamma \sum_{i=1}^{n} \left(\frac{\tilde{\mu}_i \hat{\mu}_i}{\gamma_i^\theta} + \frac{\tilde{\nu}_i \hat{\nu}_i}{\gamma_i^\lambda} \right) - \gamma \left[h - \sum_{i=1}^{n} \left(\frac{\bar{\mu}_i^2}{2\gamma_i^\theta} + \frac{\bar{\nu}_i^2}{2\gamma_i^\lambda} \right) \right]. \tag{3.16}$$

Since $\hat{\mu}_i \tilde{\mu}_i = (\mu_i - \tilde{\mu}_i)\tilde{\mu}_i \leq \frac{\mu_i^2 - \tilde{\mu}_i^2}{2} \leq \frac{\bar{\mu}_i^2 - \tilde{\mu}_i^2}{2}$ *and* $\hat{\nu}_i \tilde{\nu}_i = (\nu_i - \tilde{\nu}_i)\tilde{\nu}_i \leq \frac{\nu_i^2 - \tilde{\nu}_i^2}{2} \leq \frac{\bar{\nu}_i^2 - \tilde{\nu}_i^2}{2}$*, we have* $\dot{\bar{h}} \geq -\gamma \left[h - \sum_{i=1}^{n} \left(\frac{\tilde{\mu}_i^2}{2\gamma_i^\theta} + \frac{\tilde{\nu}_i^2}{2\gamma_i^\lambda} \right) \right] = -\gamma \bar{h}$*, which shows the correctness of the claim.*

Because $\bar{h}(x(0), 0) \geq 0$*, it is easy to see that* $\bar{h}(t) \geq 0$ *for* $t > 0$*. Since* $\bar{h} \leq h$ *by definition, we have* $h(t) \geq 0$ *for* $t > 0$*, which completes the proof.* □

Remark 3.2 *It should be noticed that the CBF condition* $\Psi_0(x) + \Psi_1(x)\mathfrak{u} \geq 0$ *shown in* (3.6) *is imposed on the intermediate variable,* u_0*, instead of the real control input,* u*. Furthermore, the CBF condition* (3.6) *only relies on the nominal values of the unknown parameters, which implies that the CBF condition (i.e., the non-emptiness of the set* K_{BF}*) can be verified conveniently by selecting the variables in Condition (ii) appropriately.*

In [45], the problem of adaptive stabilization of a nonlinear system is converted to the nonadaptive stabilization of a modified system by utilizing an aCLF. While the idea of [45] may be extended to develop an aCBF-based safe control law for (2.11b)*, the resulting CBF condition would need to be verified for any* θ_i *and* λ_i *satisfying* $\underline{\theta}_i \leq \theta_i \leq \overline{\theta}_i$ *and* $\underline{\lambda}_i \leq \lambda \leq \overline{\lambda}_i$*, which is much more restrictive than the CBF condition given in Theorem 3.1 above. On the other hand, the CBF condition given in [54] relies on estimated parameters (i.e.,* Ψ_0 *and* Ψ_1 *are functions of the estimated parameters in the adaptive laws), which renders the singular configuration (i.e., the set* K_{BF} *is empty) difficult to verify; see the discussion in Remark 1 of [54].*

Remark 3.3 *The number of ODEs for parameter estimation in Theorem 3.1 is much less than that in other aCBF-based approaches such as [46], [47], [54]. As can be seen from the adaptive laws shown in* (3.8)*, our method only requires solving* $2n$ *ODEs that estimate* scalars $\mu_i \in \mathbb{R}$ *and* $\nu_i \in \mathbb{R}$ *for* $i \in [n]$ *(cf.* (3.4)*); in contrast, other aCBF methods have to estimate the original unknown parameters* $\theta_i \in \mathbb{R}^{p_i}$ *and* $\lambda_i \in \mathbb{R}^{q_i}$ *for* $i \in [n]$*, which results in a total of* $2n\sum_{j=1}^{n}(p_j + q_j)$ *ODEs. This reduction of number of ODEs is particularly useful when* p_i *and* q_i *are large, e.g., when* θ_i *and* λ_i *are weights of deep neural networks.*

The safe control law $u(x) \triangleq [u_1, \ldots, u_n]^\top$ in Theorem 3.1 can be obtained pointwise for any $x \in \mathcal{C}$. Specifically, each $u_i, i \in [n]$, can be obtained by solving the following optimization problem:

$$\begin{aligned} \min_{u_i \in \mathbb{R}} \quad & (u_i - u_{d,i})^2 \qquad \text{(aCBF-NLP)} \\ \text{s.t.} \quad & \Phi_0^i(x) + \Phi_1^i(x) u_{0,i} \geq 0, \\ & u_i = h_{x_2,i} s_i(u_{0,i}), \end{aligned}$$

where $s_i(\cdot)$ is the function defined in (3.10), $u_{d,i}$ is the i-th entry of the nominal controller,

$$\Phi_0^i = \begin{cases} \frac{\rho_i h_{x_2,i}^2 |g_i + \lambda_i^{0\top}\psi_i|}{\sum_{j=1}^n \rho_j h_{x_2,j}^2 |g_j + \lambda_j^{0\top}\psi_j|}\Psi_0, & \text{if } \Psi_1 \neq 0, \\ \Psi_0/n, & \text{otherwise,} \end{cases} \tag{3.17a}$$

$$\Phi_1^i = h_{x_2,i}^2(g_i + \lambda_i^{0\top}\psi_i), \tag{3.17b}$$

with Ψ_0, Ψ_1 defined in Theorem 3.1, and $\rho_i > 0, i \in [n]$, are tuning parameters. Note that (3.17a) is well-defined as $\sum_{j=1}^n \rho_j h_{x,j}^2 |g_j + \lambda_j^{0\top}\psi_j| \neq 0$ if $\Psi_1 \neq 0$ and $\sum_{i=1}^n \Phi_0^i = \Psi_0$, $\sum_{i=1}^n \Phi_1^i u_{0,i} = \Psi_1 u_0$.

Different from the traditional CBF-QP formulation [6], [76], the optimization (aCBF-NLP) is an NLP because of the nonlinear function $s_i(\cdot)$. Solving an NLP is computationally challenging in general; however, optimization (aCBF-NLP) has a *closed-form* solution, which will be discussed in the next subsection.

Remark 3.4 *An alternative optimization to obtain the safe control law $u(x)$ can be formulated as:*

$$\begin{aligned} \min_{u\in\mathbb{R}^n} \quad & \|u - u_d\|^2 \\ s.t. \quad & \Psi_0 + \Psi_1 u_0 \geq 0, \\ & u = h_{x_2}^\top \odot s(u_0), \end{aligned} \tag{3.18}$$

where $\Psi_0, \Psi_1, s(\cdot)$ are defined in Theorem 3.1 and u_d is the nominal controller. The admissible set of u_0 in (3.18) *is larger than that of* (aCBF-NLP)*, but the existence of a closed-form solution to* (3.18) *is still unclear to us.*

Remark 3.5 *The main idea behind the formulation of* (aCBF-NLP) *is to split the set K_{BF} into n independent set $K_{BF}^i \triangleq \{\mathfrak{u} \in \mathbb{R} : \Phi_0^i + \Phi_1^i \mathfrak{u} \geq 0\}$, such that $u_i \in K_{BF}^i, \forall i \in [n] \implies u \in K_{BF}$. It is easy to see that if $K_{BF} \neq \emptyset$, then $K_{BF}^i \neq \emptyset$ for any $i \in [n]$ and any $x \in \mathcal{C}$: if $\Psi_1 \neq 0$, then $\Phi_1^i = 0 \implies \Phi_0^i = 0 \implies \Phi_0^i(x) + \Phi_1^i(x)u_{0,i} \geq 0$ always holds; if $\Psi_1 = 0$ and $K_{BF} \neq \emptyset \implies \Phi_1^i(x) = 0$ and $\Psi_0 \geq 0 \implies \Phi_0^i = \frac{\Psi_0}{n} \geq 0 \implies$*

$\Phi_0^i(x) + \Phi_1^i(x)u_{0,i} \geq 0$ *always holds.*

3.3.2 Closed-form Solution to The NLP

In this subsection, we will discuss the closed-form solution to (aCBF-NLP). We will focus on the case $n = 1$ because the $n > 1$ case can be easily solved by considering the n NLPs in (aCBF-NLP) independently.

When $n = 1$, the subscript i for all relevant variables defined in Theorem 3.1 will be discarded for the sake of simplicity. It is also easy to see that $\Phi_0 = \Psi_1$, $\Phi_1 = \Psi_1$, and $h_{x_2} = 0 \implies u = 0$ according to Theorem 3.1. Thus, without loss of generality, we assume that $h_{x_2} \neq 0$ in the analysis of this subsection. By substituting $u = h_{x_2}s(u_0)$ into the objective function of (aCBF-NLP), it is easy to see that (aCBF-NLP) is equivalent to the following optimization when $n = 1$:

$$\begin{aligned} \min_{u_0 \in \mathbb{R}} \quad & (s(u_0) - \bar{u}_d)^2 \\ \text{s.t.} \quad & \Psi_0 + \Psi_1 u_0 \geq 0, \end{aligned} \tag{3.19}$$

where $\bar{u}_d = u_d/h_{x_2}$ and $\Psi_0, \Psi_1, s(\cdot)$ are defined in Theorem 3.1. We first introduce the following lemma.

Lemma 3.1 *Define a function $s(\cdot)$ as*

$$s(y) = y + \frac{\kappa_1}{b} + \frac{\kappa_2^2 y^2}{b(\kappa_2|h_{x_2}||y| + \epsilon_2)}, \tag{3.20}$$

where $\kappa_1, \kappa_2 \geq 0$ and $b, \epsilon_2, |h_{x_2}| > 0$ are considered as constants. The function $s(\cdot)$ has the following properties:

(i) When $\bar{b} - \kappa_2 \geq 0$, where $\bar{b} = b|h_{x_2}|$, $s(y)$ is monotonically increasing with respect to y, and $\lim_{y\to-\infty} s(y) = -\infty$, $\lim_{y\to+\infty} s(y) = +\infty$;

(ii) When $\bar{b} - \kappa_2 < 0$, $s(y)$ has a global minimum $y^* = \frac{\bar{\epsilon}_2[(\kappa_2-\bar{b})-\sqrt{\kappa_2(\kappa_2-\bar{b})}]}{\kappa_2(\kappa_2-\bar{b})}$, where $\bar{\epsilon}_2 = \epsilon_2/|h_{x_2}|$, and $\lim_{y\to-\infty} s(y) = \lim_{y\to+\infty} s(y) = +\infty$.

Proof *Note that the derivative of $s(y)$ with respect to y can be expressed as*

$$\frac{\mathrm{d}s}{\mathrm{d}y} = \begin{cases} 1 + \frac{\kappa_2^2 y(\kappa_2 y + 2\bar{\epsilon}_2)}{\bar{b}(\kappa_2 y + \bar{\epsilon}_2)^2}, & \text{if } y \geq 0, \\ \frac{(\bar{b}-\kappa_2)\kappa_2^2 y^2 - 2\kappa_2\bar{\epsilon}_2(\bar{b}-\kappa_2)y + \bar{b}\bar{\epsilon}_2^2}{\bar{b}(-\kappa_2 y + \bar{\epsilon}_2)^2}, & \text{if } y < 0. \end{cases} \tag{3.21}$$

(i) If $\kappa_2 = 0$, then $s(y) = \frac{\kappa_1}{b} + y$, from which one can see that the statement is true. We assume $\kappa_2 \neq 0$ in the following analysis. It can be seen that if $\bar{b} - \kappa_2 \geq 0$, $\frac{\mathrm{d}s}{\mathrm{d}y} > 0$ for any $y \in \mathbb{R}$, such that $s(y)$ is monotonically increasing. Meanwhile, one can see $\lim_{y\to+\infty} s(y) = +\infty$ and $\lim_{y\to-\infty} s(y) = \lim_{y\to-\infty} \frac{y\bar{b}(-\kappa_2 y+\bar{\epsilon}_2)+\kappa_2^2 y^2}{\bar{b}(-\kappa_2 y+\bar{\epsilon}_2)} + \frac{\kappa_1}{b} \overset{z=-y}{=\!=} \lim_{z\to+\infty} \frac{-\bar{b}(\kappa_2 z^2+\bar{\epsilon}_2 z)+\kappa_2^2 z^2}{\bar{b}(\kappa_2 z+\bar{\epsilon}_2)} + \frac{\kappa_1}{b}$. Define $\alpha(z) = -\bar{b}(\kappa_2 z^2 + \bar{\epsilon}_2 z) + \kappa_2^2 z^2$, $\beta(z) = \bar{b}(\kappa_2 z + \bar{\epsilon}_2)$, and $I = (0, +\infty)$, from which one can see $\lim_{y\to-\infty} s(y) = \frac{\kappa_1}{b} + \lim_{z\to+\infty} \frac{\alpha(z)}{\beta(z)}$. Since α, β are differentiable with respect to z and $\beta'(z) \neq 0$ for any $z \in I$, applying L'Hôpital's rule gives $\lim_{y\to-\infty} s(y) = \lim_{z\to+\infty} \frac{-2(\bar{b}-\kappa_2)\kappa_2 z - \bar{b}\bar{\epsilon}_2}{\bar{b}\kappa_2} + \frac{\kappa_1}{b} = -\infty$.

(ii) If $\bar{b} - \kappa_2 < 0$, $\frac{\mathrm{d}s}{\mathrm{d}y} > 0$ still holds when $y \geq 0$. When $y < 0$, asking $\frac{\mathrm{d}s}{\mathrm{d}y} = 0$ gives a stationary point y^*. It can be verified $\left.\frac{\mathrm{d}^2 s}{\mathrm{d}y^2}\right|_{y=y^*} = \frac{2(\kappa_2(\kappa_2-\bar{b}))^{\frac{3}{2}}}{\kappa_2\bar{b}\bar{\epsilon}_2} > 0$, such that y^* is a global minimum. Similarly, one can prove $\lim_{y\to+\infty} s(y) = \infty$ and $\lim_{y\to-\infty} s(y) \overset{z=-y}{=\!=} \lim_{z\to+\infty} \frac{\kappa_2(\kappa_2-\bar{b})z^2 - \bar{b}\bar{\epsilon}_2 z}{\bar{b}(\bar{\epsilon}_2+\kappa_2 z)} + \frac{\kappa_1}{b} = \lim_{z\to+\infty} \frac{2\kappa_2(\kappa_2-\bar{b})z - \bar{b}\bar{\epsilon}_2}{\bar{b}\kappa_2} + \frac{\kappa_1}{b} = +\infty$, where the second equality arises from L'Hôpital's rule (the conditions of L'Hôpital's rule can be verified using the similar procedure in (i)). □

Based on the properties of the function $s(\cdot)$ presented in Lemma 3.1, the optimal solution to (3.19) can be obtained, from which the closed-form solution to (aCBF-NLP) can be obtained, as shown in the following proposition.

Proposition 3.1 *The closed-form solution to* (aCBF-NLP) *can be represented as*

$$u = \begin{cases} h_{x_2} \max\left(s\left(-\frac{\Psi_0}{\Psi_1}\right), \bar{u}_d\right), & \text{if } \mathcal{A}_1 \text{ holds}, \\ h_{x_2} \min\left(s\left(-\frac{\Psi_0}{\Psi_1}\right), \bar{u}_d\right), & \text{if } \mathcal{A}_2 \text{ holds}, \\ h_{x_2} \max(s(y^*), \bar{u}_d), & \text{if } \mathcal{A}_3 \text{ holds}, \\ u_d, & \text{if } \Psi_1 = 0 \wedge \bar{b} - \kappa_2 \geq 0, \\ 0, & \text{if } h_{x_2} = 0, \end{cases} \tag{3.22}$$

where κ_2, Ψ_0, Ψ_1 *are given in Theorem 3.1,* $\bar{b} = b|h_{x_2}|$, $\bar{\epsilon}_2 = \epsilon_2/|h_{x_2}|$, $y^* = \frac{\bar{\epsilon}_2[(\kappa_2 - \bar{b}) - \sqrt{\kappa_2(\kappa_2 - \bar{b})}]}{\kappa_2(\kappa_2 - \bar{b})}$, $\mathcal{A}_1 : h_{x_2} \neq 0 \wedge ((\bar{b} - \kappa_2 \geq 0 \wedge \Psi_1 > 0) \vee (\bar{b} - \kappa_2 < 0 \wedge \Psi_0 + \Psi_1 y^* < 0))$, $\mathcal{A}_2 : h_{x_2} \neq 0 \wedge \bar{b} - \kappa_2 \geq 0 \wedge \Psi_1 < 0$, *and* $\mathcal{A}_3 : h_{x_2} \neq 0 \wedge \bar{b} - \kappa_2 < 0 \wedge \Psi_0 + \Psi_1 y^* \geq 0$.

Proof *Note that similar to the aCBF-QPs presented in [46], [47], the optimization problem* (aCBF-NLP) *is solved pointwise for a given* $(x, \hat{\mu}, \hat{\nu})$, *such that* κ_1, κ_2 *defined in* (3.10) *and* h_{x_2} *should be considered as constants when solving* (3.19). *If* $\bar{b} - \kappa_2 \geq 0$, $s(y)$ *is monotonically increasing, according to Lemma 3.1. When* $\Psi_1 > 0$, *one can see that* $K_{BF} = \{\mathfrak{u} : \mathfrak{u} \geq -\frac{\Psi_0}{\Psi_1}\}$ *and* $s(u_0) \in \left[s\left(-\frac{\Psi_0}{\Psi_1}\right), +\infty\right]$ *for any* $u_0 \in K_{BF}$. *It is easy to verify that* $s(u_0^*) = \bar{u}_d$ *if* $\bar{u}_d \geq s\left(-\frac{\Psi_0}{\Psi_1}\right)$ *and* $s(u_0^*) = s\left(-\frac{\Psi_0}{\Psi_1}\right)$ *when* $\bar{u}_d < s\left(-\frac{\Psi_0}{\Psi_1}\right)$, *where* u_0^* *denotes the solution to* (3.19). *Hence, in conclusion, one has* $s(u_0^*) = \max\left\{s\left(-\frac{\Psi_0}{\Psi_1}\right), \bar{u}_d\right\}$, *such that the closed-form solution to* (aCBF-NLP) *is* $u = h_{x_2} \max\left\{s\left(-\frac{\Psi_0}{\Psi_1}\right), \bar{u}_d\right\}$. *Performing the similar analysis one can see that the closed-form solution to* (aCBF-NLP) *is* $u = h_{x_2} \min\left\{s\left(-\frac{\Psi_0}{\Psi_1}\right), \bar{u}_d\right\}$ *when* $\Psi_1 < 0$. *If* $\Psi_1 = 0$, $K_{BF} = \mathbb{R}$ *and* $s(u_0) \in \mathbb{R}$ *for any* $u_0 \in K_{BF}$, *such that* $u = u_d$.

On the other hand, if $\bar{b} - \kappa_2 < 0$, *one knows that* $s(y)$ *has a global minimal* y^*, *according to Lemma 3.1. Note that* $\Psi_0 + \Psi_1 y^* < 0$ *indicates* $y^* \notin K_{BF}$, *such that* $s(u_0) \in \left[s\left(-\frac{\Psi_0}{\Psi_1}\right), +\infty\right]$ *for any* $u_0 \in K_{BF}$ *(note that the non-emptiness of* K_{BF} *indicates* $\Psi_0 \geq 0$ *if* $\Psi_1 = 0$*). Then, one can see that* $s(u_0^*) = s\left(-\frac{\Psi_0}{\Psi_1}\right)$ *if* $\bar{u}_d \leq s\left(-\frac{\Psi_0}{\Psi_1}\right)$ *and* $s(u_0^*) = \bar{u}_d$ *when* $\bar{u}_d > s\left(-\frac{\Psi_0}{\Psi_1}\right)$, *such that* $s(u_0^*) = \max\left\{s\left(-\frac{\Psi_0}{\Psi_1}\right), \bar{u}_d\right\}$ *and the closed-form solution to* (3.19) *is* $u = h_{x_2} \max\left\{s\left(-\frac{\Psi_0}{\Psi_1}\right), \bar{u}_d\right\}$. *Furthermore,* $\Psi_0 + \Psi_1 y^* \geq 0$ *implies* $y^* \in K_{BF}$,

such that $s(u_0) \in [s(y^*), +\infty]$ *for any* $u_0 \in K_{BF}$. *Using the similar procedure shown above, one can conclude that the closed-form solution to* (3.19) *is* $u = h_{x_2} \max\{s(x^*), \bar{u}_d\}$. $\square$

3.3.3 Extension to More General Systems

In this subsection, we will generalize the aCBF-based control design method proposed in Section 3.3 to more general systems. Specifically, we will design a safe controller u for the system (3.1) with the same f_θ, θ_i, φ_i, $i \in [n]$, as those defined in (3.2) and non-diagonal g and g_λ whose (i,j)-th entries can be expressed as

$$(g)_{ij} = g_{ij}(x),\ (g_\lambda)_{ij} = \lambda_{ij}^\top \psi_{ij}(x), \tag{3.23}$$

where $g_{ij} : \mathbb{R}^{m+n} \to \mathbb{R}$, $\psi_{ij} : \mathbb{R}^{m+n} \to \mathbb{R}^{q_{ij}}$ are known functions and $\lambda_{ij} \in \mathbb{R}^{q_{ij}}$ are vectors of unknown parameters, $i \in [n], j \in [n]$.

Similar to Assumption 3.2, we assume that θ_i and λ_{ij} are upper and lower bounded by known vectors.

Assumption 3.4 For every $i, j \in [n]$, *there exist known vectors* $\overline{\theta}_i, \underline{\theta}_i \in \mathbb{R}^{p_i}$ *and* $\overline{\lambda}_{ij}, \underline{\lambda}_{ij} \in \mathbb{R}^{q_{ij}}$, *such that* $\underline{\theta}_i \le \theta_i \le \overline{\theta}_i$ *and* $\underline{\lambda}_{ij} \le \lambda_{ij} \le \overline{\lambda}_{ij}$.

Similar to [92, Assumption 1], we assume that $\tilde{g} \triangleq g + g_\lambda$ is away from the singularity point by letting the smallest singular value of $\frac{\tilde{g}(x)+\tilde{g}^\top(x)}{2}$ lower bounded by some known positive constant.

Assumption 3.5 The matrix $\frac{\tilde{g}(x)+\tilde{g}^\top(x)}{2}$ *is either uniformly positive definite or uniformly negative definite for all* $x \in \mathcal{X}$, *where* $\mathcal{C} \subseteq \mathcal{X}, \tilde{g} = g + g_\lambda$ *and* $\mathcal{X} \in \mathbb{R}^{m+n}$ *is a compact set, i.e., there exists a positive constant* $b^* > 0$ *such that* $\underline{\sigma}\left(\frac{\tilde{g}(x)+\tilde{g}^\top(x)}{2}\right) \ge b^*, \forall x \in \mathcal{X}$, *where* $\underline{\sigma}(\cdot)$ *represents the smallest singular value of a matrix.*

Without loss of generality, we assume that $\frac{\tilde{g}(x)+\tilde{g}^\top(x)}{2}$ is positive definite for any $x \in \mathcal{C}$ in this subsection. We select arbitrary values $\theta_i^0 \in \mathbb{R}^{p_i}$, $\lambda_{ij}^0 \in \mathbb{R}^{q_{ij}}$ satisfying $\underline{\theta}_i \le \theta_i^0 \le \overline{\theta}_i$,

$\underline{\lambda}_{ij} \le \lambda_{ij}^0 \le \overline{\lambda}_{ij}$, $i, j \in [n]$, as the nominal values of θ_i and λ_{ij}, respectively. We define

$$\Theta = \begin{bmatrix} \theta_1^\top & \theta_2^\top & \cdots & \theta_n^\top \end{bmatrix}^\top,\ \Theta^0 = \begin{bmatrix} \theta_1^{0\top} & \theta_2^{0\top} & \cdots & \theta_n^{0\top} \end{bmatrix}^\top, \tag{3.24a}$$

$$\Lambda = \begin{bmatrix} \lambda_{11}^\top & \lambda_{12}^\top & \cdots & \lambda_{nn}^\top \end{bmatrix}^\top,\ \Lambda^0 = \begin{bmatrix} \lambda_{11}^{0\top} & \lambda_{12}^{0\top} & \cdots & \lambda_{nn}^{0\top} \end{bmatrix}^\top, \tag{3.24b}$$

$$\Omega_\varphi = \begin{bmatrix} \varphi_1^\top & \varphi_2^\top & \cdots & \varphi_n^\top \end{bmatrix}^\top,\ \Omega_\psi = \begin{bmatrix} \psi_{11}^\top & \psi_{12}^\top & \cdots & \psi_{nn}^\top \end{bmatrix}^\top, \tag{3.24c}$$

$$f_\theta^0 = \begin{bmatrix} \theta_1^0\varphi_1 \\ \theta_2^0\varphi_2 \\ \vdots \\ \theta_n^0\varphi_n \end{bmatrix},\ g_\lambda^0 = \begin{bmatrix} \lambda_{11}^{0\top}\psi_{11} & \lambda_{12}^{0\top}\psi_{12} & \cdots & \lambda_{1n}^{0\top}\psi_{1n} \\ \lambda_{21}^{0\top}\psi_{21} & \lambda_{22}^{0\top}\psi_{22} & \cdots & \lambda_{2n}^{0\top}\psi_{2n} \\ \cdots & \cdots & \cdots & \cdots \\ \lambda_{n1}^{0\top}\psi_{n1} & \lambda_{n2}^{0\top}\psi_{n2} & \cdots & \lambda_{nn}^{0\top}\psi_{nn} \end{bmatrix}. \tag{3.24d}$$

and

$$\mu = \|\Theta - \Theta^0\|,\ \nu = \|\Lambda - \Lambda^0\|. \tag{3.25}$$

According to Assumption 3.4, one can see that

$$\mu \le \bar{\mu} \triangleq \sqrt{\sum_{j=1}^{M} \max\{(\overline{\Theta}_j - \Theta_j^0)^2, (\underline{\Theta}_j - \Theta_j^0)^2\}},$$
$$\nu \le \bar{\nu} \triangleq \sqrt{\sum_{j=1}^{N} \max\{(\overline{\Lambda}_j - \Lambda_j^0)^2, (\underline{\Lambda}_j - \Lambda_j^0)^2\}},$$

where $M = \sum_{i=1}^n p_i$ and $N = \sum_{j=1}^n \sum_{i=1}^n q_{ij}$. We introduce the following lemma.

Lemma 3.2 *For any $a \in \mathbb{R}^n$, $b \in \mathbb{R}^n$, $c \in \mathbb{R}$, the following inequalities hold:*

$$a^\top(f_\theta - f_\theta^0) \ge -\mu\|a\|\|\Omega_\varphi\|, \tag{3.26a}$$

$$b^\top(g_\lambda - g_\lambda^0)bc \ge -\nu\|\Omega_\psi\|\|b\|^2|c|, \tag{3.26b}$$

where f_θ is defined in (3.2)*, g_λ is defined in* (3.23)*, f_θ^0, g_λ^0, Ω_φ, Ω_ψ are defined in* (3.24)*, and μ, ν are defined in* (3.25)*.*

Proof *One can verify that* $a^\top(f_\theta - f_\theta^0) \ge -\|a\|\|f_\theta - f_\theta^0\| = -\|a\|\sqrt{\sum_{i=1}^n ((\theta_i - \theta_i^0)^\top\varphi_i)^2} \ge$

$-\|a\|\sqrt{\sum_{i=1}^{n}\|\theta_i-\theta_i^0\|^2\|\varphi_i\|^2} \geq -\|a\|\sqrt{\sum_{i=1}^{n}\|\theta_i-\theta_i^0\|^2}\sqrt{\sum_{i=1}^{n}\|\varphi_i\|^2} = -\|a\|\|\Theta-\Theta^0\| \times \|\Omega_\varphi\| = -\mu\|a\|\|\Omega_\varphi\|$, *where the first and second inequality are derived from Cauchy-Schwarz inequality and the third inequality comes from the fact* $\sum_{k=1}^{n}x_k^2y_k^2 \leq \left(\sum_{k=1}^{n}x_k^2\right) \times \left(\sum_{k=1}^{n}y_k^2\right),\ \forall x_k, y_k \in \mathbb{R}$. *Therefore,* (3.26a) *holds.*

Similarly, using Cauchy-Schwarz inequality, one can get $b^\top(g_\lambda - g_\lambda^0)bc \geq -|b^\top(g_\lambda - g_\lambda^0)b||c| \geq -\|g_\lambda - g_\lambda^0\|\|b\|^2|c|$. *Invoking the definition of the Frobenius norm,* $\|g_\lambda - g_\lambda^0\|$ *satisfies* $\|g_\lambda - g_\lambda^0\| = \sqrt{\sum_{i=1}^{n}\sum_{j=1}^{n}((\lambda_{ij}-\lambda_{ij}^0)^\top\psi_{ij})^2} \leq \sqrt{\sum_{i=1}^{n}\sum_{j=1}^{n}\|\lambda_{ij}-\lambda_{ij}^0\|^2\|\psi_{ij}\|^2} \leq \sqrt{\sum_{i=1}^{n}\sum_{j=1}^{n}\|\psi_{ij}\|^2}\sqrt{\sum_{i=1}^{n}\sum_{j=1}^{n}\|\lambda_{ij}-\lambda_{ij}^0\|^2} = \|\Lambda-\Lambda^0\|\|\Omega_\psi\| = \nu\|\Omega_\psi\|$. *Therefore,* (3.26b) *holds.* □

Analogous to Theorem 3.1, the following theorem provides an aCBF-based controller that ensures the safety of system (2.11b) with g and g_λ defined in (3.23).

Theorem 3.2 *Consider the system* (3.1) *with* f_θ *defined in* (3.2) *and* g, g_λ *defined in* (3.23)*, as well as the safe set* $\mathcal{C}$ *defined in* (3.3)*. Suppose that*

(i) Assumptions 3.1, 3.4 and 3.5 hold;

(ii) There exist positive constants $\gamma, \epsilon_1, \epsilon_2, \gamma_\theta, \gamma_\lambda > 0$*, such that the following set is non-empty:*

$$K_{BF}^g \triangleq \{\mathfrak{u} \in \mathbb{R} \mid \Psi_0 + \Psi_1\mathfrak{u} \geq 0\},\ \forall x \in \mathcal{C}, \tag{3.27}$$

where $\Psi_0 = \mathcal{M} + h_{x_2}f_\theta^0 - (\epsilon_1+\epsilon_2) + \gamma\left(h - \frac{\bar{\mu}^2}{2\gamma_\theta} - \frac{\bar{\nu}^2}{2\gamma_\lambda}\right)$, $\Psi_1 = h_{x_2}(g+g_\lambda^0)h_{x_2}^\top$, $h_{x_2} = \frac{\partial h}{\partial x_2}$, *and* $\mathcal{M}$ *is the same as that defined in Theorem 3.1;*

(iii) $\hat{\mu}$ *and* $\hat{\nu}$ *are parameter estimations governed by the following adaptive laws:*

$$\dot{\hat{\mu}} = -\gamma\hat{\mu} + \gamma_\theta\|h_{x_2}\|\|\Omega_\varphi\|, \tag{3.28a}$$

$$\dot{\hat{\nu}} = -\gamma\hat{\nu} + \gamma_\lambda\|h_{x_2}\|^2|u_0|\|\Omega_\psi\|, \tag{3.28b}$$

where $\hat{\mu}(0), \hat{\nu}(0) > 0$ *and* $u_0 \in \mathbb{R}$ *is a Lipschitz function satisfying* $u_0 \in K_{BF}^g(x)$*;*

(iv) The following inequality holds: $h(x(0)) \geq \frac{\hat{\mu}(0)^2+\bar{\mu}^2}{2\gamma_\theta} + \frac{\hat{\nu}(0)^2+\bar{\nu}^2}{2\gamma_\lambda}$.

Then, the control input $u = s_g(u_0)h_{x_2}^\top \in \mathbb{R}^n$ *will make* $h(x(t)) \geq 0$ *for any* $t > 0$*, where*

$$s_g(u_0) \triangleq u_0 + \frac{\kappa_{1,g}}{b^*} + \frac{\kappa_{2,g}^2 u_0^2}{b^*(\kappa_{2,g}\|h_{x_2}\||u_0| + \epsilon_2)}, \tag{3.29}$$

with $\kappa_{1,g} = \frac{\hat{\mu}^2\|\Omega_\varphi\|^2}{\hat{\mu}\|\Omega_\varphi\|\|h_{x_2}\|+\epsilon_1}$ *and* $\kappa_{2,g} = \hat{\nu}\|\Omega_\psi\|\|h_{x_2}\|$.

Proof *Assumption 3.5 indicates that, for any* $v \in \mathbb{R}^n$, $v^\top(g+g_\lambda)v \geq b^*\|v\|^2$ *[92]. Similar to the proof of Theorem 3.1, one can see that* $\hat{\mu}(t) \geq 0, \hat{\nu}(t) \geq 0, \forall t > 0$*. Define a candidate CBF* $\bar{h}$ *as*

$$\bar{h} = h - \frac{1}{2\gamma_\theta}\tilde{\mu}^2 - \frac{1}{2\gamma_\lambda}\tilde{\nu}^2, \tag{3.30}$$

where $\tilde{\mu} = \mu - \hat{\mu}$ *and* $\tilde{\nu} = \nu - \hat{\nu}$.

We claim that $\dot{\bar{h}} \geq -\gamma\bar{h}$ *where* $\dot{\bar{h}}$ *is the time derivative of* $\bar{h}$*. Indeed, it is easy to see that*

$$\dot{\bar{h}} \geq \mathcal{M} + h_{x_2}(f_\theta + (g+g_\lambda)u) + \frac{1}{\gamma_\theta}\tilde{\mu}\dot{\hat{\mu}} + \frac{1}{\gamma_\lambda}\tilde{\nu}\dot{\hat{\nu}}. \tag{3.31}$$

Substituting (3.29) *into the inequality above yields*

$$\begin{aligned}
\dot{\bar{h}} \geq\ & \frac{1}{\gamma_\theta}\tilde{\mu}\dot{\hat{\mu}} + \frac{1}{\gamma_\lambda}\tilde{\nu}\dot{\hat{\nu}} + h_{x_2}(g+g_\lambda)h_{x_2}^\top\left(\frac{\hat{\mu}^2\|\Omega_\varphi\|^2}{b^*(\hat{\mu}\|\Omega_\varphi\|\|h_{x_2}\| + \epsilon_1)} + \frac{\hat{\nu}^2\|\Omega_\psi\|^2\|\|h_{x_2}\|^2u_0^2}{b^*(\hat{\nu}|u_0|\|\Omega_\psi\|\|\|h_{x_2}\|^2 + \epsilon_2)}\right) \\
& + \mathcal{M} + h_{x_2}f_\theta + h_{x_2}(g+g_\lambda)h_{x_2}^\top u_0 \\
\geq\ & \mathcal{M} + h_{x_2}f_\theta^0 + h_{x_2}(g+g_\lambda^0)h_{x_2}^\top u_0 + \frac{1}{\gamma_\theta}\tilde{\mu}\dot{\hat{\mu}} + \frac{1}{\gamma_\lambda}\tilde{\nu}\dot{\hat{\nu}} + h_{x_2}(f_\theta - f_\theta^0) + h_{x_2}(g_\lambda - g_\lambda^0)h_{x_2}^\top u_0 \\
& + \frac{\hat{\mu}^2\|h_{x_2}\|^2\|\Omega_\varphi\|^2}{\hat{\mu}\|\Omega_\varphi\|\|h_{x_2}\| + \epsilon_1} + \frac{\hat{\nu}^2\|\Omega_\psi\|^2\|\|h_{x_2}\|^4u_0^2}{\hat{\nu}|u_0|\|\Omega_\psi\|\|\|h_{x_2}\|^2 + \epsilon_2} \\
\geq\ & \Psi_0 + \Psi_1 u_0 + \epsilon_1 + \epsilon_2 - \gamma\left(h - \frac{1}{2\gamma_\theta}\bar{\mu}^2 - \frac{1}{2\gamma_\lambda}\bar{\nu}^2\right) + \frac{1}{\gamma_\theta}\tilde{\mu}\dot{\hat{\mu}} + \frac{1}{\gamma_\lambda}\tilde{\nu}\dot{\hat{\nu}} - \mu\|h_{x_2}\|\|\Omega_\varphi\| \\
& - \nu\|h_{x_2}\|^2\|\Omega_\psi\||u_0| + \frac{\hat{\mu}^2\|h_{x_2}\|^2\|\Omega_\varphi\|^2}{\hat{\mu}\|\Omega_\varphi\|\|h_{x_2}\| + \epsilon_1} + \frac{\hat{\nu}^2\|\Omega_\psi\|^2\|h_{x_2}\|^4u_0^2}{\hat{\nu}|u_0|\|\Omega_\psi\|\|h_{x_2}\|^2 + \epsilon_2}
\end{aligned} \tag{3.32}$$

where the second inequality is from Assumption 3.5 and the third inequality comes from Lemma 3.2 shown in Appendix. Selecting $u_0 \in K_{BF}^g$ *we have*

$$\dot{\bar{h}} \geq -\gamma\left(h - \frac{1}{2\gamma_\theta}\bar{\mu}^2 - \frac{1}{2\gamma_\lambda}\bar{\nu}^2\right) + \frac{1}{\gamma_\theta}\tilde{\mu}\left(\dot{\hat{\mu}} - \gamma_\theta\|h_{x_2}\|\|\Omega_\varphi\|\right) + \frac{1}{\gamma_\lambda}\tilde{\nu}\left(\dot{\hat{\nu}} - \gamma_\lambda\|h_{x_2}\|^2\|\Omega_\psi\||u_0|\right)$$

$$-\hat{\mu}\|h_{x_2}\|\|\Omega_\varphi\| + \frac{\hat{\mu}^2\|h_{x_2}\|^2\|\Omega_\varphi\|^2}{\hat{\mu}\|\Omega_\varphi\|\|h_{x_2}\|+\epsilon_1} - \hat{\nu}\|h_{x_2}\|^2\|\Omega_\psi\||u_0| + \frac{\hat{\nu}^2\|\Omega_\psi\|^2\|h_{x_2}\|^4u_0^2}{\hat{\nu}|u_0|\|\Omega_\psi\|\|h_{x_2}\|^2+\epsilon_2}+\epsilon_1+\epsilon_2$$
$$\geq -\gamma\left(h - \frac{1}{2\gamma_\theta}\bar{\mu}^2 - \frac{1}{2\gamma_\lambda}\bar{\nu}^2\right) + \frac{1}{\gamma_\theta}\tilde{\mu}(\dot{\hat{\mu}} - \gamma_\theta\|h_{x_2}\|\|\Omega_\varphi\|) + \frac{1}{\gamma_\lambda}\tilde{\nu}(\dot{\hat{\nu}} - \gamma_\lambda\|h_{x_2}\|^2\|\Omega_\psi\||u_0|).$$

Substituting (3.28) *into the inequality above, we have* $\dot{\bar{h}} \geq -\gamma\left(h - \frac{1}{2\gamma_\theta}\bar{\mu}^2 - \frac{1}{2\gamma_\lambda}\bar{\nu}^2\right) - \frac{\gamma}{\gamma_\theta}\tilde{\mu}\hat{\mu} - \frac{\gamma}{\gamma_\lambda}\tilde{\nu}\hat{\nu}$. *Similar to the proof of Theorem 3.1, one can see* $\hat{\mu}\tilde{\mu} \leq \frac{\bar{\mu}^2}{2} - \frac{\tilde{\mu}^2}{2}$ *and* $\hat{\nu}\tilde{\nu} \leq \frac{\bar{\nu}^2}{2} - \frac{\tilde{\nu}^2}{2}$, *which implies that* $\dot{\bar{h}} \geq -\gamma\bar{h}$. *Our claim is thus proven. Note that* $\bar{h}(x(0), 0) \geq 0$ *because of condition (iv). Hence, one can conclude that* $\bar{h}(t) \geq 0, \forall t > 0$, *and thus,* $h(x(t)) \geq 0, \forall t > 0$. □

Remark 3.6 *Compared with Theorem 3.1, Theorem 3.2 provides a safety guarantee for a more general class of systems but the resulting safe controller tends to have more conservative performance. This is because the control* $u \in \mathbb{R}^n$ *is designed to have a particular structure* $u = s_g(u_0)h_{x_2}^\top$, *which requires* u *always proportional to* $h_{x_2}^\top$, *to deal with the non-diagonal structures of* g *and* g_λ. *How to improve the design to generate a less conservative safe controller will be our future work.*

The safe controller $u(x)$ in Theorem 3.2 can be obtained pointwise for any $x \in \mathcal{C}$ via solving the following optimization problem:

$$\begin{aligned} \min_{u\in\mathbb{R}^n} \quad & \|u - u_d\|^2 \\ \text{s.t.} \quad & \Psi_0 + \Psi_1 u_0 \geq 0, \\ & u = s_g(u_0)h_{x_2}^\top, \end{aligned} \tag{3.33}$$

where Ψ_0 and Ψ_1 are defined in Theorem 3.2. The closed-form solution of (3.33) can be obtained by using Proposition 3.1.

3.3.4 Data-driven Approach For Tightening Parameter Bounds

The controller design proposed in Section 3.3.1 relies on the bounds of unknown parameters as shown in Assumptions 3.2 and 3.4. If the prior knowledge of the parameter bounds

is poor, the control performance will tend to be conservative (see simulation examples in Section 3.4). In this section, we present a data-driven approach to get tighter bounds and more accurate nominal values for the unknown parameters. Combining the aCBF-based control design and the data-driven parameter tightening approach provides a mechanism to achieve safety with less conservatism.

Our data-driven method is inspired by the differential inclusion technique proposed in [97]. To better illustrate the main idea, we consider the system (3.1) with $m = 0$ and $n = 1$ shown as follows:

$$\dot{x} = f(x) + f_u(x) + \theta^\top \varphi(x) + (g(x) + \lambda^\top \psi(x))u, \tag{3.34}$$

where $x \in \mathbb{R}$ is the state, $u \in \mathbb{R}$ is the control input, $f : \mathbb{R} \to \mathbb{R}$ and $g : \mathbb{R} \to \mathbb{R}$ are known Lipschitz functions, $f_u : \mathbb{R} \to \mathbb{R}$ is an unknown Lipschitz function satisfying Assumption 3.1, $\varphi : \mathbb{R} \to \mathbb{R}^p$, $\psi : \mathbb{R} \to \mathbb{R}^q$ are known functions, and $\theta \in \mathbb{R}^p, \lambda \in \mathbb{R}^q$ are unknown parameters. The proposed method can be readily extended to systems with multiple inputs by considering each control channel separately.

Recall that x_i denotes the i-th entry of x where x is either a column or a row vector. Given a dataset $\mathcal{E} = \{x^i, \dot{x}^i, u^i\}_{i=1}^N$, the bounds of θ, λ, and f_u can be tightened as shown by the following theorem.

Theorem 3.3 *Consider the system given in* (3.34)*. Suppose that (i) Assumptions 3.1 and 3.2 hold; (ii) f_u has a known Lipschitz constants L for $x \in \mathcal{C}$; (iii) a dataset $\mathcal{E} = \{x^i, \dot{x}^i, u^i\}_{i=1}^N$ is given. Define intervals $\mathcal{P}^0 = [\underline{\theta}, \overline{\theta}]^\top \in \mathbb{IR}^{1\times p}$ and $\mathcal{Q}^0 = [\underline{\lambda}, \overline{\lambda}]^\top \in \mathbb{IR}^{1\times q}$. Let x^0 be an arbitrary state in $\mathcal{C}$ and define $\mathcal{F}^0 = [\underline{f}_u(x^0), \overline{f}_u(x^0)]$. For $i \in [N]$, $r \in [p]$, $s \in [q]$, define*

$$\mathcal{F}^i = \left(\bigcap_{j=0}^{i-1} \{\mathcal{F}^j + L\|x^i - x^j\|[-1, 1]\}\right) \bigcap [\underline{f}_u(x^i), \overline{f}_u(x^i)] \bigcap (y^i - \mathcal{P}^0\varphi^i - \mathcal{Q}^0\psi^i u^i), \tag{3.35a}$$

$$v_0^i = (y^i - \mathcal{F}^i - \mathcal{Q}^0\psi^i u^i) \cap (\mathcal{P}^{i-1}\varphi^i), \tag{3.35b}$$

$$v_r^i = (v_{r-1}^i - \mathcal{P}_r^{i-1}\varphi_r^i) \cap \left(\sum_{l=r+1}^{p} \mathcal{P}_l^{i-1}\varphi_l^i\right), \tag{3.35c}$$

$$\mathcal{P}_r^i = \begin{cases} ((v_{r-1}^i - \sum_{l=r+1}^{p} \mathcal{P}_l^{i-1}\varphi_l^i) \cap (\mathcal{P}_r^{i-1}\varphi_r^i)))\frac{1}{\varphi_r^i}, & \text{if } \varphi_r^i \neq 0, \\ \mathcal{P}_r^{i-1}, & \text{otherwise,} \end{cases} \tag{3.35d}$$

and

$$w_0^i = (y^i - \mathcal{F}^i - \mathcal{P}^N\varphi^i) \cap (\mathcal{Q}^{i-1}\psi^i u^i), \tag{3.36a}$$

$$w_s^i = (w_{s-1}^i - \mathcal{Q}_s^i\psi_s^i u^i) \cap \left(\sum_{l=s+1}^{q} \mathcal{Q}_l^{i-1}\psi_l^i u^i\right), \tag{3.36b}$$

$$\mathcal{Q}_s^i = \begin{cases} ((w_{s-1}^i - \sum_{l=s+1}^{q} \mathcal{Q}_l^{i-1}\psi_l^i u^i) \cap (\mathcal{Q}_s^{i-1}\psi_s^i u^i))\frac{1}{\psi_s^i u^i}, & \text{if } \psi_s^i u^i \neq 0, \\ \mathcal{Q}_s^{i-1}, & \text{otherwise,} \end{cases} \tag{3.36c}$$

where $\varphi^i = \varphi(x^i)$, $\psi^i = \psi(x^i)$, *and* $y^i = \dot{x}^i - f(x^i) - g(x^i)u^i$. *Then,* $\theta^\top \in \mathcal{P}^N$, $\lambda^\top \in \mathcal{Q}^N$, *and* $f_u(x) \in \mathcal{F}(x) \triangleq \bigcap_{j=0}^{N}\{\mathcal{F}^j + L\|x - x^j\|[-1,1]\}$, *for any* $x \in \mathcal{C}$.

Proof *Note that* $f_u(x^i) \in [\underline{f}_u(x^i), \overline{f}_u(x^i)]$ *from Assumption 3.1 and* $f_u(x^i) \in y^i - \mathcal{P}^0\varphi^i - \mathcal{Q}^0\psi^i u^i$ *from* $f_u(x^i) = y^i - \theta^\top\varphi^i - \lambda^\top\psi^i u^i$, $\theta^\top \in \mathcal{P}^0$, *and* $\lambda^\top \in \mathcal{Q}^0$. *Because of the Lipschitzness of* f_u, *it is obvious that for any* $i \in [N]$ *[97]*

$$f_u(x^i) \in \left(\bigcap_{j=0}^{i-1}\{f_u(x^j) + L\|x^i - x^j\|[-1,1]\}\right) \bigcap [\underline{f}_u(x^i), \overline{f}_u(x^i)] \bigcap (y^i - \mathcal{P}^0\varphi^i - \mathcal{Q}^0\psi^i u^i),$$

which indicates $f_u(x^i) \in \mathcal{F}^i$ *provided* $f_u(x^k) \in \mathcal{F}^k$ *for any* $0 \leq k < i$. *Since* $f_u(x^0) \in \mathcal{F}^0$, *using mathematical induction one can conclude that* $f_u(x^i) \in \mathcal{F}^i$, $\forall i \in [N]$; *thus, for any* $x \in \mathcal{C}$, $f_u(x) \in \bigcap_{j=0}^{N}\{f_u(x^j) + L\|x - x^j\|[-1,1]\} \subset \mathcal{F}(x)$.

Next, we will prove that if $\theta^\top \in \mathcal{P}^{i-1}$, *then* $\theta^\top\varphi^i - \sum_{l=1}^{r}\theta_l\varphi_l^i \in v_r^i$ *holds for any* $0 \leq r \leq p$. *When* $r = 0$, *one can see that* $\theta^\top\varphi^i \in v_0^i$ *since* $\theta^\top\varphi^i = y^i - f_u(x^i) - \lambda^\top\psi^i u^i \in y^i - \mathcal{F}^i - \mathcal{Q}^0\psi^i u^i$ *and* $\theta^\top\varphi^i \in \mathcal{P}^{i-1}\varphi^i$. *Then, we assume* $\theta^\top\varphi^i - \sum_{l=1}^{r-1}\theta_l\varphi_l^i \in v_{r-1}^i$ *holds. It can be seen that*

$$\theta^\top\varphi^i - \sum_{l=1}^{r}\theta_l\varphi_l^i = \theta^\top\varphi^i - \sum_{l=1}^{r-1}\theta_l\varphi_l^i - \theta_r\varphi_r^i \in v_{r-1}^i - \theta_r\varphi_r^i \in v_{r-1}^i - \mathcal{P}_r^{i-1}\varphi_r^i. \tag{3.37}$$

On the other hand, one can see

$$\theta^\top \varphi^i - \sum_{l=1}^{r} \theta_l \varphi_l^i = \sum_{l=r+1}^{p} \theta_l \varphi_l^i \in \sum_{l=r+1}^{p} \mathcal{P}_l^{i-1} \varphi_l^i. \tag{3.38}$$

Summarizing the discussion above, one can conclude that $\theta^\top \varphi^i - \sum_{l=1}^{r} \theta_l \varphi_l^i \in (v_{r-1}^i - \mathcal{P}_r^{i-1} \varphi_r^i) \cap (\sum_{l=r+1}^{p} \mathcal{P}_l^{i-1} \varphi_l^i) = v_r^i$.

Finally, we will prove $\theta^\top \in \mathcal{P}^i$ *for any* $0 \leq i \leq N$ *using mathematical induction. For* $i = 0$, $\theta^\top \in \mathcal{P}^0$ *because of Assumption 3.2. Then we assume* $\theta^\top \in \mathcal{P}^{i-1}$. *Note that* $\theta^\top \varphi^i = y^i - f_u(x^i) - \lambda^\top \psi^i u^i \in y^i - \mathcal{F}^i - \mathcal{Q}^0 \psi^i u^i$ *and* $\theta^\top \varphi^i \in \mathcal{P}^{i-1} \varphi^i$, *which implies that* $\theta^\top \varphi^i \in v_0^i$. *It can be seen that for any* $r \in [p]$ *one has*

$$\theta_r \varphi_r^i = \theta^\top \varphi^i - \sum_{l=1}^{r-1} \theta_l \varphi_l^i - \sum_{l=r+1}^{p} \theta_l \varphi_l^i \in v_{r-1}^i - \sum_{l=r+1}^{p} \mathcal{P}_l^{i-1} \varphi_l^i. \tag{3.39}$$

Moreover, noticing that $\theta_r \varphi_r^i \in \mathcal{P}_r^{i-1} \varphi_r^i$, *we have* $\theta_r \in \mathcal{P}_r^i$ *for any* $r \in [p]$, *which indicates* $\theta^\top \in \mathcal{P}^i$. *Following the similar procedure above, one can prove that* $\lambda^\top \in \mathcal{Q}^i$. □

Remark 3.7 *With tighter bounds on* θ, λ *and* f_u *provided by Theorem 3.3, a larger admissible set* $K_{BF}(x)$ *as defined in* (3.6) *can be obtained. As a result, the data-driven-augmented, aCBF-NLP controller tends to have a better control performance while always ensuring safety. It is expected that the system's performance will be improved if the dataset* $\mathcal{E}$ *is large enough and the data in* $\mathcal{E}$ *are sufficiently "diverse" (i.e., the whole state space is sufficient explored), but a formal proof is still under our investigation. The Lipschitz constant* L *is needed in Theorem 3.3 to induce the bounds of* f_u *from a finite number of data. A lot of existing work can be leveraged to estimating the Lipschitz constant of an unknown function, such as [98], [99]. Moreover, the data-driven approach can be also combined with the aCBF-based controller shown in* (3.33) *to reduce its conservatism.*

3.4 Numerical Simulations

In this section, three examples are provided to demonstrate the effectiveness of the proposed control methods.

Example 3.1 *Consider the following single-input system:*

$$\dot{x} = f_u + \theta_1 \sin(x) + \theta_2 x^2 + (\lambda_1 + \lambda_2 x^2)u, \tag{3.40}$$

where $x \in \mathbb{R}$ *is the state and* $u \in \mathbb{R}$ *is the control input. The function* $f_u = \cos(x)$ *is unknown in the controller design; we choose the bounds of* f_u *as* $f_u \in [-2, 2]$ *such that Assumption 3.1 holds. The true values of the parameters* $\theta_1 = \theta_2 = 2, \lambda_1 = 1, \lambda_2 = 2$ *are unknown in the controller design; we choose the bounds of these parameters as* $\theta_1, \theta_2, \lambda_1, \lambda_2 \in [-10, 10]$ *such that Assumption 3.2 holds. Note that loose bounds of the unknown parameters and the function are chosen deliberately. It is easy to verify that Assumption 3.3 is satisfied with* $b = 0.5$*. We choose the safe set as* $\mathcal{C} = \{x : h(x) \geq 0\}$ *where* $h(x) = x - 1$*, that is, we aim to make* $x(t) \geq 1$ *for all* $t \geq 0$*. The initial condition of* (3.1) *is chosen as* $x(0) = 2$*, the reference trajectory is selected as* $x_d = 3\sin(t)$ *and the nominal control* u_d *is designed via feedback linearization.*

First, we demonstrate the performance of the safe controller obtained from (aCBF-NLP)*. We choose the nominal values of the unknown parameters* $\theta_1^0 = \theta_2^0 = \lambda_2^0 = 0, \lambda_1^0 = 0.5$*, which result in* $\bar{\mu} = \bar{\nu} = 15$*, and positive constants* $\epsilon_1 = \epsilon_2 = 0.001, \gamma^\theta = 550, \gamma^\lambda = 300, \gamma = 800$ *and* $\hat{\mu}(0) = \hat{\nu}(0) = 0.1$*. One can verify that Condition (iv) of Theorem 3.1 holds with the given initial condition, and Condition (ii) of Theorem 3.1 holds because* $\Psi_1 = \lambda_1^0 + \lambda_2^0 x^2 = 0.5 > 0$ *for any* $x \in \mathcal{C}$*, which implies that* $K_{BF} \neq \emptyset$*. Therefore, all conditions of Theorem 3.1 are satisfied. Applying the safe controller obtained from* (aCBF-NLP)*, the state evolution of the closed-loop system is shown as the blue line in Figure 3.2(a). One can observe that safety is always guaranteed (i.e., the state does not cross the safety boundary represented by the dashed red line) in the presence of parameter uncertainties and the reference trajectory is well-tracked within the safe set. The evolution*

of the control input is shown as the blue line in Figure 3.2(b).

Next, we consider the aCBF-NLP-based safe controller combined with the data-driven approach. We assume that f_u has a Lipschitz constant $L = 1$ and a dataset of 10 points are given. By using Theorem 3.3, bounds of the unknown parameters are tightened as $\theta_1 \in [-0.5042, 4.8060]$, $\theta_2 \in [1.8848, 2.0618]$, $\lambda_1 \in [0.9050, 1.1550]$, and $\lambda_2 \in [0.8471, 3.6036]$. With these new bounds, we choose the nominal parameters as $\theta_1^0 = 2.1509, \theta_2^0 = 1.9733, \lambda_1^0 = 1.03, \lambda_2^0 = 2.2254$, which result in $\bar{\mu} = 2.6566, \bar{\nu} = 1.3839$. We select $\gamma^\theta = 60$, $\gamma^\lambda = 30$ in Theorem 3.1 with parameters $\epsilon_1, \epsilon_2, \gamma^\theta, \gamma^\lambda, \gamma, \hat{\mu}(0), \hat{\nu}(0)$ chosen the same as above. Applying the data-driven augmented, aCBF-NLP-based safe controller, the state evolution of the closed-loop system is shown as the pink line in Figure 3.2(a). One can observe that this controller can also ensure safety and has a better tracking performance than the aCBF-NLP-based controller without parameter update, since it can better track the reference trajectory inside the safe region and it can be closer to the boundary of the safe set when the reference trajectory is outside the safe region. The evolution of the control input is shown as the pink line in Figure 3.2(b).

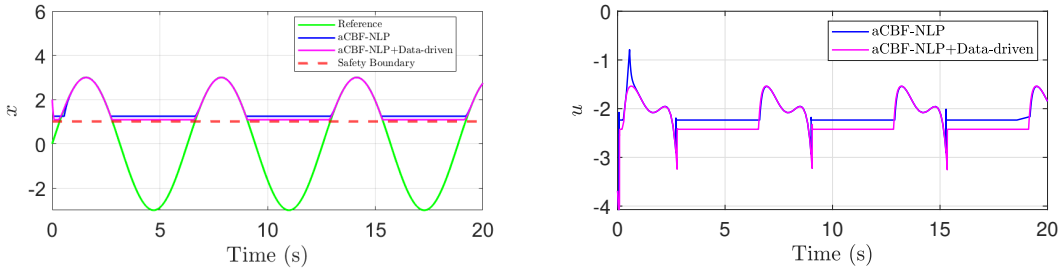

(a) Evolution of the state variable x (b) Evolution of the control input u

Figure 3.2: Simulation results of Example 3.1.

Example 3.2 *Consider the following adaptive cruise control system [76]:*

$$\frac{\mathrm{d}}{\mathrm{d}t}\begin{bmatrix} D \\ v_l \\ v_f \end{bmatrix} = \begin{bmatrix} v_l - v_f \\ a \\ -\frac{1}{m}(f_0 + f_1 v_f + f_2 v_f^2) \end{bmatrix} + \begin{bmatrix} 0 \\ 0 \\ \frac{1}{m} \end{bmatrix} u, \tag{3.41}$$

where v_l and v_f are the velocities of the lead car and the following car, respectively, D is the distance between the two vehicles, u is the control input, $F_r \triangleq f_0 + f_1 v_f + f_2 v_f^2$ is the aerodynamic drag term with constants f_0, f_1, f_2, and m is the mass of the following car. The true values of the parameters $f_0 = 0.1N, f_1 = 5N \cdot s/m, f_2 = 0.25N \cdot s^2/m, m = 1650\ kg$ are unknown in the controller design. We assume that $f_0 \in [0, 10]$, $f_1 \in [0, 50]$, $f_2 \in [0, 20]$, $m \in [100, 3000]$, and let $\theta = \frac{1}{m}[-f_0\ -f_1\ -f_2]^\top$, $\varphi(v_f) = [1\ v_f\ v_f^2]^\top$, $\lambda = \frac{1}{m}$; one can easily see that Assumption 3.2 is satisfied with $\theta_1 \in [-0.1, 0]$, $\theta_2 \in [-0.5, 0]$, $\theta_3 \in [-0.2, 0]$, $\lambda \in [0.00033, 0.01]$. Note that in (3.41) $f_u = 0$, such that we selected $\underline{f}_u = \overline{f}_u = 0$, from which one can see Assumption 3.1 is satisfied. Meanwhile, from (3.41) one can easily verify that Assumption 3.3 holds with $b = 1/3000$. The safety constraint of the following car is to keep a safe distance from the lead car, which can be expressed as $D/v_f \geq 1.8$ where 1.8 is the desired time headway in seconds. Therefore, the safe set is $\mathcal{C} = \{x : h(x) \geq 0\}$ where $h = D - 1.8v_f$. The nominal controller u_d is designed to keep the following car at a desired speed $v_{f,des} = 22\ m/s$.

Applying the safe controller obtained from (aCBF-NLP)*, the state and CBF evolution are shown as the blue lines in Figure 3.3. Next, we consider the aCBF-NLP-based controller augmented with a dataset of 5 datapoints. The state and CBF evolution of the closed-loop system with the data-driven-augmented aCBF-NLP controller are shown as the brown lines in Figure 3.3. One can see that both controllers can ensure safety in the presence of parameter uncertainties since $h(t) \geq 0$ for any $t > 0$; moreover, when the data-driven approach is employed, the aCBF-NLP controller has a better performance.*

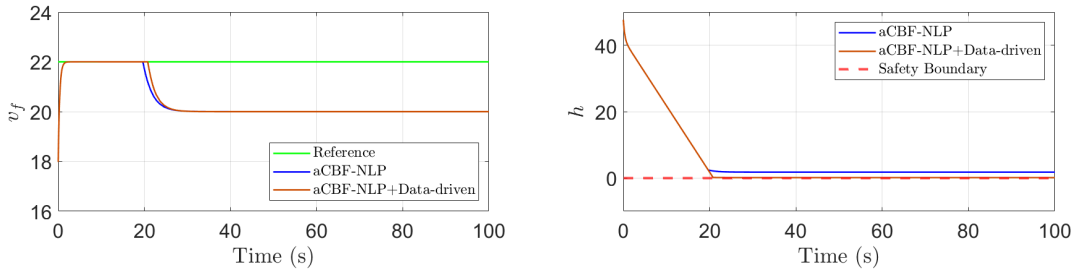

(a) Evolution of v_f (b) Evolution of h

Figure 3.3: Simulation results of Example 3.2.

Example 3.3 *Consider the mass-spring system as follows:*

$$\frac{\mathrm{d}}{\mathrm{d}t}\begin{bmatrix} x_1 \\ x_2 \\ \dot{x}_1 \\ \dot{x}_2 \end{bmatrix} = \begin{bmatrix} 0 & 0 & 1 & 0 \\ 0 & 0 & 0 & 1 \\ -\frac{k_1+k_2}{m_1} & \frac{k_2}{m_1} & 0 & 0 \\ \frac{k_2}{m_2} & -\frac{k_2}{m_2} & 0 & 0 \end{bmatrix}\begin{bmatrix} x_1 \\ x_2 \\ \dot{x}_1 \\ \dot{x}_2 \end{bmatrix} + \begin{bmatrix} 0 & 0 \\ 0 & 0 \\ \frac{1}{m_1} & 0 \\ 0 & \frac{1}{m_2} \end{bmatrix}\begin{bmatrix} u_1 \\ u_2 \end{bmatrix}, \tag{3.42}$$

where $x_1, x_2 \in \mathbb{R}$ *denote the position of two mass points,* $u_1, u_2 \in \mathbb{R}$ *are control inputs,* $m_1 = m_2 = 0.2$ *represent the mass, and* $k_1 = k_2 = 1$ *denote the stiffness of two springs. We assume that all functions in* (3.42) *are known, that is,* $f_u = 0$*. Define* $\theta_1 = [-\frac{k_1+k_2}{m_1} \ \frac{k_2}{m_1}]^\top = [-10 \ 5]^\top$*,* $\theta_2 = [\frac{k_2}{m_2} \ -\frac{k_2}{m_2}]^\top = [5 \ -5]^\top$*,* $\lambda_1 = \frac{1}{m_1} = 5$*, and* $\lambda_2 = \frac{1}{m_2} = 5$*, which are unknown parameters in control design. One can easily verify that Assumption 3.2 is fulfilled with* $m_1, m_2 \in [0.1, 0.5]$ *and* $k_1, k_2 \in [0, 5]$*, such that* $[-100 \ 0]^\top \leq \theta_1 \leq [0 \ 50]^\top$*,* $[0 \ -50]^\top \leq \theta_1 \leq [50 \ 0]^\top$*,* $\lambda_1 \in [2, 10]$*, and* $\lambda_2 \in [2, 10]$*. It is obvious that Assumption 3.3 is fulfilled with* $b_1 = b_2 = 1$*. The desired trajectories are selected as* $x_{1d} = 0$*,* $x_{2d} = 1 + \sin(t)$*, with a nominal PD controller* u_d *designed to track* x_{1d}*,* x_{2d}*, The safe set is defined as* $\mathcal{C} = \{x : h(x) \geq 0\}$ *with* $h = x_2 - x_1 - 0.5$*, which aims to keep the distance between two masses. Note that the relative degree of* h *is equal to 2.*

We first consider the aCBF-NLP-based controller proposed in Theorem 3.1. Applying the safe controller obtained from (aCBF-NLP)*, the state and CBF evolution are shown as the blue lines in Figure 3.4. Then, the aCBF-NLP-based controller is augmented with a dataset of 4 datapoints. The state and CBF evolution are represented by the brown lines in Figure 3.4. It can be seen that both controllers can guarantee the safety since* $h(x(t)) \geq 0$ *for any* $t > 0$*, while the performance of the aCBF-NLP controller is improved if the data-driven approach is adopted.*

Finally, we show how the results of Theorem 3.2 can be applied to (3.42)*. From now on we do not assume* g *and* g_λ *are diagonal matrices. It is easy to verify that Assumptions 3.1, 3.4, 3.5 hold true with* $b^* = 1$*,* $\lambda_{11}, \lambda_{22} \in [-1, 1]$*,* $\lambda_{12}, \lambda_{21} \in [2, 10]$*,* $[-100 \ 0]^\top \leq \theta_1 \leq [0 \ 50]^\top$*, and* $[0 \ -50]^\top \leq \theta_1 \leq [50 \ 0]^\top$*. Applying the safe control law obtained from*

(3.33), *the state and CBF evolution are shown in Figure 3.5, from which one can see that the safety is ensured since* $h(x(t)) \geq 0$ *for any* $t > 0$. *However, from Figure 3.5(a) and 3.5(b), it can be seen that the control performance is conservative, i.e., the desired control performance is not well preserved inside the safe region. This phenomenon verifies what we discussed in Remark 3.6, i.e.,* u *might not be close to* u_d *since it is always proportional to the partial derivative of* h.

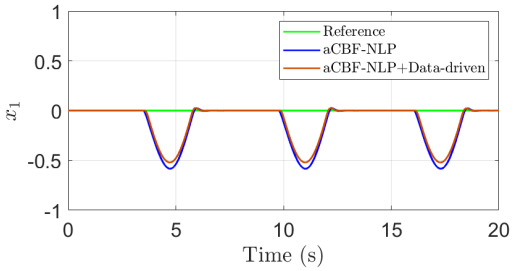

(a) Evolution of x_1

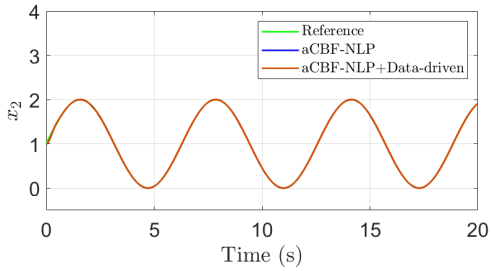

(b) Evolution of x_2

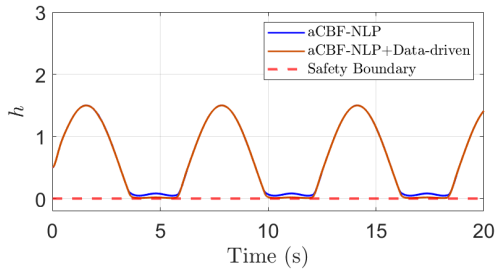

(c) Evolution of h

Figure 3.4: Simulation results of Example 3.3 using (aCBF-NLP).

3.5 Chapter Summary and Future Directions

In this chapter, we propose a singularity-free aCBF-NLP-based control strategy for systems with parametric uncertainties in both drift terms and control-input matrices, where the solution to the aCBF-NLP has a closed form. Furthermore, a data-driven approach is developed to tighten the bounds of the unknown parameters and functions such that the performance of the proposed controller can be improved. Simulation results are also presented to validate the proposed approach.

The aCBF-NLP-based controller developed in this chapter can only be applied to a

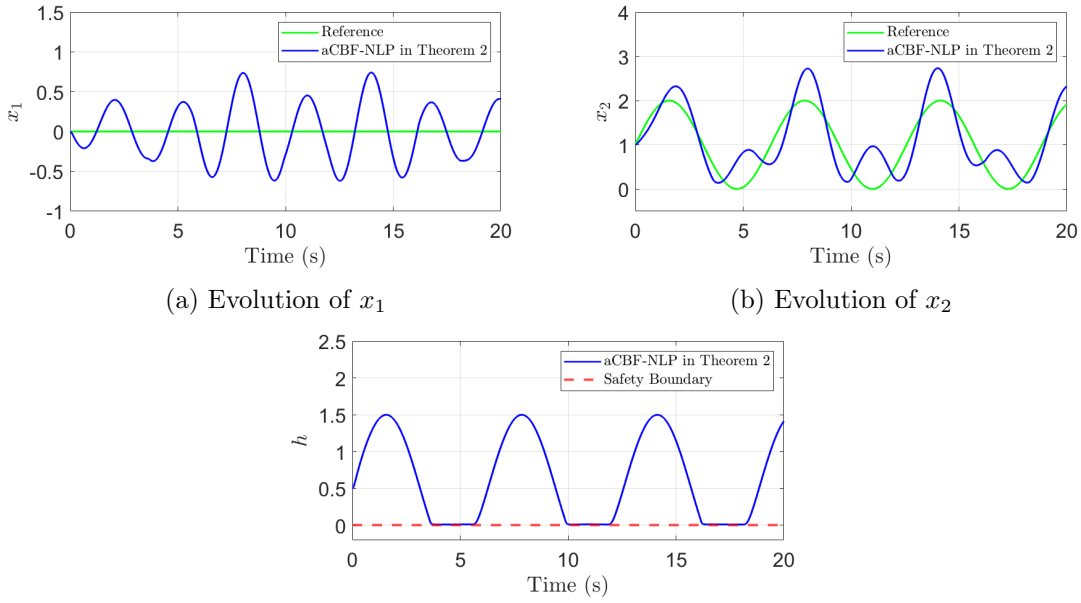

(a) Evolution of x_1

(b) Evolution of x_2

(c) Evolution of h

Figure 3.5: Simulation results of Example 3.3 using (3.33).

special class of systems with diagonal control-input matrices, which limits the applicability of this method to physical systems. Furthermore, the strong controllability assumption presented in Assumption 3.3 is hard to satisfy for many systems. Future work includes extending the proposed method to more general systems and relaxing the assumptions.

In addition, the convergence of the data-driven approach proposed in Section 3.3.4 is not investigated. Intuitively, the system's performance will be improved if the dataset is large enough and the data are sufficiently "diverse" (i.e., the whole state space is sufficient explored), but a formal proof is still lacking. Moreover, the Lipschitz constant L is needed in Theorem 3.3 to induce the bounds of f_u from a finite number of data, while obtaining Lipschitz constants is challenging in many cases. A promising direction for future work is to derive the convergence condition of the proposed data-driven method and estimate the Lipschitz constant using data.

Chapter 4

CBF-based Control for Strict-feedback Systems With Limited Model Information

4.1 Introduction

In Chapters 2 and 3, robust and adaptive CBF-based safe control approaches are developed for systems with unstructured and structured uncertainties, respectively. While these methods provide rigorous safety guarantees, they rely on the availability of certain model information. Specifically, the IIDOB-CBF-QP framework assumes the existence of a nominal system model, and the adaptive CBF-QP approach requires knowledge of the uncertainty structure. In some practical applications, however, such assumptions are difficult to satisfy. For instance, obtaining accurate expressions of the inertia matrix, Coriolis and centripetal terms, and gravity vector of a robotic manipulator can be challenging due to modeling complexity. These limitations motivate the development of CBF-based control strategies for systems with limited model information.

CBF-based safe control for systems with limited model information is not well investigated in the literature, while in contrast, several Lyapunov-based safe control methods,

such as BLFs [4] and PPC [15], have been developed to ensure safety for systems with unknown dynamics. Despite their effectiveness, Lyapunov-based approaches suffer from several inherent limitations when compared with the CBF framework. In particular, they impose more structural restrictions on constraints and require a coupled design of the control objective and safety specification, thereby reducing flexibility in controller design. Consequently, it is highly desirable to integrate the complementary strengths of Lyapunov-based and CBF-based approaches, enabling the synthesis of safe controllers for systems with limited model information while retaining the advantages of CBF-based control.

This chapter introduces a Proxy Control Barrier Function (PCBF) control strategy that follows a modular design scheme to integrate CBF-based and Lyapunov-based methods for strict-feedback systems with limited model information. Specifically, the original system is decomposed into a proxy subsystem and a virtual tracking subsystem; the proxy subsystem generates a safe (virtual) reference trajectory and is controlled by a CBF-based controller, while the virtual tracking subsystem is controlled by a Lyapunov-based output-constrained controller to ensure the boundedness of the tracking error (see Figure 4.1). The modularity of the proposed PCBF method offers superior flexibility in control design and combines the advantages of both CBF-based and Lyapunov-based approaches. By leveraging Lyapunov-based tools, the PCBF method can be employed to design safe controllers for systems with unknown dynamics that existing CBF-based methods cannot handle. Moreover, the CBF design process in the PCBF method is significantly simplified because the validity of the CBF does not rely on the full dynamics, allowing distinct systems with the same proxy subsystem to share an identical CBF design.

The main contributions of this chapter are summarized as follows.

- A PCBF control design scheme that integrates CBF-based and Lyapunov-based methods is proposed for strict-feedback systems with limited model information.
- A PCBF-based control approach is developed for strict-feedback systems with mismatched disturbances using a new filter-based DOB.

Parts of this chapter are adapted from previously published work in [100], [101]

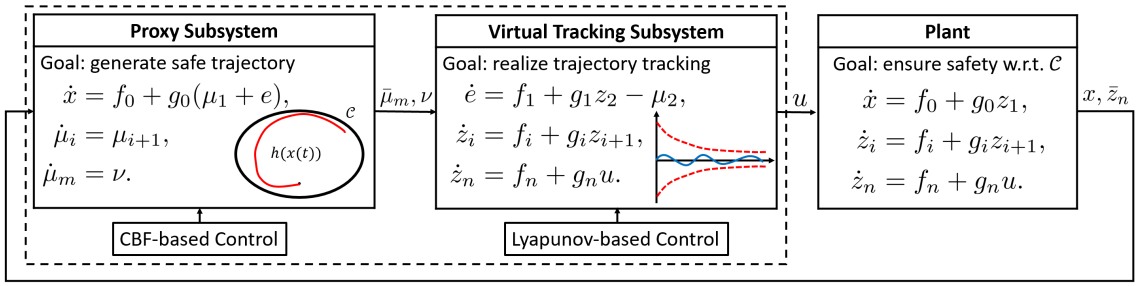

Figure 4.1: Illustration of the proposed PCBF control scheme.

4.2 Motivation and Problem Formulation

4.2.1 Motivation Example

Partly because CBFs lack favorable structural properties of Lyapunov functions (e.g., positive definiteness), there are certain systems that CBFs cannot handle but have been extensively studied by Lyapunov-based methods in the context of stabilizing control design. Consider the following Norrbin model for ship steering [102]:

$$\dot{x}_1 = x_2, \tag{4.1a}$$

$$\dot{x}_2 = bu + \theta^\top \varphi(x_2), \tag{4.1b}$$

where $x_1 = \psi \in \mathbb{R}$ is the yaw angle, $x_2 = \dot{\psi} \in \mathbb{R}$ is the yaw rate, $u \in \mathbb{R}$ is the rudder angle as the control input, $\theta = [-\frac{1}{T} \ -\frac{\alpha}{T}]^\top$, $\varphi(x_2) = [x_2 \ x_2^3]^\top$, $b = \frac{K}{T}$, $K > 0$ is the gain constant, T is the time constant, and α is the Norrbin coefficient determined via a spiral test. Here, θ and b are considered as unknown parameters, and b is either positive or negative and its sign is unknown; see [102] and [103, Section 5.5] for more explanations.

Suppose that the goal is to design a safe controller for system (4.1) with respect to a given safe set $\mathcal{C} = \{x_1 : h(x_1) \geq 0\}$ with h a continuously differentiable function. To the best of our knowledge, CBF-based control strategies are not yet developed for systems with unknown control coefficients; if robust CBF methods (e.g., [17]) are applied, the resulting QP could be infeasible since the sign of b is unknown. On the other hand, the Nussbaum-gain-based adaptive control methods have been developed to stabilize systems

with unknown control coefficients [104]. Then, one natural question is: can we combine CBF-based safe control methods and Lyapunov-based stabilizing control methods, such that we can bring the best from both worlds to design a safe controller?

Observing the structure of system (4.1), one may consider the system as two subsystems with x_2 as the input in (4.1a). To design a safe controller, one potential idea is to design a CBF-based control law for (4.1a) to generate a safe reference trajectory for x_2 that ensures the (robust) forward invariance of $\mathcal{C}$, and a Lyapunov-based output-constrained controller for (4.1b) to ensure the boundedness of the tracking error. In this chapter, we will systematize this idea and propose a modular safe control design method for strict-feedback systems with theoretical guarantees.

4.2.2 Problem Formulation

Consider a strict-feedback system described as follows:

$$\dot{x} = f_0(x) + g_0(x)z_1, \tag{4.2a}$$

$$\dot{z}_1 = f_1(x, z_1) + g_1(x, z_1)z_2, \tag{4.2b}$$

$$\vdots$$

$$\dot{z}_{n-1} = f_{n-1}(x, z_1, \ldots, z_{n-1}) + g_{n-1}(x, z_1, \ldots, z_{n-1})z_n, \tag{4.2c}$$

$$\dot{z}_n = f_n(x, z_1, \ldots, z_n) + g_n(x, z_1, \ldots, z_n)u, \tag{4.2d}$$

where $x \in \mathbb{R}^p$, $z_i \in \mathbb{R}^{p_i}$, $i \in [n]$, are state variables, $u \in \mathbb{R}^q$ is the control input, f_0 and g_0 are sufficiently smooth and known functions, and f_i, g_i, $i \in [n]$, are sufficiently smooth functions that are possibly unknown. Define a safe set $\mathcal{C}$ as follows:

$$\mathcal{C} = \{x \in \mathbb{R} : h(x) \geq 0\} \tag{4.3}$$

where $h : \mathbb{R}^p \to \mathbb{R}$ is a sufficiently smooth function.

The problem investigated in this paper is stated as follows.

Problem 4.1 *Given the system shown in* (4.2) *and the safe set* $\mathcal{C}$ *defined in* (4.3)*, design a controller* u *such that the closed-loop system is safe with respect to* $\mathcal{C}$*, i.e.,* $h(x(t)) \geq 0, \forall t \geq 0$.

The main challenge in solving Problem 2.1 lies in the presence of unknown functions f_i and g_i, $i \in [n]$. To the best of our knowledge, no safe control design method exists for system (4.2) if f_i and g_i are completely unknown. Moreover, it is reasonable to assume an exact knowledge of f_0 and g_0 for many practical systems such as Euler-Lagrange systems.

4.3 Proxy CBF-based Control Design

The PCBF method follows a modular design scheme and consists of three parts: (i) decompose system (4.2) into a proxy subsystem and a virtual tracking subsystem, (ii) design a CBF-based controller for the proxy subsystem to generate a (virtual) safe trajectory, and (iii) design a Lyapunov-based tracking controller for the virtual tracking subsystem to ensure the boundedness of the tracking error. Because the CBF-based and Lyapunov-based control design are decoupled, the PCBF method offers flexibility for safe control design as will be shown below.

4.3.1 System Decomposition Scheme

We decompose the strict-feedback system shown in (4.2) into the proxy subsystem:

$$\dot{x} = f_0(x) + g_0(x)\mu_1 + g_0(x)e, \tag{4.4a}$$

$$\dot{\mu}_1 = \mu_2, \tag{4.4b}$$

$$\vdots$$

$$\dot{\mu}_{m-1} = \mu_m, \tag{4.4c}$$

$$\dot{\mu}_m = \nu, \tag{4.4d}$$

and the virtual tracking subsystem:

$$\dot{e} = f_1(x, e+\mu_1) + g_1(x, e+\mu_1)z_2 - \mu_2, \tag{4.5a}$$

$$z_2 = f_2(x, e+\mu_1, z_2) + g_2(x, e+\mu_1, z_2)z_3, \tag{4.5b}$$

$$\vdots$$

$$\dot{z}_{n-1} = f_{n-1}(x, e+\mu_1, z_2, \ldots, z_{n-1}) + g_{n-1}(x, e+\mu_1, z_2, \ldots, z_{n-1})z_n, \tag{4.5c}$$

$$\dot{z}_n = f_n(x, e+\mu_1, z_2, \ldots, z_n) + g_n(x, e+\mu_1, z_2, \ldots, z_n)u, \tag{4.5d}$$

where $e = z_1 - \mu_1$ is the virtual tracking error, $\nu \in \mathbb{R}^{p_1}$ is the virtual control input to be designed, and $\mu_1, \mu_2, \cdots, \mu_m \in \mathbb{R}^{p_1}$ are virtual states with the number $m \leq n$ a positive integer to be determined. The initial conditions of the virtual states are selected as $\mu_1(0) = z_1(0)$ and $\mu_i(0) = 0$ for $i = 2, \cdots, m$.

The proxy subsystem (4.4) consists of dynamics of x and a chain of integrators, which mainly serve to provide the explicit forms of the derivatives of μ_1 as will be explained later; the virtual tracking subsystem (4.5) consists of error dynamics of e, which is derived from (4.2b) and (4.4b), and equations of $z_3, z_4, \ldots, z_n$.

Given the system decomposition shown in (4.4)-(4.5), the safe control design problem for system (4.2) will be solved by accomplishing the following two tasks:

- Design a CBF-based control law ν for the subsystem (4.4) to ensure $h(x(t)) \geq 0, \forall t \geq 0$, under the assumption

$$\|e(t)\| \leq \rho(t), \quad \forall t \geq 0, \tag{4.6}$$

  where $\rho : \mathbb{R}_{\geq 0} \to \mathbb{R}_{>0}$ is a predefined smooth bounded function whose derivatives up to n-th order are bounded.

- Design a Lyapunov-based control law u for the subsystem (4.5) to ensure (4.6) holds.

As will be explained in the next three subsections, these two tasks can be accomplished separately, and the controllers constructed for the two subsystems together provide a solution to Problem 4.1.

4.3.2 Proxy Subsystem Control Design

The main difficulty of designing a CBF-based controller for the proxy subsystem (4.4) lies in the existence of e, which is considered as a mismatched disturbance to be rejected and has a relative degree lower than that of the virtual input ν, implying it is difficult to completely decouple e [80]. To address this issue, we define a set of functions $b_i, i \in [m]$ as follows:

$$b_i(\bar{\mu}_i, \bar{y}_i, y_0, x, t) = \mathcal{M}_i(f_0 + g_0\mu_1) - \frac{\|\mathcal{M}_i g_0\|^2}{2\beta_i} - \frac{\beta_i}{2}\rho^2 + \lambda_i b_{i-1} + \frac{\partial b_{i-1}}{\partial t} + \sum_{j=1}^{i-1} \frac{\partial b_{i-1}}{\partial \mu_j}\mu_{j+1}, \quad (4.7)$$

where

$$\mathcal{M}_i = \frac{1}{\xi}\sum_{j=0}^{i-1} \frac{\partial b_{i-1}}{\partial y_j}\frac{\partial h}{\partial x}y_{j+1} + \frac{\partial b_{i-1}}{\partial x}, \ i \in [m+1], \quad (4.8)$$

ξ, β_i, λ_i for $i \in [m]$ are positive constants, $y_0 = \chi(h/\xi)$, $y_i = \chi^{(i)}(h/\xi)$ for $i \in [m]$, and $b_0 = y_0$. Here, $\chi : \mathbb{R} \to \mathbb{R}$ is a $(m+1)$-th order differentiable function satisfying $\chi(0) = 0$, $\chi(\tau) = 1$ for $\tau \geq 1$, and $\frac{\mathrm{d}\chi}{\mathrm{d}\tau} > 0$ for $\tau < 1$ [95].

With these notations, the following theorem presents a CBF-based control design method for proxy subsystem (4.4) to ensure $h(x(t)) \geq 0, \forall t \geq 0$, under assumption (4.6).

Theorem 4.1 *Consider the proxy subsystem* (4.4) *and the safe set* $\mathcal{C}$ *defined in* (4.3). *Suppose that condition* (4.6) *holds, and there exist* $\xi > 0$, $\lambda_i > 0$, $i \in [m+1]$, *and* $\beta_i > 0$, $i \in [m]$, *such that*

(i) for any $x \in \mathcal{C}$, $L_{g_0}h = 0 \Rightarrow h \geq \xi$ *holds;*

(ii) for any $t \geq 0$, $\sum_{j=2}^{m+1} \frac{\beta_{j-1}}{2}\left(\frac{\mathrm{d}}{\mathrm{d}t} + \lambda_j\right) \circ \cdots \circ \left(\frac{\mathrm{d}}{\mathrm{d}t} + \lambda_{m+1}\right) \circ \rho(t)^2 \leq \Pi_{j=1}^{m+1}\lambda_j$ *holds;*

(iii) $y_0(0) > 0$ *and* $b_i(\bar{\mu}_i(0), \bar{y}_i(0), y_0(0), x(0), 0) > 0$ *for* $i \in [m]$ *where* b_i *is defined in* (2.22).

Then, for any $x \in \mathcal{C}$ *and* $\mu_1, \cdots, \mu_m \in \mathbb{R}^{p_1}$, *the set*

$$K_{BF} = \{\mathfrak{v} \in \mathbb{R} : \psi_0 + \psi_1\mathfrak{v} \geq 0\} \quad (4.9)$$

is non-empty, where

$$\psi_0 = \frac{\partial b_m}{\partial t} + \sum_{j=1}^{m-1} \frac{\partial b_m}{\partial \mu_j}\mu_{j+1} + \mathcal{M}_{m+1}(f_0 + g_0\mu_1) + \lambda_{m+1}b_m - \|\mathcal{M}_{m+1}g_0\|\rho, \quad (4.10a)$$

$$\psi_1 = \frac{\partial b_m}{\partial \mu_m}, \quad (4.10b)$$

with $\mathcal{M}_{m+1}$ defined in (4.8)*. Moreover, any Lipschitz continuous controller $\nu \in K_{BF}$ ensures $h(x(t)) \geq 0$, $\forall t \geq 0$.*

Proof *The proof consists of four steps. We will first show b_i in* (4.7) *can be expressed as the sum of three functions, and then the non-emptiness of K_{BF}. After that we will show $b_m \geq 0$, and $b_i \geq 0 \implies b_{i-1} \geq 0$ holds for $i \in [m]$. Finally, we will prove $b_0 \geq 0 \implies h \geq 0, \forall t \geq 0$.*

(i) Expression of b_i. *We claim that b_i in* (2.22) *can be expressed as the sum of three functions.*

Claim. *The function b_i defined in* (2.22) *can be expressed in the following form for any $i \in [m]$:*

$$b_i = s_i(x, \bar{\mu}_i, \bar{y}_i) + l_i(y_0) + T_i(t) \quad (4.11)$$

where $s_i = \sum_{k=1}^{n_i} \varphi_i^k(x, \bar{\mu}_i)\bar{y}_i^{\alpha_i^k}$ is a polynomial function of $\bar{y}_i$ for fixed $x, \bar{\mu}_i$, $l_i = \prod_{j=1}^{i} \lambda_j y_0$ is a linear function of y_0, and

$$T_i = -\frac{\beta_i}{2}\rho^2 - \sum_{j=2}^{i} \frac{\beta_{j-1}}{2}\left(\frac{\mathrm{d}}{\mathrm{d}t} + \lambda_j\right) \circ \cdots \circ \left(\frac{\mathrm{d}}{\mathrm{d}t} + \lambda_i\right) \circ \rho(t)^2 \quad (4.12)$$

is a time-varying function. In the expression of s_i, n_i is a non-negative integer, φ_i^k is a function whose form can be uniquely determined, $\bar{y}_i^{\alpha_i^k} = y_1^{\alpha_{i1}^k} y_2^{\alpha_{i2}^k} \dots y_i^{\alpha_{ii}^k}$ where $\bar{y}_i = [y_1\ y_2\ \cdots\ y_i]^\top$ and $\alpha_i^k = [\alpha_{i1}^k\ \alpha_{i2}^k\ \dots\ \alpha_{ii}^k]^\top$ is a vector of non-negative integers satisfying $\|\alpha_i^k\|_1 \geq 1$, which implies that $\varphi_i^k(x, \bar{\mu}_i)\bar{y}_i^{\alpha_i^k}$ can not be a constant for fixed x and $\bar{\mu}_i$.

We will prove the claim using mathematical induction. For $i = 1$, from (2.22) *we can*

rewrite b_1 *in the following form:*

$$b_1 = \underbrace{\frac{1}{\xi}\frac{\partial h}{\partial x}(f_0 + g_0\mu_1)y_1 - \frac{\left\|\frac{\partial h}{\partial x}g_0\right\|^2}{2\beta_1\xi^2}y_1^2}_{s_1} + \underbrace{\lambda_1 y_0}_{l_1} \underbrace{-\frac{\beta_1}{2}\rho^2}_{T_1} \tag{4.13}$$

which implies that (4.11) *holds when* $i = 1$.

Now assume that (4.11) *holds for* $i = d \geq 1$. *We only have to prove that* (4.11) *holds for* $i = d + 1$. *From* (4.8), *we have*

$$\mathcal{M}_{d+1} = \left(\frac{1}{\xi}\frac{\partial h}{\partial x}\prod_{j=1}^{d}\lambda_j\right)y_1 + \frac{1}{\xi}\frac{\partial h}{\partial x}\sum_{j=1}^{d}\sum_{k=1}^{n_d}\varphi_d^k\frac{\partial(\bar{y}_d^{\alpha_d^k})}{\partial y_j}y_{j+1} + \sum_{k=1}^{n_d}\frac{\partial\varphi_d^k}{\partial x}\bar{y}_d^{\alpha_d^k}. \tag{4.14}$$

It is clear that every term in any entry of $\mathcal{M}_{d+1}$ *(note that* $\mathcal{M}_{d+1}$ *is a vector) can be expressed in the form of* $\varphi_{d+1}^k(x, \bar{\mu}_{d+1})\bar{y}_{d+1}^{\alpha_{d+1}^k}$ *and it can not be a constant for fixed* x, $\bar{\mu}_{d+1}$. *It is also easy to verify that each term in* $\sum_{j=1}^{d}\frac{\partial b_d}{\partial \mu_j}\mu_{j+1}$ *can be expressed in the form of* $\varphi_{d+1}^k(x, \bar{\mu}_{d+1})\bar{y}_{d+1}^{\alpha_{d+1}^k}$ *because* $\frac{\partial b_d}{\partial \mu_j}\mu_{j+1} = \sum_{k=1}^{n_d}\left(\frac{\partial\varphi_d^k}{\partial\mu_j}\mu_{j+1}\right)\bar{y}_d^{\alpha_d^k}$. *Hence,* $\mathcal{M}_{d+1}(f_0 + g_0\mu_1) - \frac{\|\mathcal{M}_{d+1}g_0\|^2}{2\beta_{d+1}} + \sum_{j=1}^{d}\frac{\partial b_d}{\partial\mu_j}\mu_{j+1}$, *which is included as part of* b_{d+1}, *can be expressed in the form of* s_{d+1}.

In addition, since $\frac{\partial b_d}{\partial t} + \lambda_{d+1}b_d - \frac{\beta_{d+1}}{2}\rho^2$, *which are the rest terms in* b_{d+1}, *are equal to* $\sum_{k=1}^{n_d}(\lambda_{d+1}\varphi_k^d)\bar{y}_d^{\alpha_d^k} + \prod_{j=1}^{d+1}\lambda_j y_0 - \frac{\beta_{d+1}}{2}\rho^2 - \sum_{j=2}^{d+1}\frac{\beta_{j-1}}{2}\left(\frac{\mathrm{d}}{\mathrm{d}t} + \lambda_j\right)\circ\cdots\circ\left(\frac{\mathrm{d}}{\mathrm{d}t} + \lambda_{d+1}\right)\circ\rho^2$, *one can express the first summation term in the form of* s_{d+1}, *consider the second term* $\prod_{j=1}^{d+1}\lambda_j y_0$ *as* l_{d+1} *and the sum of the rest two terms as* T_{d+1}. *Hence,* b_{d+1} *can be expressed as* (4.11) *for* $i = d + 1$, *which completes the proof of the claim.*

(ii) Non-emptiness of K_{BF}. *We will show the non-emptiness of* K_{BF} *by proving that* $\psi_1 = 0 \implies \psi_0 \geq 0$ *holds for any* $x \in \mathcal{C}$ *and* $\mu_1, \cdots, \mu_m \in \mathbb{R}^{p_1}$. *First we claim that* $\frac{\partial b_i}{\partial\mu_i} = \frac{y_1}{\xi}L_{g_0}h$ *for* $i \in [m]$. *For* $i = 1$, *this claim is clear from* b_1 *given in* (4.13). *Assume that the claim is true for* $i = d$ *where* $d \geq 1$, *then, because the only term in* b_{d+1} *including* μ_{d+1} *is* $\frac{\partial b_d}{\partial\mu_d}\mu_{d+1}$, *implying that* $\frac{\partial b_{d+1}}{\partial\mu_{d+1}} = \frac{\partial b_d}{\partial\mu_d} = \frac{y_1}{\xi}L_{g_0}h$ *and thus the claim is true for* $i = d + 1$. *Hence, the claim is proved.*

Next, invoking (4.10b), *one can see* $\psi_1 = \frac{y_1}{\xi}L_{g_0}h$. *Now we assume* $\psi_1 = 0$, *which*

implies $y_1 = 0$ *or* $L_{g_0}h = 0$. *If* $y_1 = 0$, *one can see that* $h \geq \xi$ *from the definition of* χ. *Meanwhile, from Condition (i) one can see that* $L_{g_0}h = 0$ *indicates* $h \geq \xi$ *for any* $x \in \mathcal{C}$. *Note that* $h \geq \xi$ *implies* $y_0 = 1$ *and* $y_1 = y_2 = \cdots = y_{m+1} = 0$, *according to their definitions shown below* (2.22). *Hence, from* (4.11) *one can conclude*

$$b_m = \prod_{j=1}^{m} \lambda_j - \frac{\beta_m}{2}\rho^2 - \sum_{j=2}^{m} \frac{\beta_{j-1}}{2} \left(\frac{\mathrm{d}}{\mathrm{d}t} + \lambda_j\right) \circ \cdots \circ \left(\frac{\mathrm{d}}{\mathrm{d}t} + \lambda_m\right) \circ \rho^2 \tag{4.15}$$

because s_m *is a polynomial of* $\bar{y}_m$ *for fixed* x *and* $\bar{\mu}_m$ *(with no constant terms), meaning that it equals* 0 *as* $y_i = 0$, $i \in [m]$. *Moreover, invoking* (4.11), *one can readily verify that* $\frac{\partial b_m}{\partial x} = \frac{\partial p_m}{\partial x} = 0$ *and* $\sum_{j=0}^{m} \frac{\partial b_m}{\partial y_j} \frac{\partial h}{\partial x} \frac{y_{j+1}}{\xi} = 0$, *implying that* $\mathcal{M}_{m+1} = 0$. *Similarly, it can be shown* $\sum_{j=1}^{m-1} \frac{\partial b_m}{\partial \mu_j} \mu_{j+1} = 0$. *Thus, according to* (4.10a) *and* (4.11), *one can see*

$$\psi_0 = \frac{\partial b_m}{\partial t} + \lambda_{m+1} b_m = \frac{\partial T_m}{\partial t} + \lambda_{m+1} b_m = \prod_{j=1}^{m+1} \lambda_j - \sum_{j=2}^{m+1} \frac{\beta_{j-1}}{2} \left(\frac{\mathrm{d}}{\mathrm{d}t} + \lambda_j\right) \circ \cdots \circ \left(\frac{\mathrm{d}}{\mathrm{d}t} + \lambda_{m+1}\right) \circ \rho^2.$$

From Condition (ii), $\psi_0 \geq 0$, *meaning that* K_{BF} *is non-empty.*

(iii) $\nu \in K_{BF} \implies b_m \geq 0$. *One can see that*

$$\begin{aligned} \dot{b}_m + \lambda_{m+1} b_m &= \frac{\partial b_m}{\partial x}\dot{x} + \sum_{j=1}^{m-1} \frac{\partial b_m}{\partial \mu_j}\mu_{j+1} + \frac{\partial b_m}{\partial t} + \frac{\partial b_m}{\partial \mu_m}\nu + \sum_{j=0}^{m} \frac{\partial b_m}{\partial y_j}\frac{y_{j+1}}{\xi}\frac{\partial h}{\partial x}\dot{x} + \lambda_{m+1} b_m \\ &\geq \mathcal{M}_{m+1}(f_0 + g_0\mu_1) + \sum_{j=1}^{m-1} \frac{\partial b_m}{\partial \mu_j}\mu_{j+1} + \frac{\partial b_m}{\partial t} + \frac{\partial b_m}{\partial \mu_m}\nu + \lambda_{m+1} b_m - \|\mathcal{M}_{m+1} g_0\|\rho \\ &= \psi_0 + \psi_1 \nu. \end{aligned} \tag{4.16}$$

Hence, selecting $\nu \in K_{BF}$ *implies* $\dot{b}_m + \lambda_{m+1} b_m \geq 0$, *and thus* $b_m \geq 0$ *because* $b_m(\bar{\mu}_m(0), \bar{y}_m(0), y_0(0), x(0), 0) > 0$, *as shown in Condition (iii).*

(iv) $b_i \geq 0 \Rightarrow b_{i-1} \geq 0$ for any $i \in [m]$. *Note that*

$$\begin{aligned} \dot{b}_{i-1} + \lambda_i b_{i-1} &= \frac{\partial b_{i-1}}{\partial x}\dot{x} + \sum_{j=1}^{i-1} \frac{\partial b_{i-1}}{\partial \mu_j}\mu_{j+1} + \frac{\partial b_{i-1}}{\partial t} + \lambda_i b_{i-1} + \sum_{j=0}^{i-1} \frac{\partial b_{i-1}}{\partial y_j}\frac{y_{j+1}}{\xi}\frac{\partial h}{\partial x}\dot{x} \\ &\geq \mathcal{M}_i(f_0 + g_0\mu_1) + \sum_{j=1}^{i-1} \frac{\partial b_{i-1}}{\partial \mu_j}\mu_{j+1} + \lambda_i b_{i-1} + \frac{\partial b_{i-1}}{\partial t} - \frac{\|\mathcal{M}_i g_0\|^2}{2\beta_i} - \frac{\beta_i}{2}\rho^2 \end{aligned}$$

$$= b_i. \tag{4.17}$$

Thus, $b_i \geq 0$ *indicates* $\dot{b}_{i-1}+\lambda_i b_{i-1} \geq 0$*, which implies* $b_{i-1} \geq 0$ *as* $b_{i-1}(\bar{\mu}_{i-1}(0), \bar{y}_{i-1}(0), y_0(0), x(0), 0) > 0$*. Hence,* $b_0 \geq 0$*, which indicates that* $h(x(t)) \geq 0, \forall t \geq 0$*. This completes the proof.* □

Remark 4.1 *If the term* $\frac{\beta_i}{2}\rho^2$ *in* (4.7) *is dropped for* $i \in [m]$*, the input-to-state safety [105] of the proxy subsystem* (4.4) *can be proven without Condition (ii) in Theorem 4.1. On the other hand, if* $L_{g_0}h \neq 0$ *for any* $x \in \mathcal{C}$*, the conclusion of Theorem 4.1 still holds by dropping Condition (i) and (ii) and replacing functions* y_0 *and* y_i *in* (4.7) *with* h *and* 0*, respectively.*

The safe control law ν in Theorem 4.1 is obtained by solving the following convex CBF-QP:

$$\begin{aligned} \min_{\nu} \quad & \|\nu - \nu_d\|^2 \\ \text{s.t.} \quad & \psi_0 + \psi_1 \nu \geq 0 \end{aligned} \tag{4.18}$$

where ψ_0, ψ_1 are given in (4.10), ν_d is any nominal control law that is possibly unsafe. Note that this QP is always feasible by the non-emptiness of the set K_{BF}. Since ν_d cannot be given directly as it is the input to the proxy subsystem, the following result provides a method for designing it.

Corollary 4.1 *Consider the proxy subsystem* (4.4) *and the safe set* $\mathcal{C}$ *defined in* (2.2)*. Suppose that the right inverse of* g_0 *exists for any* $x \in \mathcal{C}$*, condition* (4.6) *holds, and* $x_d(t)$ *is a reference trajectory that is* $(m+1)$*-th order differentiable. Then the control law* ν *given as* $\nu = \alpha_{m+1}$ *will ensure the tracking error* $x - x_d$ *is globally UUB, where* α_{m+1} *is defined recursively according to*

$$\alpha_1 = -g_0^{\dagger}(k_0\epsilon_0 + f_0 - \dot{x}_d) - \frac{g_0^{\top}\epsilon_0}{2c_0}, \tag{4.19a}$$

$$\alpha_2 = \frac{\partial \alpha_1}{\partial t} + \frac{\partial \alpha_1}{\partial x}(f_0 + g_0\mu_1) - \frac{\epsilon_1}{2c_1}\left\|\frac{\partial \alpha_1}{\partial x}g_0\right\|^2 - g_0^{\top}\epsilon_0 - k_1\epsilon_1, \tag{4.19b}$$

$$\alpha_i = \frac{\partial \alpha_{i-1}}{\partial t} + \frac{\partial \alpha_{i-1}}{\partial x}(f_0 + g_0\mu_1) + \sum_{j=1}^{i-2} \frac{\partial \alpha_{i-1}}{\partial \mu_j}\mu_{j+1} - \frac{\epsilon_{i-1}}{2c_{i-1}}\left\|\frac{\partial \alpha_{i-1}}{\partial x}g_0\right\|^2$$
$$-\epsilon_{i-2} - k_{i-1}\epsilon_{i-1},\ i = 3, \cdots, m+1, \tag{4.19c}$$

where $\epsilon_0 = x - x_d$, $\epsilon_i = \mu_i - \alpha_i$ *for* $i \in [m]$, *and positive constants* $k_i, c_i > 0$ *for* $i = 0, 1, \cdots, m$.

Proof *Define* $V_0 = \frac{1}{2}\epsilon_0^2$ *and*

$$V_i = V_0 + \frac{1}{2}\sum_{j=1}^{i} \epsilon_j^\top \epsilon_j,\ i \in [m]. \tag{4.20}$$

Clearly,

$$\begin{aligned}
\dot{V}_0 &= \epsilon_0^\top (f_0 + g_0(\alpha_1 + \epsilon_1 + e) - \dot{x}_d) \\
&= -k_0\|\epsilon_0\|^2 + \epsilon_0^\top g_0\epsilon_1 + \epsilon_0^\top g_0 e - \frac{\|g_0^\top \epsilon_0\|^2}{2c_0} \\
&\le -k_0\|\epsilon_0\|^2 + \epsilon_0^\top g_0\epsilon_1 + \|\epsilon_0^\top g_0\|\rho - \frac{\|\epsilon_0^\top g_0\|^2}{2c_0} \\
&\le -k_0\|\epsilon_0\|^2 + \epsilon_0^\top g_0\epsilon_1 + \frac{c_0}{2}\bar{\rho}^2,
\end{aligned} \tag{4.21}$$

where $\bar{\rho} = \sup_{t\ge 0}\rho(t)$. *We claim the following inequality holds for any* $i \in [m-1]$*:*

$$\dot{V}_i \le -\sum_{j=0}^{i} k_j\|\epsilon_j\|^2 + \epsilon_i^\top \epsilon_{i+1} + \frac{\bar{\rho}^2}{2}\sum_{j=0}^{i} c_j. \tag{4.22}$$

Indeed, (4.22) *holds for* $i = 1$ *as*

$$\begin{aligned}
\dot{V}_1 &= \dot{V}_0 + \epsilon_1^\top \left(\epsilon_2 - g_0^\top \epsilon_0 - k_1\epsilon_1 - \frac{\epsilon_1}{2c_1}\left\|\frac{\partial \alpha_1}{\partial x}g_0\right\|^2 - \frac{\partial \alpha_1}{\partial x}g_0 e\right) \\
&\le -k_0\|\epsilon_0\|^2 - k_1\|\epsilon_1\|^2 + \epsilon_1^\top \epsilon_2 + \frac{c_0 + c_1}{2}\bar{\rho}^2.
\end{aligned} \tag{4.23}$$

Now assume that (4.22) *holds for* $i = k-1$ *where* $k \ge 2$. *Since*

$$\dot{V}_k = \dot{V}_{k-1} + \epsilon_k^\top \left(\epsilon_{k+1} - \epsilon_{k-1} - \frac{\epsilon_k}{2c_k}\left\|\frac{\partial \alpha_k}{\partial x}g_0\right\|^2 - k_k\epsilon_k - \frac{\partial \alpha_k}{\partial x}g_0 e\right)$$

$$\leq -\sum_{j=0}^{k} k_j \|\epsilon_j\|^2 + \epsilon_k^\top \epsilon_{k+1} + \frac{\bar{\rho}^2}{2} \sum_{j=0}^{k} c_j, \tag{4.24}$$

(4.22) *holds for* $i = k$. *Hence, by mathematical induction,* (4.22) *holds for all* $i \in [m-1]$.

Note that

$$\begin{aligned}
\dot{V}_m &= \dot{V}_{m-1} + \epsilon_m^\top \dot{\epsilon}_m \\
&\overset{(4.22)}{\leq} -\sum_{j=0}^{m-1} k_j \|\epsilon_j\|^2 + \epsilon_{m-1}^\top \epsilon_m + \frac{\bar{\rho}^2}{2} \sum_{j=0}^{m-1} c_j + \epsilon_m (\nu_d - \dot{\alpha}_m) \\
&\leq -\sum_{j=0}^{m} k_j \|\epsilon_j\|^2 + \frac{\bar{\rho}^2}{2} \sum_{j=0}^{m} c_j \\
&\leq -\chi V_m + \frac{\bar{\rho}^2}{2} \sum_{j=0}^{m} c_j,
\end{aligned} \tag{4.25}$$

where $\chi = 2\min\{k_0, k_1, \cdots, k_m\}$. *Using the standard Lyapunov argument, one can conclude that* ϵ_0 *is globally UUB.* □

4.3.3 Virtual Tracking Subsystem Control Design

Control design for the virtual tracking subsystem (4.5) can be accomplished by any Lyapunov-based method that ensures (4.6) holds, such as BLFs [4], [104], [106] and PPC [5], [15]. This flexibility demonstrates modularity of our proposed approach.

In particular, by leveraging the approximation-free PPC technique shown in [15, Theorem 2], a "model-free" control law without the information of f_i and g_i can be designed, as presented in the following result whose proof is similar to [15, Theorem 2] and thus omitted.

Proposition 4.1 *Consider the virtual tracking subsystem* (4.5) *with* $q = 1$ *and* $p_i = 1$, $i \in [n]$. *Suppose that (i) the sign of* g_i *is known and* $|g_i| \geq b_i$, $i \in [n]$, *where* $b_i > 0$ *is an unknown constant, and (ii) when* $m > 1$, μ_1 *and* μ_2 *(or* μ_1 *and* ν *when* $m = 1$*) are bounded with possibly unknown bounds. Then, the control law designed as* $u = \eta_n$ *will ensure* $|e(t)| \leq \rho(t)$ *where* η_n *is defined recursively according to* $\eta_i = -k_i \log\left(\frac{1+\xi_i}{1-\xi_i}\right)$, $i \in [n]$, *with* k_i *a positive constant,* $\xi_1 = \frac{z_1 - \mu_1}{\rho}$, $\xi_i = \frac{z_i - \eta_{i-1}(\bar{z}_{i-1}, \mu_1, t)}{\rho_i}$ $(i = 2, \cdots, n)$,

and ρ_i $(i = 2, \cdots, n)$ *smooth positive functions satisfying* $\lim_{t\to\infty} \rho_i(t) > 0$ *and* $\rho_i(0) > |z_i(0) - \eta_{i-1}(\bar{z}_{i-1}(0), \mu_1(0), 0)|$.

The control law in Proposition 4.1 is robust since it does not rely on the information of f_i and g_i, $i \in [n]$. Furthermore, because the reference signal in PPC is only required to be continuously differentiable [15, Assumption 4], one may select $m = 1$ for the proxy subsystem, which will result in a simple control design in Section 4.3.1. However, in this case, the PPC controller tends to yield large and oscillating control input; see the simulation results in Example 4.2. In addition, although we assume $p_i = 1$ and $q = 1$, the approximation-free PPC can be readily extended to multi-input multi-output systems (i.e., $p_i, q > 1$), as discussed in [15, Remark 2].

4.3.4 Safety Guarantee of the Overall System

The safety of system (4.2) can be ensured by combining the controllers separately designed for the proxy subsystem and the virtual tracking subsystem in the preceding subsections, as shown in the following result.

Corollary 4.2 *Consider system* (4.2)*, the safe set defined in* (4.3)*, and the decomposition shown in* (4.4)-(4.5)*. Suppose that all conditions of Theorem 4.1 are satisfied, such that a Lipschitz continuous controller* $\nu \in K_{BF}$ *is given by the CBF-QP* (4.18)*. Then, any Lipschitz continuous control law* u *that ensures* $\|e(t)\| \leq \rho(t)$ *for the virtual tracking subsystem* (4.5) *will guarantee* $h(x(t)) \geq 0, \forall t \geq 0$*, for system* (4.2)*.*

The modular safe control design method offers several advantages: i) By leveraging both CBF-based and Lyapunov-based tools, the proposed method can design safe controllers for a general class of systems shown in (4.2) that cannot be tackled by either tool separately; ii) Because the proxy subsystem (4.4) is more structured than the original system (4.2), validity of the CBF h can be verified by a simple condition (i.e., Condition (i) of Theorem 4.1), which significantly simplifies the CBF construction and guarantees feasibility of the CBF-QP shown in (4.18) as K_{BF} is non-empty; iii) Different systems

(e.g., Euler-Lagrange systems) with the same proxy subsystem share an identical CBF design, which simplifies the whole safe control design process.

Remark 4.2 *Including a chain of integrators in the proxy subsystem is essential. Suppose that the proxy subsystem is selected as* $\dot{x} = f_0 + g_0\nu + g_0 e$ *without integrators where* ν *is the virtual control and* $e = z_1 - \nu$*. Then, in the CBF design, the constraint* $\rho(0) > \|e(0)\| = \|z_1(0) - \nu(x(0), 0)\|$ *has to be imposed on* ν*, which makes the design process complicated. Moreover, the differentiability of* ν*, which is required by most Lyapunov-based methods in the control design of the virtual tracking subsystem, is difficult to be guaranteed as* ν *is the solution of a QP. Although this issue may be addressed by using smoothing techniques as part of the ROM-based method, such controllers tend to be more conservative than their QP counterparts and are hard to obtain when additional constraints exist (e.g., multiple safe constraints) [107], [108]. In contrast, the proposed proxy subsystem form* (4.4) *can avoid these issues.*

Remark 4.3 *In contrast to the modular PCBF design method, the ROM-based methods involve coupled ROM safe control design and tracking control design [109], [110]. In these methods, the tracking controller must satisfy specific Lyapunov conditions (refer to [109, Section 6.1]), which can be challenging to achieve; for instance, the Lyapunov condition shown in [109, eqn. (71)] is not satisfiable by either the approximation-free PPC in Proposition 4.1 or the Nussbaum-based adaptive controller in Example 4.1. Furthermore, although the proxy subsystem includes additional integrators, verifying the validity of* h *(i.e., Condition (i) in Theorem 4.2) is simpler compared to ROM-based methods (such as the equation above [109, eqn. (38)]) because* f_0 *is not involved.*

Remark 4.4 *Although input constraints are not explicitly addressed in this work, techniques from CBFs [111] or BLFs [112] can be leveraged to incorporate input constraints into the design process. In particular, for proxy subsystems with polynomial dynamics, sum-of-squares optimization may be used to design CBFs that account for input constraints [113].*

4.4 DOB-PCBF-based Control Design

In this section, we introduce a novel filter-based DOB and integrate it into the PCBF framework, enabling a DOB-PCBF-based safe control design scheme that addresses limitations of existing DOB-CBF methods in handling strict-feedback systems with mismatched disturbances. The system under consideration is described as

$$\dot{x} = f_0(x) + g_0(x)z_1, \tag{4.26a}$$

$$\dot{z}_1 = f_1(x, z_1) + g_1(x, z_1)z_2 + d_1, \tag{4.26b}$$

$$z_2 = f_2(x, z_1, z_2) + g_2(x, z_1, z_2)z_3 + d_2, \tag{4.26c}$$

$$\vdots$$

$$\dot{z}_n = f_n(x, z_1, \ldots, z_n) + g_n(x, z_1, \ldots, z_n)u + d_n, \tag{4.26d}$$

where $x \in \mathbb{R}^p, z_1 \in \mathbb{R}^{p_1}, \ldots, z_n \in \mathbb{R}^{p_n}$ are state variables, $f_0, f_1, \ldots, f_n$ and $g_0, g_1, \ldots, g_n$ are all known sufficiently smooth functions, $d_1, \ldots, d_n$ represent lumped unknown disturbances/uncertainties, and $u \in \mathbb{R}^q$ is the control input. We aim to design a controller u for system (4.26) such that the closed-loop system is safe with respect to the set $\mathcal{C}$ defined in (4.3), i.e., $h(x(t)) \geq 0, \forall t \geq 0$. Note that f_i and g_i, $i \in [n]$ in system (4.26) can be considered as the known part of the model with d_i as the unknown part - this is different from the "model-free" problem setting in Proposition 4.1 where functions f_i and g_i, $i \in [n]$, in system (4.2) are assumed to be unknown.

Robust CBF methods that consider the worst-case of disturbances have been developed for disturbed systems, but their performance tends to be conservative [16], [17]. To mitigate their unnecessary conservativeness, several DOB-CBF-based control schemes that precisely estimate and compensate for disturbances are proposed [26], [75], [114], including our IIDOB-CBF-QP-based method developed in Chapter 2. However, for systems whose disturbance relative degree is lower than the input relative degree (e.g., system (4.26)), results on DOB-CBF-based control are still limited. In particular, the method presented in Chapter 2 cannot be directly applied to system (4.26), and the approach in [114] is not

applicable to systems whose input and disturbance relative degrees differ more than one.

To design a safe controller for (4.26), we will propose a new filter-based DOB and the corresponding DOB-PCBF-based safe control strategy. The following assumption is standard.

Assumption 4.1 The derivatives of disturbances d_i, $i \in [n]$, are bounded, i.e., $\|\dot{d}_i\| \leq \omega_i$, where ω_i is an unknown constant.

The DOB we use has the following form [27]:

$$\hat{d}_i = s_i + \alpha_i z_i, \tag{4.27a}$$

$$\dot{s}_i = \begin{cases} -\alpha_i(f_i + g_i z_{i+1} + \hat{d}_i), & \text{if } i \in [n-1], \\ -\alpha_n(f_n + g_n u + \hat{d}_n), & \text{if } i = n, \end{cases} \tag{4.27b}$$

where $\hat{d}_i$ is the estimation of d_i, α_i is a positive constant, and s_i is the internal state of the DOB, for $i \in [n]$. With a Lyapunov function $V_i^d = \frac{1}{2} e_{d,i}^\top e_{d,i}$, where $e_{d,i} = \hat{d}_i - d_i$, one can verify that $\dot{V}_i^d \leq -2\kappa_i V_i^d + \omega_i^d$ where $\kappa_i = \alpha_i - \frac{\nu_i}{2}$, $\nu_i < 2\alpha_i$ is a positive constant, and $\omega_i^d = \frac{\omega_i^2}{2\nu_i}$. Thus, $e_{d,i}$ is globally UUB.

Following the system decomposition scheme developed in Section 4.3.1, system (4.26) can be decomposed into the proxy subsystem shown in (4.4) with $m = n$ and the following virtual tracking subsystem:

$$\dot{e} = f_1 + g_1 z_2 + d_1 - \mu_2, \tag{4.28a}$$

$$\dot{z}_2 = f_2 + g_2 z_3 + d_2, \tag{4.28b}$$

$$\vdots$$

$$\dot{z}_n = f_n + g_n u + d_n, \tag{4.28c}$$

where $e = z_1 - \mu_1$ and μ_i, $i \in [m]$, are defined in (4.4). The CBF-based control design for the proxy subsystem follows Theorem 4.1 under condition (4.6). We will propose a new DOB-based control approach for the subsystem (4.28) to ensure (4.6) holds.

The high-order derivatives of $\hat{d}_i$, $i \in [n-1]$, are indispensable for control design because d_i is a mismatched disturbance. However, $\dot{\hat{d}}_i$ is unknown because $\dot{\hat{d}}_i = -\alpha_i e_{d,i}$ and $e_{d,i}$ rely on d_i. To address this issue, we propose a filter-based DOB, which can generate alternative disturbance estimation signals that are close to d_i and have known derivatives, as follows:

$$\dot{\hat{d}}^f_{i,j} = -T_{i,j}(\hat{d}^f_{i,j} - \hat{d}^f_{i,j-1}) \tag{4.29}$$

where $j \in [n-i], i \in [n-1]$, $\hat{d}^f_{i,0} = \hat{d}_i$, $\hat{d}^f_{i,j}$ is the filtered disturbance estimation, and $T_{i,j} > 0$ is a positive constant. The following lemma shows the convergence of the filter.

Lemma 4.1 *Consider the DOB given in* (4.27) *and the filter presented in* (4.29)*. Suppose that Assumption 4.1 holds. Then the filtered disturbance estimation error* $\delta_i = \hat{d}^f_{i,n-i} - d_i$, $i \in [n-1]$, *is globally UUB.*

Proof *Define* $E^f_i = [e^{f\top}_{i,1}\ e^{f\top}_{i,2}\ \cdots\ e^{f\top}_{i,n-i}\ e^{\top}_{d,i}]^\top$ *where* $e_{d,i}$ *is defined after* (2.24) *and* $e^f_{i,j} = \hat{d}^f_{i,j} - \hat{d}^f_{i,j-1}$ *for* $j \in [n-i]$ *and* $i \in [n-1]$*. We will demonstrate that* δ_i *is globally UUB by establishing the boundedness of* E^f_i*.*

From (4.29) *we have*

$$\dot{E}^f_i = A_i E^f_i + B_i \dot{d}_i \tag{4.30}$$

where $B_i = [\mathbf{0}\ \cdots\ \mathbf{0}\ -I_{p_i}]^\top$ *and*

$$A = \begin{bmatrix} -T_{i,1}I_{p_i} & \mathbf{0} & \cdots & \mathbf{0} & \alpha_i I_{p_i} \\ T_{i,1}I_{p_i} & -T_{i,2}I_{p_i} & \cdots & \mathbf{0} & \mathbf{0} \\ \vdots & \vdots & \ddots & \vdots & \vdots \\ \mathbf{0} & \mathbf{0} & T_{i,n-i-1}I_{p_i} & -T_{i,n-i}I_{p_i} & \mathbf{0} \\ \mathbf{0} & \cdots & \mathbf{0} & \mathbf{0} & -\alpha_i I_{p_i} \end{bmatrix}.$$

It is easy to check that all eigenvalues of A_i *are negative, so for any* $\gamma_i > 0$*, there exists a positive definite matrix* P_i *satisfying* $A_i^\top P_i + P_i A_i = -\gamma_i I_{p_i(n-i+1)}$*. Define a candidate Lyapunov function as*

$$V^f_i = E^{f\top}_i P_i E^f_i \tag{4.31}$$

whose derivative satisfies

$$\begin{aligned}\dot{V}_i^f &= E_i^{f\top}(A_i^\top P_i + P_i A_i)E_i^f + \dot{d}_i^\top B_i^\top P_i E_i^f + E_i^{f\top} P_i B_i \dot{d}_i \\ &\leq -\gamma_i \|E_i^f\|^2 + 2\sqrt{p_i}\omega_i \|P_i\| \|E_i^f\| \\ &\leq -\gamma_i^f \|E_i^f\|^2 + \omega_i^f \end{aligned} \tag{4.32}$$

where $0 < \theta_i < \gamma_i$, $\gamma_i^f = \gamma_i - \theta_i > 0$, *and* $\omega_i^f = \frac{p_i \omega_i^2 \|P_i\|^2}{\theta_i}$. *From* (4.32) *one can conclude that* E_i^f *is globally UUB, which indicates that* δ_i *is also globally UUB since*

$$\|\delta_i\| \leq \|e_{d,i}\| + \sum_{j=1}^{n-i} \|e_{i,j}^f\| \leq \sqrt{n-i+1}\|E_i^f\|, \tag{4.33}$$

which completes the proof. □

From Lemma 4.1 one can see that $\hat{d}_{i,n-i}^f$, whose derivatives up to the $(n-i)$-th order are explicitly given, is close to d_i in the sense that $\|\delta_i\|$ is bounded by a known decaying function, implying that one can replace $\hat{d}_i$ with $\hat{d}_{i,j}^f$ in DOB design. Note that the ultimate bound of δ_i can be made arbitrarily small by selecting appropriate parameters.

The following theorem provides a filtered-DOB-based controller for the virtual tracking subsystem (4.28) to ensure $\|e\| \leq \rho$. The control design follows backstepping [35], and the filtered disturbance estimation error δ_i is compensated by virtual control signals.

Theorem 4.2 *Consider system* (4.26), *the safe set defined in* (4.3), *and the decomposition given by* (4.4) *and* (4.28) *with* $m = n$. *Suppose that all conditions of Theorem 4.1 are satisfied, such that a Lipschitz continuous controller* ν *is given by the CBF-QP* (4.18). *Suppose that Assumption 4.1 holds, the right inverse of* g_i *exists for any* $x \in \mathcal{C}$ *and* $z_1 \in \mathbb{R}^{p_1}, \cdots, z_i \in \mathbb{R}^{p_i}$ $(i \in [n])$, *the DOB is given in* (4.27), *and the filter is given in* (4.29). *If*

$$\begin{aligned} u = g_n^\dagger \Bigg(&\sum_{j=1}^{n-1} \frac{\partial \tau_{n-1}}{\partial z_j} \hat{d}_{j,n-j}^f - \sum_{j=1}^{n-1} \frac{(n-j+1)\epsilon_n}{4\gamma_j^f} \left\| \frac{\partial \tau_{n-1}}{\partial z_j} \right\|^2 - \hat{d}_n - f_n - \frac{\epsilon_n}{4(\kappa_n - \sigma_n)} \\ &- k_n \epsilon_n - g_{n-1}^\top l_n + \mathcal{N}_n \Bigg), \end{aligned} \tag{4.34}$$

where

$$\tau_1 = g_1^\dagger \left(\frac{\dot{\rho}}{\rho} e - k_1 e - \hat{d}_{1,n-1}^f - \frac{ne}{4(\gamma_1^f - \sigma_1)(\rho^2 - \|e\|^2)} - f_1 + \mu_2 \right), \tag{4.35a}$$

$$\begin{aligned} \tau_i = g_i^\dagger \Bigg(& \sum_{j=1}^{i-1} \frac{\partial \tau_{i-1}}{\partial z_j} \hat{d}_{j,n-j}^f - \sum_{j=1}^{i-1} \frac{(n-j+1)\epsilon_i}{4\gamma_j^f} \left\| \frac{\partial \tau_{i-1}}{\partial z_j} \right\|^2 - \hat{d}_{i,n-i}^f - f_i \\ & - \frac{(n-i+1)\epsilon_i}{4(\gamma_i^f - \sigma_i)} - k_i \epsilon_i - g_{i-1}^\top l_i + \mathcal{N}_i \Bigg), \ i = 2, \cdots, n-1, \end{aligned} \tag{4.35b}$$

are virtual control signals designed by following backstepping, κ_n *is defined after* (2.24)*,* $k_i > 0$ $(i \in [n])$*,* $\gamma_i^f > 0$ $(i \in [n-1])$*,* $0 < \sigma_i < \gamma_i^f$ $(i \in [n-1])$*,* $0 < \sigma_n < \kappa_n$*,* $\epsilon_1 = e$*,* $\epsilon_i = z_i - \tau_{i-1}$ $(i = 2, \cdots, n)$*,* $l_2 = \frac{e}{\rho^2 - \|e\|^2}$*,* $l_i = \epsilon_{i-1}$ $(i = 3, \cdots, n)$*,* $\mathcal{N}_i = \frac{\partial \tau_{i-1}}{\partial t} + \sum_{j=1}^{i-1} \frac{\partial \tau_{i-1}}{\partial z_j}(f_j + g_j z_{j+1}) + \sum_{j=1}^{i} \frac{\partial \tau_{i-1}}{\partial \mu_j} \mu_{j+1} - \sum_{j=1}^{i-1} \sum_{m=j}^{i-1} \frac{\partial \tau_{i-1}}{\partial \hat{d}_{j,n-m}^f} T_{j,n-m}(\hat{d}_{j,n-m}^f - \hat{d}_{j,n-m-1}^f) + \frac{\partial \tau_{i-1}}{\partial x}(f_0 + g_0 z_1)$ *for* $i = 2, \cdots, n$*, and* $\mu_{n+1} = \nu$*, then* (4.6) *holds.*

Proof *Note that for* $i \in [n-1]$*,* τ_i *is a function of* x,$\bar{z}_i$,$\bar{\mu}_{i+1}$,t,$\hat{d}_{j,n-j}^f$,$\ldots$, $\hat{d}_{j,n-i}^f$ $(j \in [i])$*. Define candidate BLFs* V_i $(i = 2, \cdots, n)$ *as*

$$V_i(e, \bar{\epsilon}_i, \bar{E}_i^f) = V_{i-1}(e, \bar{\epsilon}_{i-1}, \bar{E}_{i-1}^f) + \frac{1}{2}\|\epsilon_i\|^2 + \sum_{j=1}^{i} V_j^f, \tag{4.36}$$

where $V_1(e, E_1^f) = \frac{1}{2}\log\left(\frac{\rho^2}{\rho^2 - \|e\|^2}\right) + V_1^f$*,* V_i^f $(i \in [n-1])$ *are defined in* (4.31)*,* $V_n^f = V_n^d$*, and* V_n^d *is defined after* (4.27)*. The control design follows the BLF backstepping technique [4], and the disturbances are compensated by their estimates presented in* (4.27) *and* (4.29)*.*

Clearly $\dot{V}_1$ *in the open set* $\mathcal{Z}(t) = \{e \in \mathbb{R} : \|e\| < \rho\}$ *satisfies*

$$\begin{aligned} \dot{V}_1 \overset{(4.32)}{\leq} & \frac{e^\top}{\rho^2 - \|e\|^2}\big(f_1 + g_1\tau_1 + g_1\epsilon_2 + d_1 - \mu_2 - \frac{\dot{\rho}}{\rho}e\big) - \gamma_1^f\|E_1^f\|^2 + \omega_1^f \\ \overset{(4.35a)}{=} & \frac{e^\top}{\rho^2 - \|e\|^2}(-k_1 e + g_1\epsilon_2 - \delta_1) - \sigma_1\|E_1^f\|^2 - \frac{n\|e\|^2}{4(\gamma_1^f - \sigma_1)(\rho^2 - \|e\|^2)^2} \\ & -(\gamma_1^f - \sigma_1)\|E_1^f\|^2 + \omega_1^f \\ \overset{(4.33)}{\leq} & -\frac{k_1\|e\|^2}{\rho^2 - \|e\|^2} + \frac{e^\top g_1\epsilon_2}{\rho^2 - \|e\|^2} + \frac{\sqrt{n}\|e\|\|E_1^f\|}{\rho^2 - \|e\|^2} - \sigma_1\|E_1^f\|^2 + \omega_1^f - \frac{n\|e\|^2}{4(\gamma_1^f - \sigma_1)(\rho^2 - \|e\|^2)^2} \\ & -(\gamma_1^f - \sigma_1)\|E_1^f\|^2 \end{aligned}$$

$$\leq \quad -\frac{k_1 e^2}{\rho^2 - \|e\|^2} - \sigma_1 \|E_1^f\|^2 + \frac{e^\top g_1 \epsilon_2}{\rho^2 - \|e\|^2} + \omega_1^f. \tag{4.37}$$

Then, we will show for any $i = 2, \cdots, n-1$,

$$\dot{V}_i \leq \frac{-k_1\|e\|^2}{\rho^2 - \|e\|^2} - \sum_{j=2}^{i} k_j \|\epsilon_j\|^2 - \sum_{j=1}^{i} \sigma_j \|E_j^f\|^2 + \sum_{j=1}^{i} (i-j+1)\omega_j^f + \epsilon_i^\top g_i \epsilon_{i+1}. \tag{4.38}$$

One can verify that

$$\begin{aligned}
\dot{V}_2 &= \dot{V}_1 + \epsilon_2^\top (\dot{z}_2 - \dot{\tau}_1) + \dot{V}_1^f + \dot{V}_2^f \\
&= \epsilon_2^\top \bigg(f_2 + g_2\tau_2 + g_2\epsilon_3 + d_2 - \frac{\partial \tau_1}{\partial x}\dot{x} - \frac{\partial \tau_1}{\partial z_1}\dot{z}_1 - \sum_{j=1}^{2} \frac{\partial \tau_1}{\partial \mu_j}\mu_{j+1} - \frac{\partial \tau_1}{\partial \hat{d}_{1,n-1}^f}\dot{\hat{d}}_{1,n-1}^f - \frac{\partial \tau_1}{\partial t} \bigg) \\
&\quad + \dot{V}_1 + \dot{V}_1^f + \dot{V}_2^f \\
&\overset{(4.35b)}{\leq} -\frac{k_1\|e\|^2}{\rho^2 - \|e\|^2} - k_2\|\epsilon_2\|^2 - \sigma_1\|E_1^f\|^2 - \sigma_2\|E_2^f\|^2 + 2\omega_1^f + \omega_2^f - (\gamma_2^f - \sigma_2)\|E_2^f\|^2 \\
&\quad - \frac{(n-1)\|\epsilon_2\|^2}{4(\gamma_2^f - \sigma_2)} + \|\epsilon_2\| \Big\| \frac{\partial \tau_1}{\partial z_1} \Big\| \sqrt{n} \|E_2^f\| - \frac{n\epsilon_2^2}{4\gamma_1^f} \Big\| \frac{\partial \tau_1}{\partial z_1} \Big\|^2 + \epsilon_2^\top g_2 \epsilon_3 \\
&\quad + \|\epsilon_2\| \sqrt{n-1} \|E_2^f\| - \gamma_1^f \|E_1^f\| \\
&\leq -\frac{k_1\|e\|^2}{\rho^2 - \|e\|^2} - k_2\|\epsilon_2\|^2 - \sigma_1\|E_1^f\|^2 - \sigma_2\|E_2^f\|^2 + 2\omega_1^f + \omega_2^f + \epsilon_2^\top g_2 \epsilon_3,
\end{aligned} \tag{4.39}$$

so (4.38) *holds for* $i = 2$. *Assume* (4.38) *holds for* $i = k-1$. *Since*

$$\begin{aligned}
\dot{V}_k &= \dot{V}_{k-1} + \sum_{j=1}^{k} \dot{V}_j^f + \epsilon_k^\top (\dot{z}_k - \dot{\tau}_{k-1}) \\
&\overset{(4.32)}{\leq} -\frac{k_1\|e\|^2}{\rho^2 - \|e\|^2} - \sum_{j=2}^{k-1} k_j \|e_j\|^2 - \sum_{j=1}^{k-1} \sigma_j \|E_j^f\|^2 + \sum_{j=1}^{k} (k-j+1)\omega_j^f + \epsilon_{k-1}^\top g_{k-1}\epsilon_k \\
&\quad - \sum_{j=1}^{k} \gamma_j^f \|E_j^f\|^2 + \epsilon_k^\top (f_k + g_k\tau_k + g_k\epsilon_{k+1} + d_k - \dot{\tau}_{k-1}) \\
&\overset{(4.35b)}{\leq} -\frac{k_1\|e\|^2}{\rho^2 - \|e\|^2} - \sum_{j=2}^{k} k_j \|e_j\|^2 - \sum_{j=1}^{k} \sigma_j \|E_j^f\|^2 + \sum_{j=1}^{k} (k-j+1)\omega_j^f - \sum_{j=1}^{k-1} \gamma_j^f \|E_j^f\|^2 \\
&\quad - (\gamma_k^f - \sigma_k)\|E_k^f\|^2 + \epsilon_k^\top \bigg(g_k\epsilon_{k+1} - \delta_k + \sum_{j=1}^{k-1} \frac{\partial \tau_{k-1}}{\partial z_j}\delta_j - \sum_{j=1}^{k-1} \frac{(n-j+1)\epsilon_k}{4\gamma_j^f} \bigg\| \frac{\partial \tau_{k-1}}{\partial z_j} \bigg\|^2 \\
&\quad - \frac{(n-k+1)\epsilon_k}{4(\gamma_k^f - \sigma_k)} \bigg)
\end{aligned}$$

$$
\begin{aligned}
\overset{(4.33)}{\leq} & -\frac{k_1\|e\|^2}{\rho^2-\|e\|^2}-\sum_{j=2}^{k}k_j\|e_j\|^2-\sum_{j=1}^{k}\sigma_j\|E_j^f\|^2+\sum_{j=1}^{k}(k-j+1)\omega_j^f-\sum_{j=1}^{k-1}\gamma_j^f\|E_j^f\|^2 \\
& -(\gamma_k^f-\sigma_k)\|E_k^f\|^2+\epsilon_k^\top g_k\epsilon_{k+1}+\|\epsilon_k\|\sqrt{n-k+1}\|E_k^f\|-\frac{(n-k+1)\|\epsilon_k\|^2}{4(\gamma_k^f-\sigma_k)} \\
& +\sum_{j=1}^{k-1}\Big\|\frac{\partial\tau_{k-1}}{\partial z_j}\Big\|\|\epsilon_k\|\sqrt{n-j+1}\|E_j^f\|-\sum_{j=1}^{k-1}\frac{(n-j+1)\|\epsilon_k\|^2}{4\gamma_j^f}\Big\|\frac{\partial\tau_{k-1}}{\partial z_j}\Big\|^2 \\
\leq & -\frac{k_1\|e\|^2}{\rho^2-\|e\|^2}-\sum_{j=2}^{k}k_j\|\epsilon_j\|^2-\sum_{j=1}^{k}\sigma_j\|E_j^f\|^2+\sum_{j=1}^{k}(k-j+1)\omega_j^f+\epsilon_k^\top g_k\epsilon_{k+1}, \quad (4.40)
\end{aligned}
$$

(4.38) *holds for* $i=k$. *By induction,* (4.38) *holds for* $i=2,\cdots,n-1$. *From* (4.36) *one can see*

$$
V_n=\frac{1}{2}\log\left(\frac{\rho^2}{\rho^2-\|e\|^2}\right)+\frac{1}{2}\sum_{j=2}^{n}\|\epsilon_j\|^2+\sum_{j=1}^{n}(n-j+1)V_j^f. \quad (4.41)
$$

Meanwhile, it is easy to verify

$$
\begin{aligned}
\dot{V}_n \leq & \frac{-k_1\|e\|^2}{\rho^2-\|e\|^2}-\sum_{j=2}^{n}k_j\|\epsilon_j\|^2-\sum_{j=1}^{n}\sigma_j\|E_j^f\|^2-\sum_{j=1}^{n}(n-j+1)\omega_j^f \\
\leq & -k_1\log\left(\frac{\rho^2}{\rho^2-\|e\|^2}\right)-\sum_{j=2}^{n}k_j\|\epsilon_j\|^2-\sum_{j=1}^{n}\sigma_j\|E_j^f\|^2+\sum_{j=1}^{n}(n-j+1)\omega_j^f, \quad (4.42)
\end{aligned}
$$

where $\omega_n^f=\omega_n^d$, $E_n^f=e_{d,n}$, ω_n^d *and* $e_{d,n}$ *are defined after* (2.24), *the first inequality follows a similar procedure above, and the second inequality is derived from* $\log\left(\frac{\rho^2}{\rho^2-\|e\|^2}\right)\leq\frac{\|e\|^2}{\rho^2-\|e\|^2}$, *which holds in* $\mathcal{Z}(t)$ *[4]. Hence,* $\dot{V}_n\leq-\zeta V_n+\sum_{j=n}^{i}(i-j+1)\omega_j^f$, *where* $\zeta=\min\left\{2k_1,\cdots,2k_n,\min_{j\in[n-1]}\left\{\frac{\sigma_j}{(n-j+1)\lambda_{\min}(P_j)}\right\},2\sigma_n\right\}$. *Thus,* V_n *is bounded, implying* $\|e\|\leq\rho$ *for any* $t\geq0$, *according to [4, Lemma 1].* □

From Corollary 4.2, one can see that the safety of the closed-loop system (4.26) with the controller u is ensured because of the modularity of the proposed method.

4.5 Numerical Simulations

In this section, two examples are provided to demonstrate the effectiveness of the proposed methods.

Example 4.1 *Consider system* (4.1) *with parameters* $T = 31, K = 0.5, \alpha = 0.4$ *as in [102]. Recall that* θ *and* b *are both unknown parameters, which makes the problem unsolvable by existing CBF methods. The safe set is given as* $\mathcal{C} = \{\psi : \frac{\pi^2}{81} - \psi^2 \geq 0\}$ *that aims to keep* $|\psi| \leq 20°$*; the reference trajectory is* $x_d = 30\sin(0.02t)$ *in degrees. We select* $\rho(t) = 0.02$ *and decompose the system into* (4.4)-(4.5) *where the proxy subsystem is* $\dot{x} = \mu_1 + e$*,* $\dot{\mu}_1 = \nu$*, and the virtual tracking subsystem is* $\dot{e} = bu + \theta^\top \varphi - \nu$*. With parameters* $\lambda_1 = 6, \lambda_2 = 1, \beta_1 = 20, \xi = \frac{\pi^2}{81}$*, one can verify that all conditions of Theorem 4.1 are satisfied, so that* ν *is obtained by solving CBF-QP* (4.18)*. We design a Nussbaum-based adaptive controller* $u = N(\zeta)\alpha$ *[104], where*

$$\alpha = ke - \nu + \hat{\theta}^\top \varphi, \tag{4.43}$$

$N(\cdot)$ *is a Nussbaum-type function,* ζ *and* $\hat{\theta}$ *are governed by adaptive laws*

$$\dot{\zeta} = \frac{e\alpha}{\rho^2 - e^2}, \tag{4.44a}$$

$$\dot{\hat{\theta}} = \frac{\gamma_1^{-1} e\varphi}{\rho^2 - e^2} - \gamma_2 \hat{\theta}, \tag{4.44b}$$

and $\gamma_1 = 10, \gamma_2 = 2, k = 2$*. By Corollary 4.2, the safety of the closed-loop system is satisfied. From the simulation result shown in Figure 4.2, one can see that the trajectory of* ψ *indeed stays within the safe region, while the desired tracking performance is well preserved inside* $\mathcal{C}$*.*

Example 4.2 *Consider the following electromechanical system with mismatched disturbances adapted from [115]:*

$$\dot{x} = z_1, \tag{4.45a}$$

$$\dot{z}_1 = f_1(x, z_1) + g_1 z_2 + d_1, \tag{4.45b}$$

$$\dot{z}_2 = f_2(x, z_1, z_2) + g_2 u + d_2, \tag{4.45c}$$

where $f_1 = -(Bz_1 + N_0 \sin(x))/M_0$*,* $g_1 = 1/M_0$*,* $f_2 = -(K_b z_1 + R_m z_2)/L_m$*,* $g_2 = 1/L_m$*,*

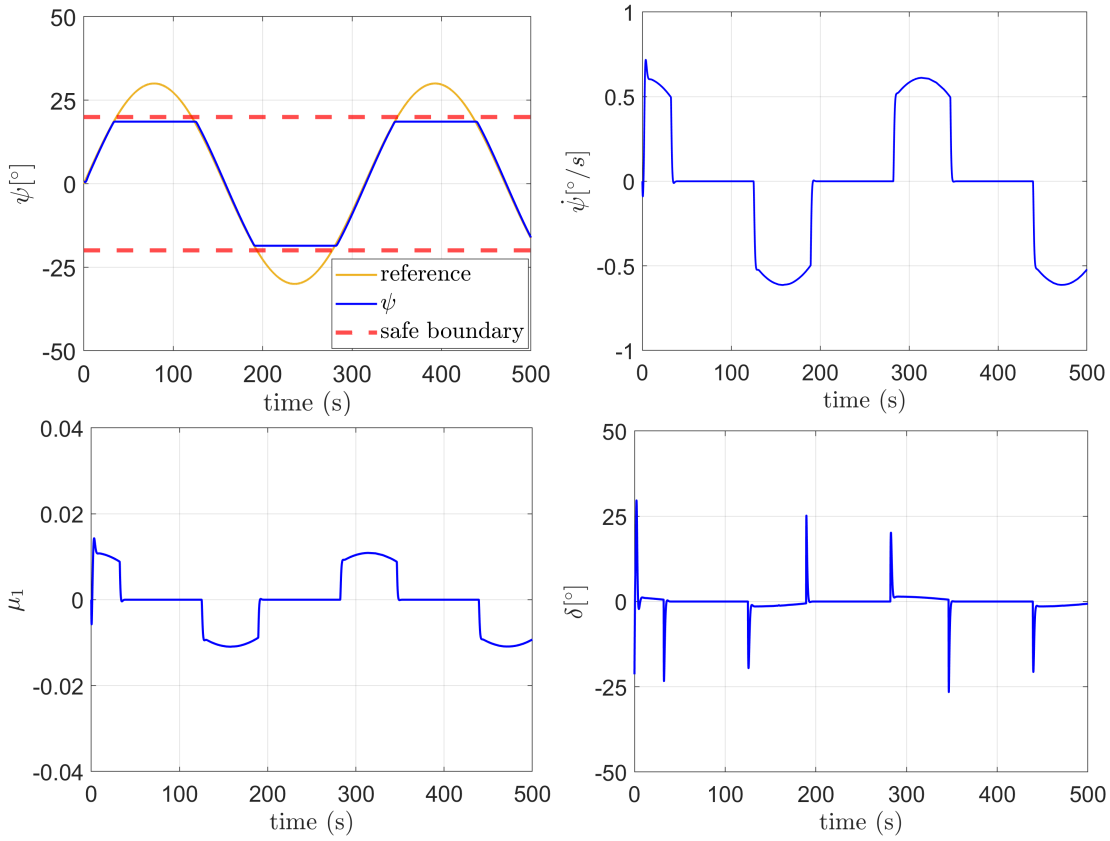

Figure 4.2: Simulation results of Example 4.1.

d_1, d_2 are external disturbances, and $M_0, B, N_0, L_m, R_m, K_b$ are physical parameters whose values are the same as those in [115]. The safe set is $\mathcal{C} = \{x \in \mathbb{R}^n : -0.5 \leq x \leq 0.3\}$, so we select two CBFs $h_1 = x + 0.5$ and $h_2 = -x + 0.3$. For comparison, we implement three methods in simulation: (i) the DOB-PCBF method by utilizing Corollary 4.1, Corollary 4.2, and Theorem 4.2; (ii) the model-free PCBF-based control law by using Corollary 4.1, Corollary 4.2, and Proposition 4.1; and (iii) the DOB-CBF-QP proposed in [26]. The disturbances are selected as $d_1 = d_2 = \sin(t) + 0.2\sin(2t) - 0.5\cos(5t) + \cos(3t)$, from which one can verify that Assumption 4.1 holds with $\omega_1 = \omega_2 = 6$; the reference trajectory is $x_d = \sin(t)$; and the control parameters for the DOB-PCBF method are $\beta_1 = \beta_2 = 0.05, \rho(t) = 0.8e^{-10t} + 0.05, \lambda_1 = \lambda_2 = 10, \lambda_3 = 15, \alpha_1 = \alpha_2 = 30, \gamma_1 = 50, \theta_1 = 10, T_{1,1} = 100, k_1 = k_2 = 10, \sigma_1 = \sigma_2 = 15, \nu_1 = \nu_2 = 1$. The Symbolic Math Toolbox in MATLAB is used to compute ψ_0, ψ_1 in (4.10), as well as u in (4.34) and (4.35). The simulation results are presented in Figure 4.3, which demonstrates that all three methods can ensure safety but their tracking performance and control input profiles are different: the DOB-PCBF method has perfect tracking performance with the smoothest control input profile; the model-free PCBF approach generates almost identical tracking performance as the DOB-PCBF method but its control input profile is more oscillatory; the DOB-CBF-QP approach has a poor tracking performance compared with other two methods.

4.6 Chapter Summary and Future Directions

This chapter proposes a PCBF safe control design scheme that integrates Lyapunov-based and CBF-based control approaches for strict-feedback systems with limited model information. Moreover, a DOB-PCBF-based controller is presented for systems with mismatched disturbances. Simulation results demonstrate the effectiveness of the proposed methods.

The PCBF control framework proposed in this chapter still relies on exact knowledge of f_0 and g_0, which can be restrictive for certain physical systems. This assumption may be further relaxed by developing alternative system decomposition schemes that reduce dependence on model information. Meanwhile, the PCBF framework is only applicable to

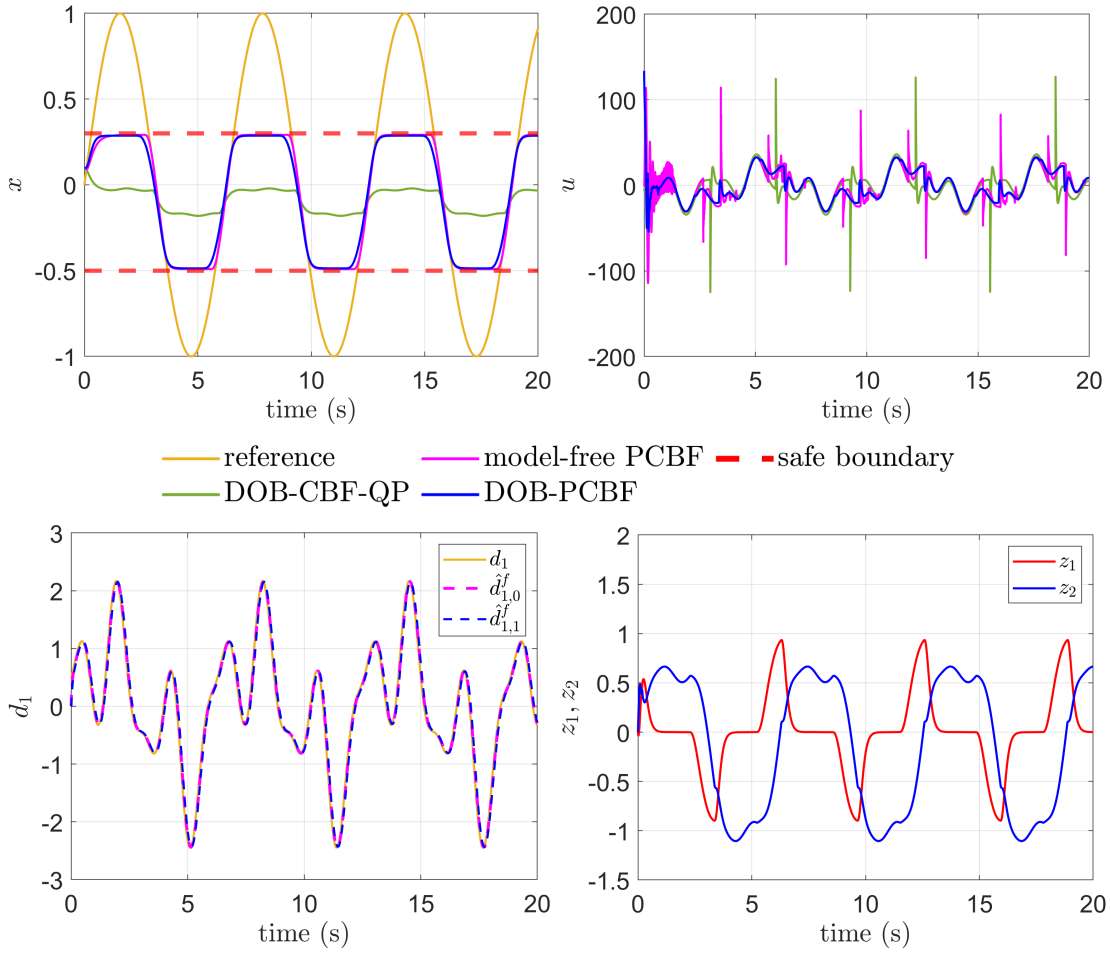

Figure 4.3: Simulation results of Example 4.2.

strict-feedback systems, which limits the applicability of the method to general systems. Future work includes extending the results to more generic systems.

Another limitation of the PCBF framework is that input constraints, which are ubiquitous and arise from physical limitations of actuators, are not explicitly considered in control design. Techniques from CBFs [111] or BLFs [112] can be leveraged to incorporate input constraints into the design process. In particular, for proxy subsystems with polynomial dynamics, sum-of-squares optimization may be used to design CBFs that account for input constraints [113].

Chapter 5

MPC-CBF-based Hierarchical Control for Visual Servoing Under Measurement Uncertainties

5.1 Introduction

Vision-based control has emerged as a powerful paradigm for robotic systems, enabling interaction with dynamic environments through direct use of visual feedback. Various approaches have been developed and implemented across diverse applications [116], [117], [118], [119], [120], [121]. However, most existing approaches lack rigorous safety guarantees in the presence of measurement (perception) uncertainties, which can result in performance degradation or even catastrophic failure in safety-critical applications. Although several recent works have focused on developing vision-based controllers with formal safety guarantees [122], [123], [124], these methods rely on restrictive assumptions or result in small safe regions, thereby limiting their applicability in complex, real-world systems.

Among vision-based control strategies, visual servoing, which uses image features as feedback signals for control, is a well-established and widely adopted framework with a rich history [125], [126], [127]. Its structured formulation facilitates the systematic devel-

opment of rigorous guarantees. Visual servoing is typically divided into Position-Based Visual Servoing (PBVS), which reconstructs 3D pose information, and Image-Based Visual Servoing (IBVS), which regulates image features directly without explicit 3D reconstruction. Compared to PBVS, IBVS avoids solving nonlinear pose estimation problems online, offering greater computational efficiency and reduced sensitivity to calibration errors [125]. These advantages make IBVS particularly well-suited for applications demanding real-time performance or where precise calibration is challenging.

Despite significant progress, most IBVS algorithms are not designed for complex environments where targets may be occluded and assume accurate vision feedback. In safety-critical applications such as surgical robotics [128], even brief visual occlusion is unacceptable. To address this challenge, several occlusion-free IBVS methods have been proposed using optimization-based control approaches [129], [130], [131], [132], [133], [134]. More recently, CBF-based methods have gained attention for occlusion avoidance because they provide strict safety guarantees and integrate seamlessly into convex QPs. While CBF-based methods ensure real-time constraint satisfaction, they are inherently myopic and lack long-term optimality. In contrast, MPC-based approaches utilize predictive models to achieve better long-term performance but impose heavy online computational burdens and cannot guarantee continuous-time occlusion avoidance, since constraints are enforced only at discrete time steps.

In this chapter, we present a hierarchical optimization-based visual servoing framework for robotic manipulators that ensures occlusion-free operation in the presence of perception uncertainties. The framework integrates two main components: a high-level MPC with uncertainty compensation and a low-level robust CBF-based controller (see Figure 5.1). The high-level MPC regulates target feature points and generates a nominal reference input, while the low-level controller strictly enforces occlusion-avoidance constraints. This hierarchical design inherits the advantages of both MPC and CBFs. The main contributions of this chapter are summarized as follows.

- We reformulate the occlusion-avoidance constraints as differentiable convex con-

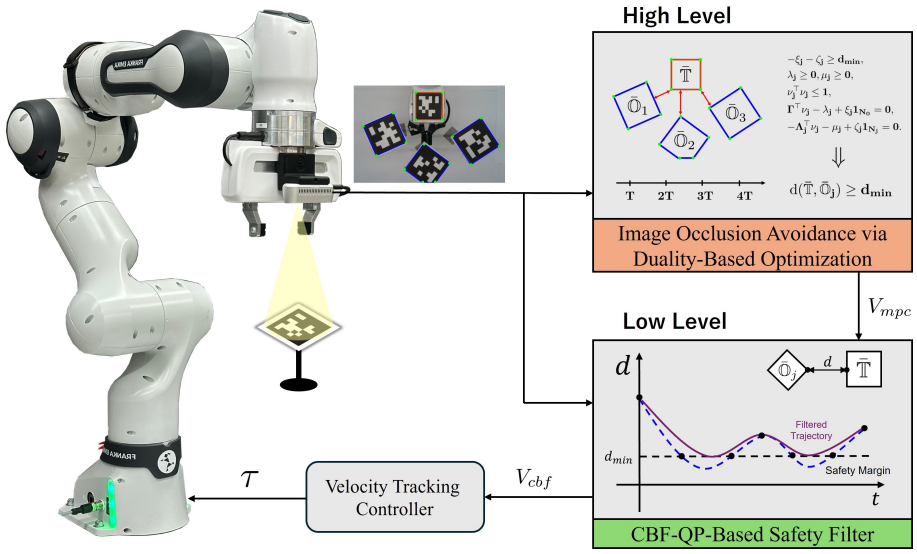

Figure 5.1: Architecture of the proposed hierarchical optimization-based visual servoing framework for robotic manipulators designed to ensure occlusion-free operation.

straints by leveraging a vertex-based image representation and a duality-based optimization approach. This reformulation enables the design of an MPC problem that regulates target feature points while ensuring occlusion avoidance in discrete time.

- We design a robust CBF-QP-based controller that strictly enforces occlusion-avoidance constraints in continuous time while tracking the MPC reference input. The CBFs are constructed from the relaxed minimum distance between polytopes, with distance derivatives computed using the KKT conditions of the corresponding optimization problem, and their validity established via nonsmooth analysis.

- We experimentally validate the proposed hierarchical framework on a Franka Research 3 manipulator, demonstrating occlusion-free visual servoing and real-time implementability. Extensive comparisons highlight the effectiveness and advantages of the approach.

5.2 Preliminaries and Problem Formulation

5.2.1 Camera Model

Consider a point $P = [x, y, z]^\top \in \mathbb{R}^3$ in the camera coordinate frame, and let $\eta = [u_x \ u_y]^\top \in \mathbb{R}^2$ denote the image coordinates of its projection. By the perspective projection model [125], the image coordinates are given by

$$\eta = \frac{f}{z} \begin{bmatrix} x \\ y \end{bmatrix} \in \mathbb{R}^2, \tag{5.1}$$

where f is the camera focal length. By augmenting η with z, we define the augmented state as

$$\bar{\eta} = \begin{bmatrix} u_x \\ u_y \\ z \end{bmatrix} \in \mathbb{R}^3. \tag{5.2}$$

Its dynamics are given by [135]

$$\dot{\bar{\eta}} = J(\bar{\eta}) \begin{bmatrix} v \\ \omega \end{bmatrix} - S(\bar{\eta}) w, \tag{5.3}$$

where $v \in \mathbb{R}^3$ and $\omega \in \mathbb{R}^3$ denote the translational and angular velocities of the camera in the camera frame, respectively, $w \in \mathbb{R}^3$ is the feature point velocity in the camera frame, and

$$S(\bar{\eta}) = \begin{bmatrix} -\frac{f}{z} & 0 & \frac{u_x}{z} \\ 0 & -\frac{f}{z} & \frac{u_y}{z} \\ 0 & 0 & -1 \end{bmatrix}, \tag{5.4a}$$

$$J(\bar{\eta}) = \begin{bmatrix} -\frac{f}{z} & 0 & \frac{u_x}{z} & \frac{u_x u_y}{f} & -\frac{f^2+u_x^2}{f} & u_y \\ 0 & -\frac{f}{z} & \frac{u_y}{z} & \frac{f^2+u_y^2}{f} & -\frac{u_x u_y}{f} & -u_x \\ 0 & 0 & -1 & -\frac{u_y z}{f} & \frac{u_x z}{f} & 0 \end{bmatrix}. \tag{5.4b}$$

For notational convenience, we denote

$$V = \begin{bmatrix} v \\ \omega \end{bmatrix} \in \mathbb{R}^6 \tag{5.5}$$

as the concatenation of the translational and angular velocity vectors, and rewrite (5.3) equivalently as

$$\dot{\bar{\eta}} = J(\bar{\eta})V - S(\bar{\eta})w. \tag{5.6}$$

5.2.2 Vertex-Based Representation of Object Images

In computer vision, an image feature refers to any structural attribute extracted from an image, and a good feature point is one that can be located unambiguously across different views [125]. In this work, the images of the target and occluding objects are assumed to be over-approximated by the convex hulls of their respective feature points.

Let $\eta_0^i \in \mathbb{R}^2$ denote the image coordinates of the i-th feature point on the target object, where $i \in [N_0]$ with $N_0 \in \mathbb{Z}_{>0}$; let η_j^i denote the image coordinates of the i-th feature point on the j-th occluding object, where $i \in [N_j], j \in [M]$ with $N_j, M \in \mathbb{Z}_{>0}$. Denote by $\mathbb{T}$ the image of the target object and by $\mathbb{O}_j$ the image of the j-th occluding object. Then,

$$\mathbb{T} \subseteq \text{conv}(\eta_0^1, \cdots, \eta_0^{N_0}) \triangleq \bar{\mathbb{T}}, \tag{5.7a}$$

$$\mathbb{O}_j \subseteq \text{conv}(\eta_j^1, \cdots, \eta_j^{N_j}) \triangleq \bar{\mathbb{O}}_j, \ j \in [M], \tag{5.7b}$$

where $\text{conv}(\cdot)$ denotes the convex hull operator defined in Section 1.4 (see Figure 5.2). Note that N_0 and N_j may vary depending on the specific image processing algorithm used to extract the feature point coordinates. Nevertheless, the control framework presented in the subsequent sections remains valid as long as (5.7) holds.

In contrast to existing approaches that rely on the half-space representation (H-rep) of convex polytopes [132], [136], we adopt the vertex representation (V-rep) [137] in our con-

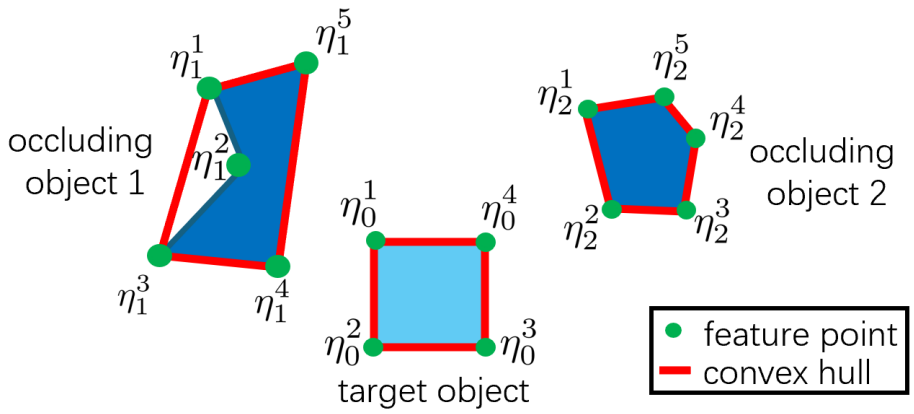

Figure 5.2: Illustration of the vertex-based representation of image objects.

trol framework. This choice offers several advantages: it aligns directly with image data, enhances numerical robustness, and enables a differentiable formulation. More detailed discussions are provided in Section 5.3.

5.2.3 Problem Formulation

Consider the robotic manipulator described as [138]

$$D(q)\ddot{q} + C(q,\dot{q})\dot{q} + G(q) = \tau, \tag{5.8}$$

where $q \in \mathbb{R}^n$ is the joint angle, $\dot{q} \in \mathbb{R}^n$ is the angular velocity, $\tau \in \mathbb{R}^n$ is the control input, $D : \mathbb{R}^n \to \mathbb{R}^{n\times n}$ is the inertia matrix, $C : \mathbb{R}^n \times \mathbb{R}^n \to \mathbb{R}^{n\times n}$ is the Coriolis/centripetal matrix, and $G : \mathbb{R}^n \to \mathbb{R}^n$ is the gravity term.

The problem addressed in this paper is formally stated as follows:

Problem 5.1 *Consider a robotic manipulator equipped with a camera on its end-effector, where the robot dynamics are given by* (5.8) *and the visual dynamics by* (5.6)*. The goal is to design a control law for the robot that achieves the following two tasks simultaneously:*

1. *Target feature points regulation: The image coordinates of all feature points on the*

target object, $\eta_0^i \in \mathbb{R}^2$, are regulated to their desired values, $\eta_{0,d}^i$, i.e.,

$$\eta_0^i(t) \to \eta_{0,d}^i(t) \text{ as } t \to \infty, \ \forall i \in [N_0]. \tag{5.9}$$

2. *Occlusion avoidance: Visual occlusion with any of the M occluding objects is avoided during the execution, i.e.,*

$$\mathbb{O}(t) \cap \mathbb{T}_j(t) = \emptyset, \ \forall t \geq 0, \forall j \in [M]. \tag{5.10}$$

We propose a hierarchical, optimization-based, and occlusion-free visual servoing framework to solve Problem 5.1. As illustrated in Figure 5.1, the control scheme comprises two main components: a high-level MPC (Section 5.3) and a low-level CBF-based controller (Section 5.4). The high-level MPC ensures target regulation and provides a desired input to the CBF-based controller, while the low-level controller strictly enforces occlusion-avoidance constraints. The reference velocity generated by the CBF-based controller is then tracked by a standard Cartesian velocity controller to yield the final control input τ for the robot.

5.3 High-level MPC via Duality-Based Optimization

In this section, we present an MPC as the high-level control scheme of the hierarchical framework, which generates the desired Cartesian velocity in discrete time, enabling the robot to regulate target feature points (Task 1 of Problem 5.1) and avoid visual occlusion. By leveraging a vertex-based representation of object images and duality theory in optimization, the nonsmooth distance constraints are reformulated as smooth functions that can be seamlessly incorporated into the MPC.

The discrete-time MPC model of the visual dynamics is obtained by applying explicit Euler discretization to (5.6). For the i-th feature point on the j-th object, the dynamic

model is

$$\bar{\eta}_j^i(k+1) = \bar{\eta}_j^i(k) + TJ(\bar{\eta}_j^i(k))V(k) - TS(\bar{\eta}_j^i(k))w_j^i(k), \tag{5.11}$$

where k is the discrete time step, T is the sampling period, and $\bar{\eta}_j^i$ and w_j^i are the augmented state and velocity of the i-th feature point on the j-th object, respectively. Recall that $j = 0$ in η_j^i corresponds to the target object, while $j \in [M]$ indexes the occluding objects. The feature point velocity w_j^i must be estimated over the prediction horizon (see Remark 5.1).

We use the distance between two sets to formulate the occlusion-avoidance constraints $\mathbb{O}(t) \cap \mathbb{T}_j(t) = \emptyset$ shown in (5.10). The distance between the target object and the j-th occluding object is defined as

$$\mathrm{d}(\mathbb{T}, \mathbb{O}_j) = \min_{x,y} \{\|x - y\| : x \in \mathbb{T}, y \in \mathbb{O}_j\}. \tag{5.12}$$

It is obvious that $\mathrm{d}(\mathbb{T}, \mathbb{O}_j) > 0$ implies $\mathbb{O}(t) \cap \mathbb{T}_j(t) = \emptyset$. With the vertex representations of the convex hulls defined in (5.7), the distance $\mathrm{d}(\bar{\mathbb{T}}, \bar{\mathbb{O}}_j)$ can be obtained by solving the following optimization problem

$$\begin{aligned}
\mathrm{d}(\bar{\mathbb{T}}, \bar{\mathbb{O}}_j) = \min_{\alpha,\beta,\theta} \ & \|\theta\| && \text{(5.13a)}\\
\text{s.t.} \ & \alpha \geq 0, \beta \geq 0, && \text{(5.13b)}\\
& \mathbf{1}_{N_0}^\top \alpha = 1, \mathbf{1}_{N_j}^\top \beta = 1, && \text{(5.13c)}\\
& \Gamma\alpha - \Lambda_j \beta = \theta, && \text{(5.13d)}
\end{aligned}$$

where $\alpha \in \mathbb{R}^{N_0}$, $\beta \in \mathbb{R}^{N_j}$, and $\theta \in \mathbb{R}^2$ are decision variables,

$$\Gamma = [\eta_0^1, \eta_0^2, \cdots, \eta_0^{N_0}], \tag{5.14}$$

$$\Lambda_j = [\eta_j^1, \eta_j^2, \cdots, \eta_j^{N_j}], \ j \in [M]. \tag{5.15}$$

Since $\mathrm{d}(\mathbb{T}, \mathbb{O}_j) \geq \mathrm{d}(\bar{\mathbb{T}}, \bar{\mathbb{O}}_j)$, the occlusion-avoidance constraints $\mathbb{O}(t) \cap \mathbb{T}_j(t) = \emptyset$ shown

in (5.10) can be relaxed to $\mathrm{d}(\bar{\mathbb{T}}, \bar{\mathbb{O}}_j) > 0$. We add a safety margin so that the relaxed occlusion-avoidance constraints are given as

$$\mathrm{d}(\bar{\mathbb{T}}, \bar{\mathbb{O}}_j) \geq d_{\min}, \tag{5.16}$$

for any $j \in [M]$, where $d_{\min} > 0$ denotes the safety margin. However, condition (5.16) cannot be directly incorporated in an MPC since $\mathrm{d}(\bar{\mathbb{T}}, \bar{\mathbb{O}}_j)$ involves solving the optimization problem (5.13) and its Jacobian and Hessian are hard to obtain. To address this issue, inspired by [139], we formulate a set of differentiable constraints to enforce the occlusion-avoidance constraints (5.16), as shown in the following theorem.

Theorem 5.1 *The occlusion-avoidance constraint* (5.16) *is satisfied if there exist* $\lambda_j \in \mathbb{R}^{N_0}$, $\mu_j \in \mathbb{R}^{N_j}$, $\xi_j, \zeta_j \in \mathbb{R}$, *and* $\nu_j \in \mathbb{R}^2$ *such that the following conditions hold true*

$$-\xi_j - \zeta_j \geq d_{\min}, \tag{5.17a}$$

$$\lambda_j \geq 0, \mu_j \geq 0, \tag{5.17b}$$

$$\nu_j^\top \nu_j \leq 1, \tag{5.17c}$$

$$\Gamma^\top \nu_j - \lambda_j + \xi_j \mathbf{1}_{N_0} = 0, \tag{5.17d}$$

$$-\Lambda_j^\top \nu_j - \mu_j + \zeta_j \mathbf{1}_{N_j} = 0. \tag{5.17e}$$

Proof *The Lagrangian of optimization problem* (5.13) *is*

$$\begin{aligned} L(\lambda_j, \mu_j, \xi_j, \nu_j, \zeta_j, \alpha, \beta, \theta) = \|\theta\| - \lambda_j^\top \alpha - \mu_j^\top \beta + \xi_j(\mathbf{1}_{N_0}^\top \alpha - 1) \\ + \zeta_j(\mathbf{1}_{N_j}^\top \beta - 1) + \nu_j^\top(\Gamma\alpha - \Lambda_j\beta - \theta). \end{aligned} \tag{5.18}$$

Therefore, the Lagrange dual function is

$$\begin{aligned} g(\lambda_j, \mu_j, \xi_j, \nu_j, \zeta_j) &= \inf_{\alpha,\beta,\theta} L(\lambda_j, \mu_j, \xi_j, \nu_j, \zeta_j, \alpha, \beta, \theta) \\ &= -\xi_j - \zeta_j + \inf_{\theta} \left(\|\theta\| - \nu_j^\top \theta \right) + \inf_{\alpha} (\nu_j^\top \Gamma - \lambda_j^\top + \xi_j \mathbf{1}_{N_0}^\top)\alpha \end{aligned}$$

$$+\inf_{\beta}(-\nu_j^\top \Lambda_j - \mu_j^\top + \zeta_j \mathbf{1}_{N_j}^\top)\beta. \tag{5.19}$$

Note that $\inf_\theta \left(\|\theta\| - \nu_j^\top \theta\right) = -f^*(\nu)$ *where* $f(\theta) = \|\theta\|$ *and* f^* *is the convex conjugate. Since the conjugate of the norm is the indicator function of the unit ball of the dual norm, we have* $f^*(\nu) = 0$ *if* $\|\nu_j\| \leq 1$ *and* $+\infty$ *if* $\|\nu_j\| > 1$*, which implies* $\inf_\theta \left(\|\theta\| - \nu_j^\top \theta\right) = 0$ *if* $\|\nu_j\| \leq 1$ *and* $-\infty$ *if* $\|\nu_j\| > 1$*. It is clear that* $\inf_\alpha(\nu_j^\top \Gamma - \lambda_j^\top + \xi_j \mathbf{1}_{N_0}^\top)\alpha = 0$ *if* $\nu_j^\top \Gamma - \lambda_j^\top + \xi_j \mathbf{1}_{N_0}^\top = 0$*, and* $-\infty$ *otherwise; similarly,* $\inf_\beta(-\nu_j^\top \Lambda_j - \mu_j^\top + \zeta_j \mathbf{1}_{N_j}^\top)\beta = 0$ *if* $-\nu_j^\top \Lambda_j - \mu_j^\top + \zeta_j \mathbf{1}_{N_j}^\top = 0$*, and* $-\infty$ *otherwise. Therefore, the dual problem of* (5.13) *is*

$$\begin{aligned} \tilde{d}_j = \max_{\lambda_j, \mu_j, \xi_j, \zeta_j, \nu_j} \quad & -\xi_j - \zeta_j \\ s.t. \quad & \lambda_j \geq 0, \mu_j \geq 0, \\ & \|\nu_j\| \leq 1, \\ & \nu_j^\top \Gamma - \lambda_j^\top + \xi_j \mathbf{1}_{N_0}^\top = 0, \\ & -\nu_j^\top \Lambda_j - \mu_j^\top + \zeta_j \mathbf{1}_{N_j}^\top = 0. \end{aligned} \tag{5.20}$$

Thus, the conditions in (5.17) *implies* $\tilde{d}_j \geq d_{\min}$*. By the weak duality,* $\mathrm{d}(\bar{\mathbb{T}}, \bar{\mathbb{O}}_j) \geq \tilde{d}_j \geq d_{\min}$*. This completes the proof.* □

In contrast to existing works [132], [139], which employ the H-rep of polytopes for occlusion constraints, Theorem 3.1 establishes equivalent conditions using the vertex representation. The V-rep offers several important advantages over the H-rep for handling the image-based occlusion avoidance.

- *Direct compatibility with image data*: Image processing algorithms typically provide only the pixel coordinates of feature points, which usually correspond to boundary points. Using V-rep eliminates the need of computing half-space conversion, which can be computationally expensive.

- *Numerical robustness*: H-rep can suffer from numerical issues when some feature points lie inside the polytope, potentially leading to redundant or ill-conditioned

constraints. In contrast, V-rep is less sensitive to such degeneracies.

- *Differentiability and analytical convenience*: If the H-rep of the target object's image is expressed as $\{\eta \in \mathbb{R}^2 \mid A(\eta_0^1, \ldots, \eta_0^{N_0})\eta \leq b(\eta_0^1, \ldots, \eta_0^{N_0})\}$, then the gradients of A and b are difficult or impossible to compute, posing a significant challenge for CBF-based control design. V-rep avoids this issue by maintaining a smooth and direct dependence on the coordinates of feature points.

The MPC problem (5.21) is solved in a receding horizon manner at each discrete time step. At time k, the end-effector velocity $V(0|k)$ obtained from (5.21) is provided to the low-level CBF as the nominal input V_{mpc}. Although the occlusion constraint (5.16) is enforced only at discrete time instants in (5.21), its continuous satisfaction is ensured by the low-level CBF condition, which will be described in the next section.

By incorporating the dual-form safety constraints (5.17) in discrete time, we formulate the MPC shown in (5.21) to regulate the target feature points to their desired values. In (5.21a), the positive definite matrices Q, R, Q_N penalize the stage states, control inputs, and terminal states, respectively; $[\bar{\eta}_0^i(n|k)]_{1:2}$, which is equal to $\eta_0^i(n|k)$, represent the image coordinates of the i-th feature point on the target; and $\eta_{0,d}^i$ is the desired image coordinates of the target. Condition (5.21b) specifies the initial condition of $\bar{\eta}_j^i$; condition (5.21c) is the system dynamics constraint from (5.11); conditions (5.21d)-(5.21g) impose the occlusion-avoidance constraints from (5.17); condition (5.21h) bounds the control inputs, where $V_{\min}, V_{\max} \in \mathbb{R}^6$ denote the minimum and maximum end-effector velocities; and condition (5.21i) imposes the field-of-view constraints, where $\eta_{\min}, \eta_{\max} \in \mathbb{R}^2$ denote the bounds on the pixel coordinates of target feature points. The term Γ_n in (5.21f) and Λ_{jn} in (5.21g) are defined according to (5.14) and (5.15): $\Gamma_n = [\eta_0^1(n|k), \eta_0^2(n|k), \cdots, \eta_0^{N_0}(n|k)]$, $\Lambda_{jn} = [\eta_j^1(n|k), \eta_j^2(n|k), \cdots, \eta_j^{N_j}(n|k)]$, and the term $\hat{w}_j^i$ in (5.21c) denotes the estimated velocity of the i-th feature point of object j.

Remark 5.1 *In practice, we assume that the estimated velocity $\hat{w}_j^i$ in* (5.21c) *remains constant over the prediction horizon and determine its value from the measurement of $\bar{\eta}_j^i$.*

$$\min_{\substack{\{\bar{\eta}_j^i(n|k),V(n|k),\\ \xi_{jn},\zeta_{jn},\nu_{jn},\lambda_{jn},\mu_{jn}\},\\ j\in[0,M],i\in[N_i],n\in[0,N]}} \sum_{n=0}^{N-1}\sum_{i=1}^{N_0}(\|[\bar{\eta}_0^i(n|k)]_{1:2}-\eta_{0,d}^i\|_Q^2+\|V(n|k)\|_R^2)+\sum_{i=1}^{N_0}\|[\bar{\eta}_0^i(N|k)]_{1:2}-\eta_{0,d}^i\|_{Q_N}^2 \tag{5.21a}$$

$$\text{s.t.} \quad \bar{\eta}_j^i(0|k)=\bar{\eta}_j^i(k),\ j\in[0,M], i\in[N_i], \tag{5.21b}$$

$$\bar{\eta}_j^i(n+1|k)=\bar{\eta}_j^i(n|k)+TJ(\bar{\eta}_j^i(n|k))V(n|k) -TS(\bar{\eta}_j^i(n|k))\hat{w}_j^i(k),\ j\in[0,M], i\in[N_i], n\in[0,N], \tag{5.21c}$$

$$-\xi_{jn}-\zeta_{jn}\geq d_{\min},\ j\in[M], n\in[N], \tag{5.21d}$$

$$\lambda_{jn}\geq 0, \mu_{jn}\geq 0, \|\nu_{jn}\|\leq 1,\ j\in[M], n\in[N], \tag{5.21e}$$

$$\Gamma_n^\top\nu_{jn}-\lambda_{jn}+\xi_{jn}\mathbf{1}_{N_0}=0,\ j\in[M], n\in[N], \tag{5.21f}$$

$$-\Lambda_{jn}^\top\nu_{jn}-\mu_{jn}+\zeta_{jn}\mathbf{1}_{N_j}=0,\ j\in[M], n\in[N], \tag{5.21g}$$

$$V_{\min}\leq V(n|k)\leq V_{\max},\ n\in[0,N], \tag{5.21h}$$

$$\eta_{\min}\leq \eta_0^i(n|k)\leq \eta_{\max},\ n\in[0,N], i\in[N_0]. \tag{5.21i}$$

Below, we present two methods for estimating w using the state measurement $\bar{\eta}$ based on the visual dynamics (5.6).

Extended Kalman Filter (EKF): Note that the visual dynamics (5.6) *can be discretized and reformulated as*

$$\begin{bmatrix}\bar{\eta}(k+1)\\ w(k+1)\end{bmatrix}=\begin{bmatrix}\bar{\eta}(k)+TJ(\bar{\eta}(k))V(k)-TS(\bar{\eta}(k))w(k)\\ w(k)+T\dot{w}(k)\end{bmatrix}, \tag{5.22a}$$

$$y(k)=\bar{\eta}(k), \tag{5.22b}$$

where T is the sampling time, $w(k)$ is the state variable to be estimated, $y(k)$ is the output measurement, and $\dot{w}(k)$ is treated as process noise. An EKF can then be deployed to simultaneously estimate $\bar{\eta}$ and w.

Disturbance Observer: Suppose that the acceleration of the feature point satisfies $\|\dot{w}\|\leq W$, where $W>0$ is a constant, and that $z(t)\neq 0$ for any $t\geq 0$. These assumptions are mild and readily satisfied in practice. Under these conditions, the DOB from [27] can be employed to obtain $\hat{w}$ as the estimate of w

$$\hat{w}=m+\alpha p,$$

$$\dot{m} = -\alpha L_d \left(J(\bar{\eta}) V - S(\bar{\eta}) \hat{w} \right),$$

where $\alpha > \frac{1}{2}$ *is a constant, and*

$$p = [-\frac{u_x z}{f}, -\frac{u_y z}{f}, -z]^\top, L_d = \begin{bmatrix} -\frac{z}{f} & 0 & -\frac{u_x}{f} \\ 0 & -\frac{z}{f} & -\frac{u_y}{f} \\ 0 & 0 & -1 \end{bmatrix}.$$

We define the estimation error as $\tilde{w} = \hat{w} - w$ *and consider the candidate Lyapunov function* $V = \frac{1}{2}\tilde{w}^\top \tilde{w}$. *It follows that* $\dot{V} = -\alpha \tilde{w}^\top \tilde{w} - \tilde{w}^\top \dot{w} \leq -\tilde{w}^\top \dot{w} + \|\tilde{w}\| W \leq -\left(\alpha - \frac{1}{2}\right) \|\tilde{w}\|^2 + \frac{W^2}{2} = -(2\alpha - 1)\mathrm{V} + \frac{W^2}{2}$, *which implies that* $\tilde{w}$ *is uniformly ultimately bounded [26].*

The two methods above each have their advantages and limitations. With a sufficiently high measurement update frequency, the DOB can estimate w *accurately, and its estimation error bound is known and can be incorporated into the control design. However, in our experiments, the camera update rate is limited to 30 Hz, resulting in insufficient estimation accuracy. By contrast, the EKF performs well empirically, but its estimation error cannot be explicitly quantified.*

Remark 5.2 *In practice, the optimization problem* (5.21) *can become infeasible, particularly when the distance between the target and occluding objects approaches* $d_{\min}$. *To address this issue, we introduce slack variables* $\delta_j(n|k)$, *which satisfies* $0 \leq \delta_j(n|k) \leq d_{\min}$, *into constraint* (5.21d), *reformulating it as*

$$-\xi_j(n|k) - \zeta_j(n|k) \geq d_{\min} - \delta_j(n|k). \tag{5.23}$$

A quadratic penalty term $p\delta_j(n|k)^2$, *with* $p > 0$, *is then added to the objective function* (5.21a). *While this relaxation may allow occlusion when MPC is applied alone, occlusion avoidance is still guaranteed under the proposed hierarchical control framework, as the low-level CBFs strictly enforce the occlusion-avoidance constraints.*

Furthermore, in J *given in* (5.6), *the variable* z *appears in the denominators, mak-*

ing the system highly nonlinear and potentially causing failures in solving (5.21)*, as the optimization algorithm may drive z close to zero. In practice, however, z varies slowly over time, suggesting it can be treated as fixed in* (5.21)*. Specifically, upon receiving state feedback and initiating the MPC computation, the control sequence V from the previous iteration is used to forward propagate a sequence of z via the visual dynamics* (5.6)*. Then, in* (5.21)*, the values $z(n|k)$, $n \in [N]$, are set to this sequence and treated as known constants rather than decision variables.*

5.4 Low-Level CBF-QP-based Safe Control

In this section, we present a robust CBF-QP-based controller as the low-level scheme of the hierarchical framework, which strictly enforces the occlusion-avoidance constraint (5.16) for all $t \geq 0$ in continuous time, thereby achieving Task 2 of Problem 5.1.

We consider the image coordinate dynamics of the i-th feature point on object j from (5.6)

$$\dot{\eta}_j^i = \bar{J}(\bar{\eta}_j^i)V - \bar{S}(\bar{\eta}_j^i)w_j^i, \tag{5.24}$$

where $\eta_j^i \in \mathbb{R}^2$ denotes the image coordinates defined in (5.1), and $\bar{J}(\bar{\eta}_i^j)$ and $\bar{S}(\bar{\eta}_i^j)$ consist of the first two rows of $J(\bar{\eta}_i^j)$ and $S(\bar{\eta}_i^j)$, respectively, from (5.4). Compared with the model (5.6) used for the MPC design, the model (5.24) excludes the dynamics of z since they are not required in the CBF design.

To compactly express $\mathrm{d}(\bar{\mathbb{T}}, \bar{\mathbb{O}}_j)$, the distance between $\bar{\mathbb{T}}$ and $\bar{\mathbb{O}}_j$, we define the vector obtained by concatenating all feature points of $\bar{\mathbb{T}}$ and $\bar{\mathbb{O}}_j$

$$\boldsymbol{\eta}_j = [\eta_0^{1\top}, \cdots, \eta_0^{N_0\top}, \eta_j^{1\top}, \cdots, \eta_j^{N_j\top}]^\top \in \mathbb{R}^{2(N_0+N_j)}. \tag{5.25}$$

From (5.24), the dynamics of $\boldsymbol{\eta}_j$ can be expressed as

$$\dot{\boldsymbol{\eta}}_j = J_j(\bar{\boldsymbol{\eta}}_j)V - S_j(\bar{\boldsymbol{\eta}}_j)\boldsymbol{w}_j, \tag{5.26}$$

where $\bar{\boldsymbol{\eta}}_j = [\bar{\eta}_0^{1\top}, \cdots, \bar{\eta}_0^{N_0\top}, \bar{\eta}_j^{1\top}, \cdots, \bar{\eta}_j^{N_j\top}]^\top \in \mathbb{R}^{3(N_0+N_j)}$, $J_j = [\bar{J}(\bar{\eta}_0^1)^\top, \cdots, \bar{J}(\bar{\eta}_0^{N_0})^\top, \bar{J}(\bar{\eta}_j^1)^\top, \cdots, \bar{J}(\bar{\eta}_j^{N_j})^\top]^\top$, $S_j(\bar{\boldsymbol{\eta}}_j) = \text{blkdiag}(\bar{S}(\bar{\boldsymbol{\eta}}_0^1), \cdots, \bar{S}(\bar{\boldsymbol{\eta}}_0^{N_0}), \bar{S}(\bar{\boldsymbol{\eta}}_j^1), \cdots, \bar{S}(\bar{\boldsymbol{\eta}}_j^{N_j}))$, and $\boldsymbol{w}_j = [w_0^{1\top}, \cdots, w_0^{N_0\top}, w_j^{1\top}, \cdots, w_j^{N_j\top}]^\top$, $j \in [M]$.

We aim to design CBFs that ensure the occlusion-avoidance constraints (5.16) for all $t \geq 0$ and $j \in [M]$. However, $\text{d}(\bar{\mathbb{T}}, \bar{\mathbb{O}}_j)$ is computed by solving the optimization problem (5.13), whose objective function is not strictly convex. This leads to a non-unique minimizer and a non-Lipschitz continuous distance function, which poses challenges in computing the gradient of $\text{d}(\bar{\mathbb{T}}, \bar{\mathbb{O}}_j)$. To address this issue, we define the following function $\tilde{h}_j(\boldsymbol{\eta}_j)$ for any $j \in [M]$

$$\begin{aligned} \tilde{h}_j(\boldsymbol{\eta}_j) = \min_{\alpha,\beta,\theta} \ & \theta^\top\theta + \delta_1\alpha^\top\alpha + \delta_2\beta^\top\beta \\ \text{s.t.} \ & \text{(5.13b)} - \text{(5.13d)}, \end{aligned} \tag{5.27}$$

where $\delta_1, \delta_2 > 0$ are positive constants representing the penalty weights. It is clear that $\tilde{h}_j \geq \text{d}(\bar{\mathbb{T}}, \bar{\mathbb{O}}_j)^2$. Furthermore, although $\tilde{h}_j$ can be shown to be Lipschitz continuous with respect to $\boldsymbol{\eta}_j$, it may be nondifferentiable at points where the strict complementarity condition fails for the optimization problem (5.27) [140]. To address this issue, we employ nonsmooth CBF techniques [141], [142].

For a set A, define $\bar{\mathcal{P}}(A) = \mathcal{P}(A)\backslash A$, where $\mathcal{P}(A)$ denotes the power set of A. Given two sets $\mathcal{I}_\alpha \in \bar{\mathcal{P}}([N_0]), \mathcal{I}_\beta \in \bar{\mathcal{P}}([N_j])$, and any $j \in [M]$, we define a function $F_j(\boldsymbol{\eta}_j; \mathcal{I}_\alpha, \mathcal{I}_\beta)$ as

$$F_j(\boldsymbol{\eta}_j; \mathcal{I}_\alpha, \mathcal{I}_\beta) = \min_{\alpha,\beta,\theta} \ \theta^\top\theta + \delta_1\alpha^\top\alpha + \delta_2\beta^\top\beta \tag{5.28a}$$

$$\text{s.t.} \quad \alpha \geq 0, \beta \geq 0, \tag{5.28b}$$

$$\alpha_k = 0, \ \forall k \in \mathcal{I}_\alpha, \tag{5.28c}$$

$$\beta_l = 0, \ \forall l \in \mathcal{I}_\beta, \tag{5.28d}$$

$$\mathbf{1}_{N_0}^\top\alpha = 1, \mathbf{1}_{N_j}^\top\beta = 1, \tag{5.28e}$$

$$\Gamma\alpha - \Lambda_j\beta = \theta. \tag{5.28f}$$

The following result characterizes the differentiability of F_j and its relation to $\tilde{h}_j$.

Theorem 5.2 *Consider the functions $\tilde{h}_j$ defined in* (5.27) *and F_j defined in* (5.28)*. The following statements hold true:*

1. *The function F_j is well-defined and differentiable for any $\boldsymbol{\eta}_j$, $\mathcal{I}_\alpha \in \bar{\mathcal{P}}([N_0])$, and $\mathcal{I}_\beta \in \bar{\mathcal{P}}([N_j])$.*

2. *For any $\boldsymbol{\eta}_j$, there exists $\mathcal{I}_\alpha \in \bar{\mathcal{P}}([N_0])$ and $\mathcal{I}_\beta \in \bar{\mathcal{P}}([N_j])$ such that $F_j(\boldsymbol{\eta}_j; \mathcal{I}_\alpha, \mathcal{I}_\beta) = \tilde{h}_j(\boldsymbol{\eta}_j)$.*

Proof *Given $\mathcal{I}_\alpha \in \bar{\mathcal{P}}([N_0])$ and $\mathcal{I}_\beta \in \bar{\mathcal{P}}([N_j])$, we define a matrix*

$$M(\mathcal{I}_\alpha, \mathcal{I}_\beta) = \begin{bmatrix} -[\mathrm{I}_{N_0}]_{\mathcal{I}_\alpha} & 0 & 0 \\ 0 & -[\mathrm{I}_{N_j}]_{\mathcal{I}_\beta} & 0 \\ \boldsymbol{1}_{N_0}^\top & 0 & 0 \\ 0 & \boldsymbol{1}_{N_j}^\top & 0 \\ \Gamma & -\Lambda_j & -\mathrm{I}_2 \end{bmatrix}, \tag{5.29}$$

where $[\mathrm{I}_{N_0}]_{\mathcal{I}_\alpha}$ and $[\mathrm{I}_{N_j}]_{\mathcal{I}_\beta}$ denote the matrix formed by selecting the rows of I_{N_0} and I_{N_j} indexed by the sets $\mathcal{I}_\alpha$ and $\mathcal{I}_\beta$, respectively. We will first show that the linear independence constraint qualification (LICQ) is satisfied for the optimization problems (5.27) *and* (5.28)*. Suppose the solution to* (5.27) *is $(\alpha^*, \beta^*, \theta^*)$ and the corresponding active sets are $\mathcal{I}_\alpha^* = \{i \in [N_0] : \alpha_i^* = 0\}$ and $\mathcal{I}_\beta^* = \{i \in [N_j] : \beta_i^* = 0\}$. Note that LICQ holds if the matrix $M(\mathcal{I}_\alpha^*, \mathcal{I}_\beta^*)$ has full row rank. It is straightforward to verify that $\alpha_i^* = 0$ cannot hold for all $i \in [N_0]$ (i.e., $\mathcal{I}_\alpha^* \neq [N_0]$); otherwise the equality constraints $\boldsymbol{1}_{N_0}^\top \alpha = 1$ cannot be satisfied. A similar argument applies to the constraints $\beta \geq 0$. Hence, the matrix defined in* (5.29) *has full row rank, indicating that LICQ is satisfied. It can be shown that LICQ holds for* (5.28) *by similar reasoning.*

1) Since the QP (5.28) *is strictly convex, the value of F_j is uniquely determined for a given $\boldsymbol{\eta}_j$, implying that F_j is well defined. Moreover, because the LICQ condition holds for* (5.28)*, the optimal multiplier is also unique [143, Section 12.2], and the KKT conditions*

can be written as

$$\underbrace{\begin{bmatrix} Qz^* + A^\top(\boldsymbol{\eta}_j)\lambda_A^* + G^\top\lambda_G^* \\ Gz^* \\ A(\boldsymbol{\eta}_j)z^* - b \end{bmatrix}}_{\triangleq R(z^*,\lambda_G^*,\lambda_A^*,\boldsymbol{\eta}_j)} = 0. \tag{5.30}$$

where $z^* = [\theta^{*\top}, \alpha^{*\top}, \beta^{*\top}]^\top$, λ_A^*, λ_G^* *denote the multipliers,* $Q = blkdiag(2\mathrm{I}_2, 2\delta_1\mathrm{I}_{N_0}, 2\delta_2\mathrm{I}_{N_j})$, $b = [0, 0, 1, 1]^\top$, *and*

$$G = \begin{bmatrix} -[\mathrm{I}_{N_0}]_{\mathcal{I}_\alpha} & 0_{N_0\times N_j} & 0_{N_0\times 2} \\ 0_{N_j\times N_0} & -[\mathrm{I}_{N_j}]_{\mathcal{I}_\beta} & 0_{N_j\times 2} \end{bmatrix}, \tag{5.31a}$$

$$A(\boldsymbol{\eta}_j) = \begin{bmatrix} \Gamma & -\Lambda_j & -\mathrm{I}_2 \\ \boldsymbol{1}_{N_0}^\top & 0_{N_j\times 1} & 0_{1\times 2} \\ 0_{N_0\times 1} & \boldsymbol{1}_{N_j}^\top & 0_{1\times 2} \end{bmatrix}. \tag{5.31b}$$

Let $x^* = [z^{*\top}, \lambda_A^{*\top}, \lambda_G^{*\top}]^\top$. *Then,*

$$\frac{\partial R}{\partial x^*} = \begin{bmatrix} Q & A^\top & G^\top \\ G & 0 & 0 \\ A & 0 & 0 \end{bmatrix}. \tag{5.32}$$

Since Q *is positive definite and* $[G^\top, A^\top]^\top$ *has full row rank following the argument after* (5.29), *it is easy to show that* $\frac{\partial R}{\partial x^*}$ *is nonsingular for any* $\boldsymbol{\eta}_j \in \mathbb{R}^{2(N_0+N_j)}$ *[143, Lemma 16.1]. According to the implicit function theorem, one can see that* F_j, *which corresponds to the solution to* (5.28), *is differentiable.*

2) The second statement follows from the fact that $F_j(\boldsymbol{\eta}_j; \mathcal{I}_\alpha^*, \mathcal{I}_\beta^*) = \tilde{h}_j(\boldsymbol{\eta}_j)$, *where* $\mathcal{I}_\alpha^*$ *and* $\mathcal{I}_\beta^*$ *are active sets of the problem* (5.27). □

From Theorem 5.2, the gradient of $F_j(\boldsymbol{\eta}_j; \mathcal{I}_\alpha, \mathcal{I}_\beta)$ with respect to $\boldsymbol{\eta}_j$ can be computed, which is required for the implementation of the CBF controller. Specifically, denote the i-th entry of $\boldsymbol{\eta}_j$ by $\boldsymbol{\eta}_{ji}$, $i \in [2N_0 + 2N_j]$, and take the partial derivative with respect to $\boldsymbol{\eta}_{ji}$

on both sides of (5.30)

$$\begin{bmatrix} Q & A^\top(\boldsymbol{\eta}_j) & G^\top \\ G & 0 & 0 \\ A(\boldsymbol{\eta}_j) & 0 & 0 \end{bmatrix} \begin{bmatrix} \frac{\partial z^*}{\partial \boldsymbol{\eta}_{ji}} \\ \frac{\partial \lambda_A^*}{\partial \boldsymbol{\eta}_{ji}} \\ \frac{\partial \lambda_G^*}{\partial \boldsymbol{\eta}_{ji}} \end{bmatrix} = \begin{bmatrix} -\frac{\partial A^\top(\boldsymbol{\eta}_j)}{\partial \boldsymbol{\eta}_{ji}} \lambda_A^* \\ 0 \\ -\frac{\partial A^\top(\boldsymbol{\eta}_j)}{\partial \boldsymbol{\eta}_{ji}} z^* \end{bmatrix}. \tag{5.33}$$

Since Q is positive definite and $[G^\top, A^\top]^\top$ has full row rank, the linear system (5.33) admits a unique solution. Collecting the solutions for all entries of $\boldsymbol{\eta}_j$, we define $\frac{\partial z^*}{\partial \boldsymbol{\eta}_j} = \begin{bmatrix} \frac{\partial z^*}{\partial \boldsymbol{\eta}_{j1}} & \frac{\partial z^*}{\partial \boldsymbol{\eta}_{j2}} & \cdots & \frac{\partial z^*}{\partial \boldsymbol{\eta}_{j(2N_0+2N_j)}} \end{bmatrix}$. Since $F = \frac{1}{2} z^{*\top} Q z^*$, the gradient $\frac{\partial F}{\partial \boldsymbol{\eta}_j}$ can be computed as

$$\frac{\partial F}{\partial \boldsymbol{\eta}_j} = z^{*\top} Q \frac{\partial z^*}{\partial \boldsymbol{\eta}_j}. \tag{5.34}$$

From Theorem 5.2, we can also see that $\tilde{h}_j$ is piecewise differentiable [141, Definition II.9]. By [141, Proposition III.3], for any $\boldsymbol{\eta}_j \in \mathbb{R}^{2(N_0+N_j)}$, there exists a locally encapsulating index set $I_{h_j}(\boldsymbol{\eta}_j) \subseteq \{(\mathcal{I}_\alpha, \mathcal{I}_\beta) : \mathcal{I}_\alpha \in \bar{\mathcal{P}}([N_0]), \mathcal{I}_\beta \in \bar{\mathcal{P}}([N_j])\}$ such that the generalized gradient of $\tilde{h}_j$ with respect to $\boldsymbol{\eta}_j$ satisfies

$$\partial \tilde{h}_j \subset \operatorname{conv} \left\{ \frac{\partial F(\boldsymbol{\eta}_j; \mathcal{I}_\alpha, \mathcal{I}_\beta)}{\partial \boldsymbol{\eta}_j} : (\mathcal{I}_\alpha, \mathcal{I}_\beta) \in I_{h_j}(\boldsymbol{\eta}_j) \right\}. \tag{5.35}$$

A straightforward way to compute $I_{h_j}(\boldsymbol{\eta}_j)$ is to check the KKT conditions (5.30) for all $\mathcal{I}_\alpha \in \bar{\mathcal{P}}([N_0])$ and $\mathcal{I}_\beta \in \bar{\mathcal{P}}([N_j])$.

Based on the results above, we define the following candidate CBF for any $j \in [M]$

$$h_j(\boldsymbol{\eta}_j) = \tilde{h}_j(\boldsymbol{\eta}_j) - (d_{\min}^2 + \delta_1^2 + \delta_2^2), \tag{5.36}$$

where $\delta_1, \delta_2 > 0$ are small positive constants. Note that this CBF is implicitly constructed from the solution $\tilde{h}_j$ of optimization (5.27), which represents a relaxed minimum distance between polytopes [142].

The following result ensures that the occlusion-avoidance constraints (5.16) are strictly enforced by the CBF-based controller for all $t \geq 0$.

Theorem 5.3 *Consider the system in* (5.26) *and the CBF defined in* (5.36)*. Suppose the feature point velocities are bounded, i.e.,* $\|w_j^i\| \leq W$*, for some constant* $W > 0$*,* $\forall j \in [0, M]$ *and* $\forall i \in [N_j]$*. If* $h_j(\boldsymbol{\eta}_j(0)) > 0, \forall j \in [0, M]$*, then any Lipschitz controller* $V(\boldsymbol{\eta}_j) \in K_{BF}(\boldsymbol{\eta}_j) \triangleq \{V \in \mathbb{R}^6 : \psi_{0,j}(\boldsymbol{\eta}_j; \mathcal{I}_\alpha, \mathcal{I}_\beta) + \psi_{1,j}(\boldsymbol{\eta}_j; \mathcal{I}_\alpha, \mathcal{I}_\beta)V \geq 0, \forall (\mathcal{I}_\alpha, \mathcal{I}_\beta) \in I_{h_j}(\boldsymbol{\eta}_j)\}$ *ensures that the occlusion-avoidance constraints* (5.16) *are strictly enforced for all* $t \geq 0$*, where* $\gamma > 0$ *is a constant and*

$$\psi_{0,j} = \gamma h_j - W\sqrt{N_0 + N_j}\left\|\frac{\partial F(\boldsymbol{\eta}_j; \mathcal{I}_\alpha, \mathcal{I}_\beta)}{\partial \boldsymbol{\eta}_j} S_j(\bar{\boldsymbol{\eta}}_j)\right\|, \tag{5.37a}$$

$$\psi_{1,j} = \frac{\partial F(\boldsymbol{\eta}_j; \mathcal{I}_\alpha, \mathcal{I}_\beta)}{\partial \boldsymbol{\eta}_j} J_j(\bar{\boldsymbol{\eta}}_j). \tag{5.37b}$$

Proof *First, we prove that*

$$h_j \geq 0 \implies \mathrm{d}(\bar{\mathbb{T}}, \bar{\mathbb{O}}_j) \geq d_{\min}. \tag{5.38}$$

Let $(\alpha^*, \beta^*, \theta^*)$ *and* $(\alpha_h^*, \beta_h^*, \theta_h^*)$ *be the solutions to the optimization problems* (5.13) *and* (5.27)*, respectively. Clearly,* $\|\theta^*\|^2 = \mathrm{d}(\bar{\mathbb{T}}, \bar{\mathbb{O}}_j)^2$*,* $\tilde{h}_j = \|\theta_h^*\|^2 + \delta_1\|\alpha_h^*\|^2 + \delta_2\|\beta_h^*\|^2$*, and* $\|\theta^*\|^2 + \delta_1\|\alpha^*\|^2 + \delta_2\|\beta^*\|^2 \geq \|\theta_h^*\|^2 + \delta_1\|\alpha_h^*\|^2 + \delta_2\|\beta_h^*\|^2$*.*

By the definition of h_j*,* $h_j \geq 0 \implies \|\theta_h^*\|^2 + \delta_1\|\alpha_h^*\|^2 + \delta_2\|\beta_h^*\|^2 \geq d_{\min}^2 + \delta_1^2 + \delta_2^2$*. Therefore,*

$$h_j \geq 0 \Rightarrow \|\theta^*\|^2 + \delta_1\|\alpha^*\|^2 + \delta_2\|\beta^*\|^2 \geq d_{\min}^2 + \delta_1^2 + \delta_2^2. \tag{5.39}$$

Since $\alpha^* \geq 0$ *and* $\mathbf{1}_{N_0}^\top \alpha^* = 1$*, it follows that* $0 \leq \alpha_i^* \leq 1$ *for* $i \in [N_0]$*, which implies* $0 \leq \alpha_i^{*2} \leq \alpha_i^* \leq 1$*, and thus* $\|\alpha^*\| \leq 1$*. Following the similar argument,* $\|\beta^*\| \leq 1$*. Therefore, from* (5.39) *we have*

$$h_j \geq 0 \implies \|\theta^*\|^2 \geq d_{\min}^2,$$

which implies that (5.38) *holds since* $\|\theta^*\|^2 = \mathrm{d}(\bar{\mathbb{T}}, \bar{\mathbb{O}}_j)^2$*.*

Next, one can easily see that selecting $V \in K_{BF}$ *yields*

$$\begin{aligned}\frac{\partial F(\boldsymbol{\eta}_j;\mathcal{I}_\alpha,\mathcal{I}_\beta)}{\partial \boldsymbol{\eta}_j}(J_jV - S_j\boldsymbol{w}_j) &\geq \frac{\partial F(\boldsymbol{\eta}_j;\mathcal{I}_\alpha,\mathcal{I}_\beta)}{\partial \boldsymbol{\eta}_j}J_jV - \left\|\frac{\partial F(\boldsymbol{\eta}_j;\mathcal{I}_\alpha,\mathcal{I}_\beta)}{\partial \boldsymbol{\eta}_j}S_j\right\|\|\boldsymbol{w}_j\| \\ &\geq -\gamma h_j + \psi_{0,j} + \psi_{1,j}V \\ &\geq -\gamma h_j \end{aligned} \tag{5.40}$$

for any $(\mathcal{I}_\alpha,\mathcal{I}_\beta) \in I_{h_j}(\boldsymbol{\eta}_j)$*. Then, from [141, Theorem III.5],*

$$\min_{v\in\partial h_j} v^\top(J_jV - S_j\boldsymbol{w}_j) \geq -\gamma h_j, \tag{5.41}$$

where ∂h_j *denotes the generalized gradient of* h_j *with respect to* $\boldsymbol{\eta}_j$*. According to [141, Theorem II.7], one can conclude that* (5.41) *implies* $h_j \geq 0$*, which completes the proof.* □

By Theorem 5.3, the filtered end-effector velocity V_{cbf} can be obtained by solving the following CBF-QP

$$\begin{aligned} V_{\text{cbf}} = \arg\min_{V}\ & \|V - V_{\text{mpc}}\|^2 \\ \text{s.t.}\quad & \psi_{0,j}(\boldsymbol{\eta}_j;\mathcal{I}_\alpha,\mathcal{I}_\beta) + \psi_{1,j}(\boldsymbol{\eta}_j;\mathcal{I}_\alpha,\mathcal{I}_\beta)V \geq 0, \\ & \forall j \in [M],\ \forall(\mathcal{I}_\alpha,\mathcal{I}_\beta) \in I_{h_j}(\boldsymbol{\eta}_j), \end{aligned} \tag{5.42}$$

where V_{mpc} is obtained from solving the optimization problem (5.21) and $\psi_{0,j}, \psi_{1,j}$ are defined in (5.37). The velocity bound W in Theorem 5.3 can be chosen using the prior knowledge of the scene or data-driven methods.

Finally, the control input τ in (5.8) can be designed using standard methods to enable the robot's end-effector velocity to track the safe reference velocity V_{cbf}. For example, defining the velocity tracking error defined as $e = V - V_{\text{cbf}}$ with dynamics $\dot{e} = \dot{\text{J}}\dot{q} + \text{J}D^{-1}(\tau - C\dot{q} - G) - \dot{V}_{\text{cbf}}$, where J is the Jacobian, the control input τ can be chosen as $\tau = C\dot{q} + G + D\text{J}^\dagger(-Ke - \dot{\text{J}}\dot{q} + \dot{V}_{\text{cbf}})$ where $\text{J}^\dagger$ denotes the pseudo-inverse of J and $K \in \mathbb{R}^{6\times 6}$ is a positive definite gain matrix.

Remark 5.3 *If the strict complementarity condition ([143, Definition 12.2]) holds for* (5.27)*, then* $\tilde{h}_j$ *is differentiable at the corresponding point [140, Theorem 1], and the encapsulating index set coincides with the active sets of* (5.27)*. Consequently, the gradient of* h_j *can be obtained by solving the linear system* (5.33) *with* $\mathcal{I}_\alpha = \mathcal{I}_\alpha^*$ *and* $\mathcal{I}_\beta = \mathcal{I}_\beta^*$*, where* $\mathcal{I}_\alpha^*$ *and* $\mathcal{I}_\beta^*$ *denote the active sets of* (5.27)*.*

Remark 5.4 *In practice, the CBF-QP* (2.56) *cannot be solved in continuous time; instead,* V *is updated in a sampled-data fashion. To compensate for potential safety violations introduced by sampling, a correction term can be added into the CBF condition, modifying the constraint of* (2.56) *to*

$$\psi_{0,j}(\boldsymbol{\eta}_j; \mathcal{I}_\alpha, \mathcal{I}_\beta) + \psi_{1,j}(\boldsymbol{\eta}_j; \mathcal{I}_\alpha, \mathcal{I}_\beta) V \geq \Delta_j$$

where $\Delta_j > 0$ *is a constant that compensates for the sampling effect [144], [145], [146].*

Remark 5.5 *In the high-level MPC, the velocity* w_j^i *is estimated, whereas the low-level CBF-QP accounts for its worst-case value. This distinction reflects a trade-off between performance and guaranteed occlusion avoidance. MPC prioritizes performance and operates at discrete time instances; it cannot ensure strict occlusion avoidance, so using velocity estimates - despite potential inaccuracies - is acceptable. When sufficiently accurate, these estimates can improve control performance compared with using the worst-case value. In contrast, the CBF-QP prioritizes strict occlusion avoidance, requiring the worst-case velocity to guarantee safety.*

5.5 Experimental Results

In this section, we present experimental results that validate the proposed hierarchical control framework for occlusion-free visual servoing. All experiments are conducted on a Franka Research 3 manipulator equipped with an Intel RealSense D435i camera mounted on its end-effector, as illustrated in Figure 5.3. The camera streams RGB images at 30 Hz with a resolution of 1280×720 pixels. An AprilTag is attached on the end-effector

of a UFactory xArm 7 manipulator to serve as the target object. The control framework is implemented on an workstation (Intel Core i5-13500 @ 2.5 GHz, 16 GB RAM) for MPC and CBF computations, and an NVIDIA Jetson AGX Orin (2048 CUDA cores, 64 Tensor Cores) for image processing. The two devices communicate via a direct Ethernet connection using the UDP protocol with 72-byte datagrams.

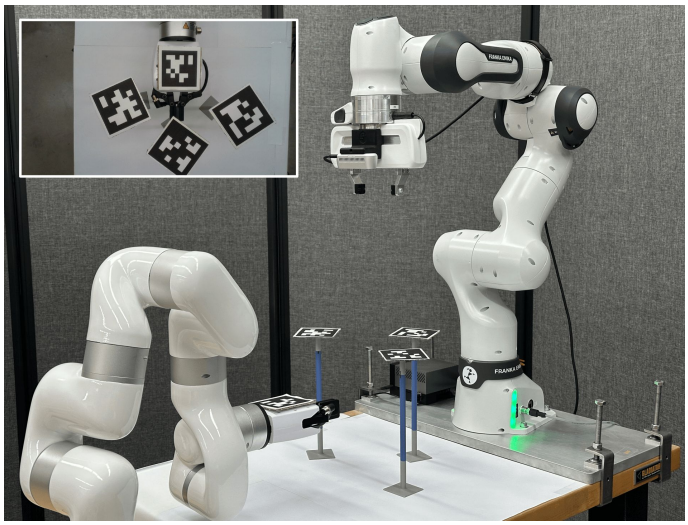

Figure 5.3: Experimental setup for validating the proposed hierarchical control framework for occlusion-free visual servoing.

5.5.1 Experimental Setup

Object Representation

AprilTag markers from the Tag36h11 family are used to represent both the target and occluding objects. The target is an AprilTag (ID: 0) mounted on the end-effector of the xArm 7 manipulator. Up to three additional AprilTags (IDs: 1–3) are mounted on adjustable support stands and serve as occluding objects.

Image Processing

We employ a GPU-accelerated AprilTag detection pipeline implemented in NVIDIA Isaac ROS, fed by an Intel RealSense D435i connected via USB 3.0. RGB images are processed to detect tag corners, rectify tag regions, and decode tag IDs. For each verified tag, a

Perspective-n-Point problem is solved to estimate its 6-DOF pose $\left({}^{c}p_j, {}^{c}q_j\right)$, including position and unit-quaternion orientation in the camera frame. From this, the depth of each corner is also obtained. The detection output, $\mathcal{D}_j \coloneqq \left(j,\ \{c_j^i\}_{i=1}^4,\ {}^{c}p_j,\ {}^{c}q_j\right)$, provides the ID, image corners, and 3D pose, which are then used by the visual servoing controller.

MPC Setup

The high-level MPC is implemented using CasADi [147] with automatic C code generation and solved using IPOPT at 10 Hz. At each time step k, the image coordinates $\bar{\eta}$ of the AprilTag feature points are extracted, and their velocities $\hat{w}_j^i(k)$ are estimated using the EKF described in Remark 5.1, yielding the filtered states $\bar{\eta}_j^i(k)$. Using these, the point set matrices Γ_n and Λ_{jn} are computed and the optimization problem (5.21) is solved.

CBF-QP Setup

The low-level CBF controller employs OSQP [148] to solve the QP (2.56), using the CBFs h_j from (5.36) and the nominal input $V_{\text{mpc}} = V(0|k)$ provided by the high-level MPC. Its solution, V_{cbf}, is sent to the Franka Control Interface to command the robot. The CBF-QP-based controller runs at 30 Hz, synchronized with the camera's RGB image stream.

5.5.2 Experimental Results

We consider scenarios with one, two, and three static occluding objects, as well as a scenario with one dynamic occluding objects. These scenarios are constructed with progressively increasing occlusion complexity. The proposed hierarchical control framework is evaluated against the high-level MPC (5.21) alone, i.e., without the low-level CBF-QP controller. For all experiments, the safety margin in (5.16) is set to $d_{\min} = 20$ (pixels), with δ_1, δ_2 selected as $\delta_1 = \delta_2 = 0.1$. Here $d_{\min}$ is a tuning parameter which can be adjusted based on specific requirements of the task. In (5.21), the prediction horizon is $N = 7$, and the weight matrices are selected as $Q = \mathrm{I}_8 \in R^{8\times 8}$, $Q_N = 5\mathrm{I}_8 \in R^{8\times 8}$ and $R = 10^6 \times \mathrm{diag}(1.5, 1.5, 1.5, 1, 1, 1) \in \mathbb{R}^{6\times 6}$.

Figure 5.5 shows snapshots of experiments with static and dynamic occluding objects, while Figure 5.6 illustrates the evolution of the distances between the target and the obstacles.

Static Scenarios

In the static scenarios, the occluding objects remain stationary along the moving target's path, while the target follows a trajectory toward the Franka manipulator. The velocity bound W in Theorem 5.3 is set to $W = 0.015$.

Figure 5.5 (a)-(c) shows camera snapshots for experiments with one, two, and three static occluding objects. AprilTag centers are annotated with their IDs, and tag corners are numbered clockwise from 0 to 3. Occlusion zones are highlighted by yellow squares with a 20-pixel safety margin, meaning the occlusion-avoidance constraint (5.16) is satisfied whenever the target's feature points remain outside the overlaid yellow squares. The target (AprilTag 0) is enclosed in a green box when persistently visible; the absence of the box indicates loss of recognition due to occlusion. In each scenario, the top row depicts the proposed hierarchical controller (high-level MPC with low-level CBF-QP), while the bottom row shows the high-level MPC alone, where $V(0|k)$ is sent directly as the reference input to the Cartesian velocity tracking controller. Each row presents the initial (left), intermediate (middle), and terminal (right) phases from both the camera and a third-person view.

Figure 5.6 (a)-(c) shows the distance profiles between the target and the occluding objects for the three static scenarios. The results indicate that the high-level MPC alone fails to consistently enforce the occlusion-avoidance constraint (5.16): in the one-occluding-object case, the minimum distance drops to $d_{\min} = 12.87$ pixels at $t \approx 4.4$ s; in the two-occluding-object case, the minimum distances are $d_{\min} = 7.43$ pixels at $t \approx 9.3$ s with Object 1 and $d_{\min} = 11.25$ pixels at $t \approx 10$ s with Object 2; and in the three-occluding-object case, the distance between the target and Object 3 reduces to zero at $t \approx 12$ s. By contrast, the hierarchical controller strictly enforces the distances near or above the

20-pixel safety margin in all three scenarios (with only minor single-pixel deviations due to measurement noise or hardware disturbances).

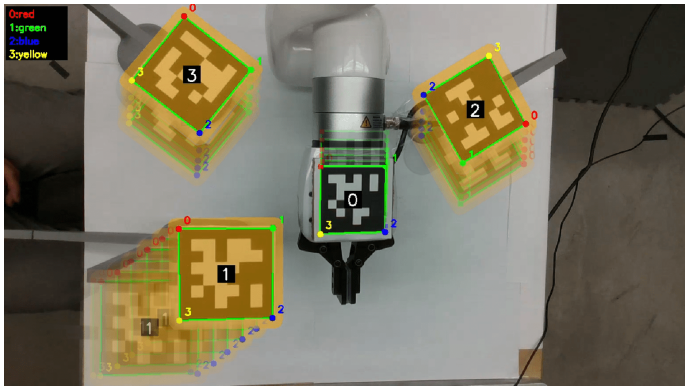

Figure 5.4: Superimposed camera frames illustrating the dynamic occluding object scenario.

Dynamic Scenario

To further demonstrate the real-time reactive capability of the hierarchical control framework, we consider a dynamic scenario in which both the target and an occluding object are moving. Figure 5.4 shows superimposed camera frames, with three occluding objects (AprilTag ID: 1-3): objects 2 and 3 remain stationary, while object 1 moves toward the target, creating a dynamic occlusion threat. The velocity of objective 1 is estimated using the EKF. The obstacles are manually displaced by dragging the base linkage of the support structure, thereby simulating occluding objects with unpredictable velocities, as often encountered in real-world environments. The velocity bound W in Theorem 2.2 is set to $W = 0.075$.

Figure 5.5 (d) shows camera snapshots for the dynamic scenario. As shown in Figure 5.6 (d), $\mathrm{d}(\bar{\mathbb{T}}, \bar{\mathbb{O}}_1)$ decreases to 20 at $t \approx 6.6$ s and drops to zero at $t \approx 11.5$ s, resulting in persistent occlusion and target recognition failure. In contrast, the hierarchical controller successfully navigates around the moving obstacle with a considerable margin, strictly enforcing the occlusion-avoidance constraint (5.16) throughout the entire operation. Objects 2 and 3 exit the camera's field of view at $t \approx 11$ s for both controllers.

Results from the static and dynamic experiments above demonstrate the effectiveness of the hierarchical control framework, where the high-level MPC ensures performance and target regulation, while the low-level CBF-QP controller enforces strict safety by filtering the MPC inputs in real time.

Table 5.1 summarizes the computation times, which are computed over 1000 iterations, for both the MPC and CBF-QP controllers across all scenarios. The results confirm that the MPC problem (10 Hz) and the CBF-QP (30 Hz) can each be solved within their respective sampling periods. Moreover, it is shown that the computational time of MPC grows almost linearly with the number of occluding objects, while the computational time of CBF-QP is negligible.

Table 5.1: Computation Times for Different Scenarios

	Controller	**Computation Time (ms)**			
		Mean	**Min.**	**Max.**	**Std.**
Static Scenarios					
1 occluding object	MPC	23.721	16.450	33.102	3.145
	CBF-QP	0.116	0.085	0.152	0.012
2 occluding objects	MPC	35.311	31.220	40.895	1.988
	CBF-QP	0.205	0.160	0.265	0.021
3 occluding objects	MPC	41.338	29.550	58.112	4.875
	CBF-QP	0.303	0.255	0.380	0.019
Dynamic Scenario					
3 occluding objects	MPC	42.515	35.101	51.440	3.220
	CBF-QP	0.331	0.275	0.410	0.025

5.6 Chapter Summary and Future Directions

This chapter presents a hierarchical, optimization-based visual servoing control scheme for robotic manipulators that guarantees occlusion-free operation by integrating a high-level MPC with a low-level CBF-QP controller. By leveraging the vertex-based representation of object images and a duality-based optimization approach, we reformulate occlusion avoidance into differentiable constraints that can be seamlessly incorporated into both the MPC and CBF design. The resulting framework achieves simultaneous regulation of target

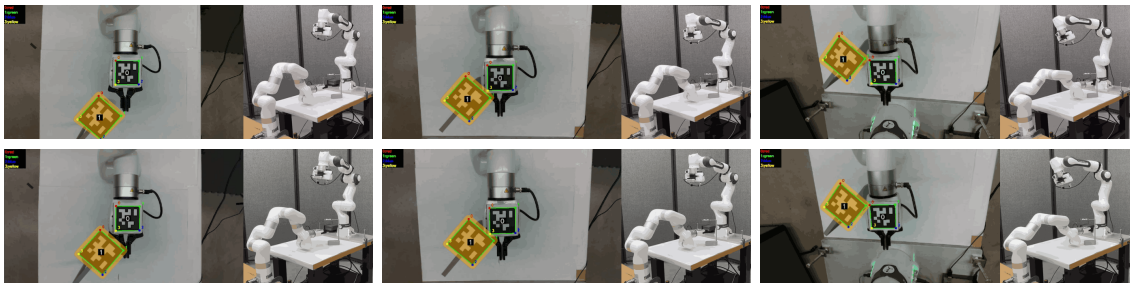

(a) Scenario 1 with one static occluding object: hierarchical controller (top row) versus MPC alone (bottom row).

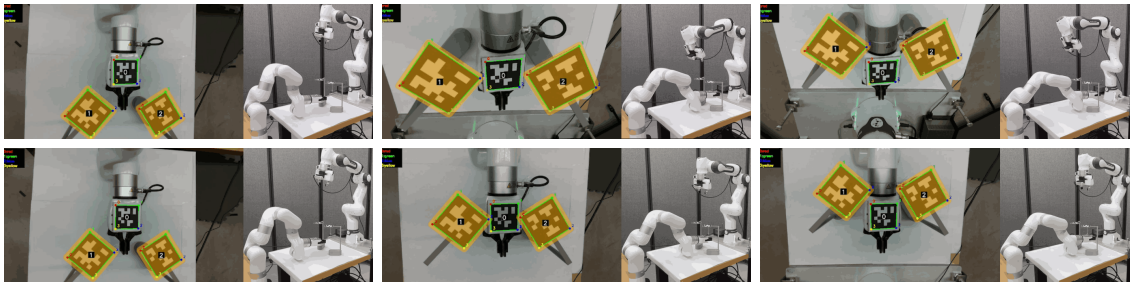

(b) Scenario 2 with two static occluding objects: hierarchical controller (top row) versus MPC alone (bottom row)

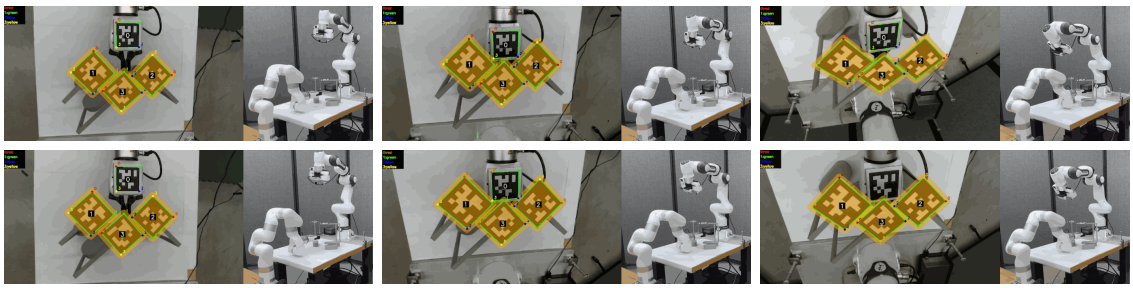

(c) Scenario 3 with three static occluding objects: hierarchical controller (top row) versus MPC alone (bottom row)

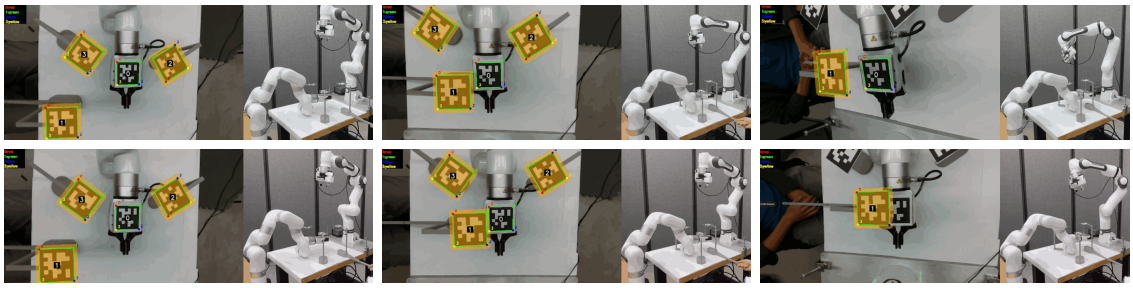

(d) Scenario 4 with one dynamic occluding objects: hierarchical controller (top row) versus MPC alone (bottom row)

Figure 5.5: Snapshots of experiments for static and dynamic occluding objects.

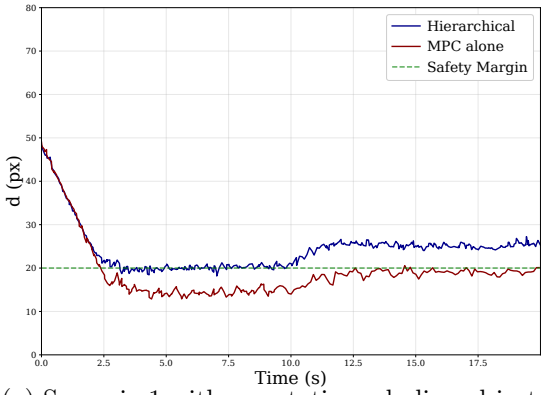

(a) Scenario 1 with one static occluding object.

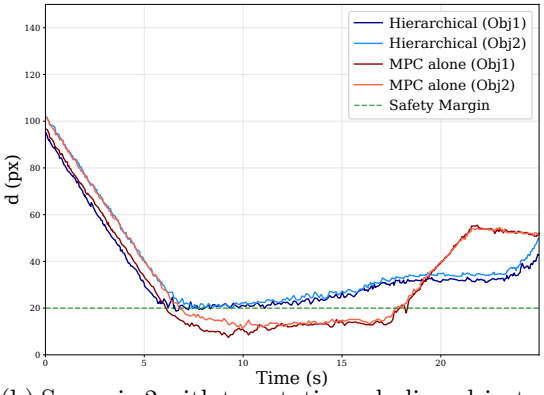

(b) Scenario 2 with two static occluding objects.

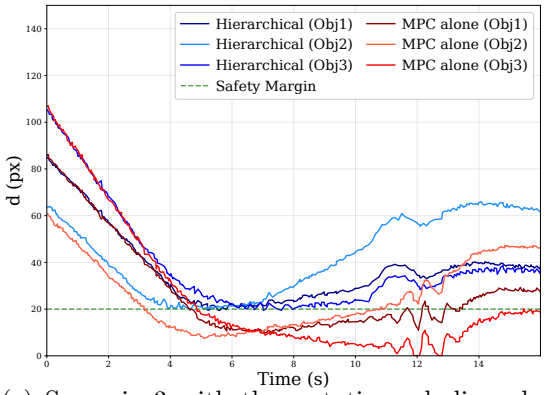

(c) Scenario 3 with three static occluding objects.

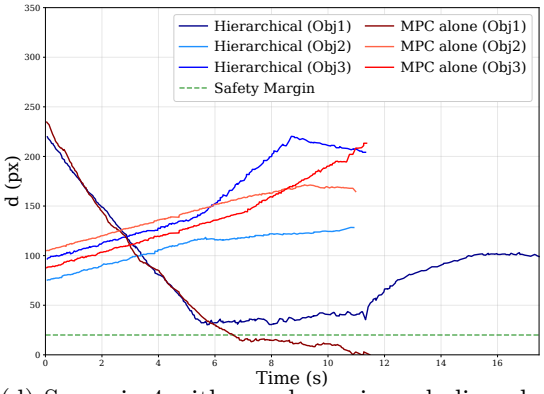

(d) Scenario 4 with one dynamic occluding object.

Figure 5.6: Evolution of the distance between the target and the occluding objects across four experimental scenarios.

feature points and strict continuous-time occlusion avoidance. Hardware experiments on the Franka Research 3 manipulator validate the effectiveness of the proposed approach.

Although V-rep offers several advantages over H-rep, as highlighted in Section 5.3, it inevitably introduces more decision variables, thereby increasing the computational burden of (5.21). One future direction is investigating computational methods to mitigate the computational burden of solving (5.21), such as the culling techniques to reduce the decision variables and the parallel computation techniques via structure exploitation. In particular, the alternating direction method of multipliers, which has been employed in several studies to reduce the computation time of MPC [149], provides a promising framework for accelerating the solving process of the MPC problem in (5.21).

The CBF-QP formulation in (5.42) incorporates multiple safety constraints arising from the presence of different occluding objects. The simultaneous enforcement of these constraints may render the CBF-QP infeasible, particularly in the presence of input constraints. Therefore, another important direction for future research is investigating the compatibility of multiple CBFs for robotic manipulators to address feasibility issues in the CBF-QP with multiple constraints, exploring both formal characterization of compatibility conditions and the synthesis of a single CBF from multiple occlusion constraints.

Chapter 6

Conclusion and Future Directions

6.1 Conclusions and Contributions

This dissertation has developed a systematic and rigorous safe control framework for uncertain systems. Motivated by the increasing deployment of safety-critical control in autonomous systems, this work addresses the fundamental safety challenges posed by uncertainties and disturbances when embedded in closed-loop dynamical systems. The main contributions of this dissertation are summarized as follows.

DOB-CBF-based Control for Systems With Unstructured Uncertainties

Chapter 2 develops a novel IIDOB design approach for generic nonlinear control-affine systems subject to unstructured uncertainties. In contrast to conventional DOB design methods that rely on restrictive assumptions, such as the solvability of PDEs, the proposed IIDOB framework provides a systematic and broadly applicable DOB design approach without imposing such strong assumptions. Based on the proposed IIDOB, a filter-based IIDOB-CBF-QP safe control design approach is developed to strictly enforce safety constraints. By introducing an auxiliary filter, the disturbance estimation signal admits a known and well-defined derivative, enabling tractable incorporation into the CBF-QP while preserving formal safety guarantees. These methods significantly broaden the class of systems to which DOB-CBF-QP methods can be applied.

Adaptive CBFs for Systems With Structured Uncertainties

Chapter 3 proposes an adaptive CBF-based safe control approach for systems with structured (parametric) uncertainties that appear in both drift terms and control-input matrices. A new adaptive CBF approach is developed to generate a safe controller via solving an NLP that admits an explicit closed-form solution. A key advantage of the proposed approach is that the non-emptiness of the admissible safe control set can be verified independently of online parameter estimation, thereby avoiding singularity and loss-of-controllability issues. In addition, a data-driven bound-tightening algorithm is introduced to reduce conservatism and improve control performance.

PCBF for Systems With Limited Model Information

Chapter 4 proposes a CBF-based safe control design method for strict-feedback systems with limited model information. A novel PCBF framework is developed by integrating barrier-based and Lyapunov-based control techniques. The proposed method adopts a modular design by decomposing the original strict-feedback system into a proxy subsystem (handled by CBF-based methods) and a virtual tracking subsystem (handled by Lyapunov-based approaches). By systematically coupling the controllers designed for different subsystems, the safety of the overall closed-loop system can be ensured under limited modeling information.

MPC-CBF-based Hierarchical Control for Visual Servoing With Measurement Uncertainties

Chapter 5 develops an occlusion-free, multi-rate visual servoing framework for robotic manipulators under measurement uncertainty. The proposed framework integrates a high-level MPC planner with a low-level CBF-based controller. Occlusion avoidance is formulated into differentiable constraints, enabling incorporation into both MPC and CBF layers. Disturbance estimation is incorporated into the MPC to mitigate the effects of perception uncertainties, while robust CBF methods enforce strict continuous-time occlu-

sion avoidance. Hardware experiments on a Franka Research 3 manipulator validate the effectiveness of the proposed approach.

Overall Impact

Collectively, the contributions of this dissertation establish a comprehensive and unified framework for safety-critical control of uncertain systems. By combining robust control, adaptive control, and data-driven methods, this work advances the state of the art in providing provable safety guarantees for autonomous systems. The developed methods strike a balance between rigor and scalability, laying a solid foundation for safety-critical control.

6.2 Future Directions

6.2.1 Compatibility and Synthesis of Multiple CBFs

The deployment of CBF-QP-based controllers in realistic, constraint-rich environments introduces additional complications. In practice, a system must simultaneously satisfy dozens or even hundreds of safety constraints. For example, the safe operation of a robotic manipulator in an unstructured environment may involve numerous constraints related to joint limits, velocity bounds, torque constraints, and dynamic obstacle avoidance, as reported in the recent work [150]. When multiple constraints are encoded as individual CBFs, their compatibility becomes a central concern: if the CBF constraints conflict or the resulting QP becomes infeasible, the controller may fail to generate a safe control action. Verifying compatibility among multiple CBFs, especially in the context of nonlinear or partially known dynamics, remains a technically difficult and often intractable problem, necessitating novel analytical tools and scalable verification procedures.

A promising direction to address these challenges lies in the use of simplified models for CBF construction and compatibility verification, while the Lyapunov-based methods are used to address the full dynamics, similar to the PCBF framework developed in Chapter

5. However, selecting appropriate simplified models is not well studied in the literature and warrants further investigation.

6.2.2 Towards Real-World and Hardware Implementation

Although this dissertation demonstrates the effectiveness of the proposed control methods through numerical simulations and simple experiments, their deployment on real-world hardware platforms remains an important open challenge. Hardware implementation introduces additional constraints, including limited computational resources, actuator limitations, and more complex environments. Addressing these challenges will require the development of more robust and computationally efficient algorithms that can operate under such constraints.

Future research may focus on further validating the robustness and improving the computational efficiency of the methods developed in this dissertation under complex and practical scenarios. In particular, high-fidelity simulators such as Project Chrono [12] provide powerful platforms for systematically evaluating the performance, robustness, and scalability of the proposed safe controllers under realistic dynamics and contact-rich interactions. Progress in this direction is essential for enabling the practical deployment of CBF-based controllers in safety-critical applications such as autonomous systems and robotics.

6.2.3 Learning-Enabled Safe Control with Formal Guarantees

In many applications, model information is unavailable, and learning-based components (e.g., learned dynamics, learned perception, or learned controllers) are increasingly used. A promising direction is to integrate machine learning techniques with CBF-based safety filters, which includes: (i) learning uncertainty bounds or disturbance models that are explicitly compatible with robust/adaptive CBF conditions; (ii) synthesizing CBFs directly from data while preserving forward invariance guarantees; and (iii) combining statistical learning tools with set-based methods to obtain less conservative yet formally justified

safety constraints.

6.2.4 Computational Scalability and Real-Time Optimization

The V-rep-based occlusion avoidance formulation developed in Chapter 5 can introduce additional decision variables, increasing the computational burden of the MPC. A promising direction for future research is to investigate computational strategies that alleviate this burden, including culling techniques for reducing unnecessary decision variables and parallel computation methods that exploit problem structure. In particular, the alternating direction method of multipliers, which has been adopted in recent studies to accelerate MPC computation [149], provides a promising framework for improving the efficiency of solving the MPC problem in Chapter 5.

Bibliography

[1] P. Liu, R. Yang, and Z. Xu, "How safe is safe enough for self-driving vehicles?" *Risk Analysis*, vol. 39, no. 2, pp. 315–325, 2019.

[2] T. Haidegger, "Autonomy for surgical robots: Concepts and paradigms," *IEEE Transactions on Medical Robotics and Bionics*, vol. 1, no. 2, pp. 65–76, 2019.

[3] J. B. Rawlings, D. Q. Mayne, M. Diehl, et al., *Model Predictive Control: Theory, Computation, and Design*. Nob Hill Publishing, LLC, 2017.

[4] K. P. Tee, S. S. Ge, and E. H. Tay, "Barrier Lyapunov functions for the control of output-constrained nonlinear systems," *Automatica*, vol. 45, no. 4, pp. 918–927, 2009.

[5] C. P. Bechlioulis and G. A. Rovithakis, "Robust adaptive control of feedback linearizable MIMO nonlinear systems with prescribed performance," *IEEE Transactions on Automatic Control*, vol. 53, no. 9, pp. 2090–2099, 2008.

[6] A. D. Ames, X. Xu, J. W. Grizzle, and P. Tabuada, "Control barrier function based quadratic programs for safety critical systems," *IEEE Transactions on Automatic Control*, vol. 62, no. 8, pp. 3861–3876, 2016.

[7] A. Bemporad, "Reference governor for constrained nonlinear systems," *IEEE Transactions on Automatic Control*, vol. 43, no. 3, pp. 415–419, 2002.

[8] T. G. Molnar, R. K. Cosner, A. W. Singletary, W. Ubellacker, and A. D. Ames, "Model-free safety-critical control for robotic systems," *IEEE Robotics and Automation Letters*, vol. 7, no. 2, pp. 944–951, 2021.

[9] J. Seo, J. Lee, E. Baek, R. Horowitz, and J. Choi, "Safety-critical control with nonaffine control inputs via a relaxed control barrier function for an autonomous vehicle," *IEEE Robotics and Automation Letters*, vol. 7, no. 2, pp. 1944–1951, 2022.

[10] B. Xu and K. Sreenath, "Safe teleoperation of dynamic UAVs through control barrier functions," in *IEEE International Conference on Robotics and Automation (ICRA)*, 2018, pp. 7848–7855.

[11] E. Todorov, T. Erez, and Y. Tassa, "MuJoCo: A physics engine for model-based control," in *2012 IEEE/RSJ International Conference on Intelligent Robots and Systems (IROS)*, pp. 5026–5033.

[12] A. Tasora et al., "Chrono: An open source multi-physics dynamics engine," in *International Conference on High Performance Computing in Science and Engineering*, Springer, 2015, pp. 19–49.

[13] C. E. Garcia, D. M. Prett, and M. Morari, "Model predictive control: Theory and practice – A survey," *Automatica*, vol. 25, no. 3, pp. 335–348, 1989.

[14] B. Ren, S. S. Ge, K. P. Tee, and T. H. Lee, "Adaptive neural control for output feedback nonlinear systems using a barrier Lyapunov function," *IEEE Transactions on Neural Networks*, vol. 21, no. 8, pp. 1339–1345, 2010.

[15] C. P. Bechlioulis and G. A. Rovithakis, "A low-complexity global approximation-free control scheme with prescribed performance for unknown pure feedback systems," *Automatica*, vol. 50, no. 4, pp. 1217–1226, 2014.

[16] M. Jankovic, "Robust control barrier functions for constrained stabilization of nonlinear systems," *Automatica*, vol. 96, pp. 359–367, 2018.

[17] Q. Nguyen and K. Sreenath, "Robust safety-critical control for dynamic robotics," *IEEE Transactions on Automatic Control*, vol. 67, no. 3, pp. 1073–1088, 2021.

[18] K. Garg and D. Panagou, "Robust control barrier and control Lyapunov functions with fixed-time convergence guarantees," in *American Control Conference (ACC)*, IEEE, 2021, pp. 2292–2297.

[19] J. Buch, S.-C. Liao, and P. Seiler, "Robust control barrier functions with sector-bounded uncertainties," *IEEE Control Systems Letters*, 2021.

[20] E. Daş and R. M. Murray, "Robust safe control synthesis with disturbance observer-based control barrier functions," in *61th IEEE Conference on Decision and Control (CDC)*, 2022, pp. 5566–5573.

[21] J. Sun, J. Yang, and Z. Zeng, "Safety-critical control with control barrier function based on disturbance observer," *IEEE Transactions on Automatic Control*, vol. 69, no. 7, pp. 4750–4756, 2024.

[22] X. Wang, J. Yang, C. Liu, Y. Yan, and S. Li, "Safety-critical disturbance rejection control of nonlinear systems with unmatched disturbances," *IEEE Transactions on Automatic Control*, 2024.

[23] A. Alan, T. G. Molnar, E. Daş, A. D. Ames, and G. Orosz, "Disturbance observers for robust safety-critical control with control barrier functions," *IEEE Control Systems Letters*, vol. 7, pp. 1123–1128, 2022.

[24] Z. Tian, X. Wang, J. Yang, S. Li, D. Niu, and Q. Li, "Safety-critical disturbance rejection control of overhead crane systems: Methods and experimental validation," *IEEE Transactions on Control Systems Technology*, vol. 32, no. 6, pp. 2253–2266, 2024.

[25] R. Cheng, G. Orosz, R. M. Murray, and J. W. Burdick, "End-to-end safe reinforcement learning through barrier functions for safety-critical continuous control tasks," in *Proceedings of the AAAI Conference on Artificial Intelligence*, vol. 33, 2019, pp. 3387–3395.

[26] Y. Wang and X. Xu, "Disturbance observer-based robust control barrier functions," in *American Control Conference (ACC)*, 2023, pp. 3681–3687.

[27] W.-H. Chen, J. Yang, L. Guo, and S. Li, "Disturbance-observer-based control and related methods – An overview," *IEEE Transactions on Industrial Electronics*, vol. 63, no. 2, pp. 1083–1095, 2015.

[28] A. Mohammadi, H. J. Marquez, and M. Tavakoli, "Nonlinear disturbance observers: Design and applications to Euler-Lagrange systems," *IEEE Control Systems Magazine*, vol. 37, no. 4, pp. 50–72, 2017.

[29] E. Sariyildiz, R. Oboe, and K. Ohnishi, "Disturbance observer-based robust control and its applications: 35th anniversary overview," *IEEE Transactions on Industrial Electronics*, vol. 67, no. 3, pp. 2042–2053, 2019.

[30] S. Li, J. Yang, W.-H. Chen, and X. Chen, *Disturbance Observer-based Control: Methods and Applications*. CRC press, 2014.

[31] W.-H. Chen, "Disturbance observer based control for nonlinear systems," *IEEE/ASME Transactions on Mechatronics*, vol. 9, no. 4, pp. 706–710, 2004.

[32] W.-H. Chen, D. J. Ballance, P. J. Gawthrop, J. J. Gribble, and J. O'Reilly, "Nonlinear PID predictive controller," *IEE Proceedings-Control Theory and Applications*, vol. 146, no. 6, pp. 603–611, 1999.

[33] K. S. Narendra and A. M. Annaswamy, *Stable Adaptive Systems*. Prentice-Hall, 1989.

[34] K. J. Åström and B. Wittenmark, *Adaptive Control*. Addison-Wesley, 1995.

[35] M. Krstic, P. V. Kokotovic, and I. Kanellakopoulos, *Nonlinear and Adaptive Control Design*. New York, NY, USA: Wiley, 1995.

[36] P. A. Ioannou and J. Sun, *Robust Adaptive Control*. Prentice-Hall, 1996.

[37] A. Astolfi, D. Karagiannis, and R. Ortega, *Nonlinear and Adaptive Control with Applications*. Springer-Verlag, 2008.

[38] S. S. Sastry and A. Isidori, "Adaptive control of linearizable systems," *IEEE Transactions on Automatic Control*, vol. 34, no. 11, pp. 1123–1131, 1989.

[39] I. Kanellakopoulos, P. V. Kokotović, and A. S. Morse, "Systematic design of adaptive controllers for feedback linearizable systems," *IEEE Transactions on Automatic Control*, vol. 36, pp. 1241–1253, 11 1991.

[40] M. Krstić, I. Kanellakopoulos, and P. V. Kokotović, "Adaptive nonlinear control without overparametrization," *Systems & Control Letters*, vol. 19, no. 3, pp. 177–185, 1992.

[41] B. D. Anderson et al., *Stability of Adaptive Systems: Passivity and Averaging Analysis*. MIT Press, 1986.

[42] R. Kosut, B. Anderson, and I. Mareels, "Stability theory for adaptive systems: Method of averaging and persistency of excitation," *IEEE Transactions on Automatic Control*, vol. 32, no. 1, pp. 26–34, 1987.

[43] G. Tao, "Multivariable adaptive control: A survey," *Automatica*, vol. 50, no. 11, pp. 2737–2764, 2014.

[44] A. M. Annaswamy and A. L. Fradkov, "A historical perspective of adaptive control and learning," *Annual Reviews in Control*, vol. 52, pp. 18–41, 2021.

[45] M. Krstić and P. V. Kokotović, "Control Lyapunov functions for adaptive nonlinear stabilization," *Systems & Control Letters*, vol. 26, no. 1, pp. 17–23, 1995.

[46] A. J. Taylor and A. D. Ames, "Adaptive safety with control barrier functions," in *American Control Conference (ACC)*, 2020, pp. 1399–1405.

[47] B. T. Lopez, J.-J. E. Slotine, and J. P. How, "Robust adaptive control barrier functions: An adaptive and data-driven approach to safety," *IEEE Control Systems Letters*, vol. 5, no. 3, pp. 1031–1036, 2020.

[48] P. Zhao, Y. Mao, C. Tao, N. Hovakimyan, and X. Wang, "Adaptive robust quadratic programs using control lyapunov and barrier functions," in *59th IEEE Conference on Decision and Control (CDC)*, 2020, pp. 3353–3358.

[49] M. Black, E. Arabi, and D. Panagou, "A fixed-time stable adaptation law for safety-critical control under parametric uncertainty," in *European Control Conference (ECC)*, 2021, pp. 1328–1333.

[50] A. Isaly, O. S. Patil, R. G. Sanfelice, and W. E. Dixon, "Adaptive safety with multiple barrier functions using integral concurrent learning," in *American Control Conference (ACC)*, 2021, pp. 3719–3724.

[51] M. H. Cohen and C. Belta, "High order robust adaptive control barrier functions and exponentially stabilizing adaptive control Lyapunov functions," in *American Control Conference (ACC)*, 2022, pp. 2233–2238.

[52] C. Huang and L. Long, "Safety-critical model reference adaptive control of switched nonlinear systems with unsafe subsystems: A state-dependent switching approach," *IEEE Transactions on System, Man, Cybernetics: Systems*, 2022.

[53] V. Azimi and S. Hutchinson, "Exponential control Lyapunov-barrier function using a filtering-based concurrent learning adaptive approach," *IEEE Transactions on Automatic Control*, 2021.

[54] C. K. Verginis, "Funnel control for uncertain nonlinear systems via zeroing control barrier functions," *IEEE Control Systems Letters*, 2022.

[55] A. J. Taylor, *Robust Safety-Critical Control: A Lyapunov and Barrier Approach*. California Institute of Technology, 2023.

[56] S. Dean, A. Taylor, R. Cosner, B. Recht, and A. Ames, "Guaranteeing safety of learned perception modules via measurement-robust control barrier functions," in *Conference on Robot Learning*, PMLR, 2021, pp. 654–670.

[57] M. Abu-Khalaf, S. Karaman, and D. Rus, "Feedback from pixels: Output regulation via learning-based scene view synthesis," in *Learning for Dynamics and Control*, PMLR, 2021, pp. 828–841.

[58] H. A. Poonawala, N. Lauffer, and U. Topcu, "Training classifiers for feedback control with safety in mind," *Automatica*, vol. 128, p. 109 509, 2021.

[59] R. Takano and M. Yamakita, "Robust constrained stabilization control using control Lyapunov and control barrier function in the presence of measurement noises," in *IEEE Conference on Control Technology and Applications (CCTA)*, 2018, pp. 300–305.

[60] Y. Wang and X. Xu, "Observer-based control barrier functions for safety critical systems," in *2022 American Control Conference (ACC)*, 2022, pp. 709–714.

[61] T. Wongpiromsarn, U. Topcu, N. Ozay, H. Xu, and R. M. Murray, "TuLip: A software toolbox for receding horizon temporal logic planning," in *Proceedings of the 14th International Conference on Hybrid Systems: Computation and Control*, 2011, pp. 313–314.

[62] P. Tabuada and G. J. Pappas, "Linear time logic control of discrete-time linear systems," *IEEE Transactions on Automatic Control*, vol. 51, no. 12, pp. 1862–1877, 2006.

[63] S. Kousik, S. Vaskov, F. Bu, M. Johnson-Roberson, and R. Vasudevan, "Bridging the gap between safety and real-time performance in receding-horizon trajectory design for mobile robots," *The International Journal of Robotics Research*, vol. 39, no. 12, pp. 1419–1469, 2020.

[64] Y. S. Shao, C. Chen, S. Kousik, and R. Vasudevan, "Reachability-based trajectory safeguard (RTS): A safe and fast reinforcement learning safety layer for continuous control," *IEEE Robotics and Automation Letters*, vol. 6, no. 2, pp. 3663–3670, 2021.

[65] S. L. Herbert, M. Chen, S. Han, S. Bansal, J. F. Fisac, and C. J. Tomlin, "Fastrack: A modular framework for fast and guaranteed safe motion planning," in *56th IEEE Annual Conference on Decision and Control (CDC)*, 2017, pp. 1517–1522.

[66] N. Csomay-Shanklin, A. J. Taylor, U. Rosolia, and A. D. Ames, "Multi-rate planning and control of uncertain nonlinear systems: Model predictive control and control Lyapunov functions," in *61st IEEE Conference on Decision and Control (CDC)*, 2022, pp. 3732–3739.

[67] U. Rosolia, A. Singletary, and A. D. Ames, "Unified multirate control: From low-level actuation to high-level planning," *IEEE Transactions on Automatic Control*, vol. 67, no. 12, pp. 6627–6640, 2022.

[68] H. M. Al-Rahmani and G. F. Franklin, "Multirate control: A new approach," *Automatica*, vol. 28, no. 1, pp. 35–44, 1992.

[69] N. Matni, A. D. Ames, and J. C. Doyle, "A quantitative framework for layered multirate control: Toward a theory of control architecture," *IEEE Control Systems Magazine*, vol. 44, no. 3, 2024.

[70] U. Rosolia and A. D. Ames, "Multi-rate control design leveraging control barrier functions and model predictive control policies," *IEEE Control Systems Letters*, vol. 5, no. 3, pp. 1007–1012, 2020.

[71] A. Astolfi and R. Ortega, "Immersion and invariance: A new tool for stabilization and adaptive control of nonlinear systems," *IEEE Transactions on Automatic Control*, vol. 48, no. 4, pp. 590–606, 2003.

[72] R. E. Moore, R. B. Kearfott, and M. J. Cloud, *Introduction to Interval Analysis*. SIAM, 2009.

[73] E. Daş, S. X. Wei, and J. W. Burdick, "Robust control barrier functions with uncertainty estimation," *arXiv preprint arXiv:2304.08538*, 2023.

[74] A. Astolfi, R. Ortega, and A. Venkatraman, "A globally exponentially convergent immersion and invariance speed observer for n degrees of freedom mechanical systems," in *48th IEEE Conference on Decision and Control (CDC)*, 2009, pp. 6508–6513.

[75] Y. Wang and X. Xu, "Immersion and invariance-based disturbance observer and its application to safe control," *IEEE Transactions on Automatic Control*, vol. 69, no. 12, pp. 8782–8789, 2024.

[76] X. Xu, P. Tabuada, A. Ames, and J. Grizzle, "Robustness of control barrier functions for safety critical control," in *IFAC-PapersOnLine*, vol. 48, 2015, pp. 54–61.

[77] H. An, J. Liu, C. Wang, and L. Wu, "Disturbance observer-based antiwindup control for air-breathing hypersonic vehicles," *IEEE Transactions on Industrial Electronics*, vol. 63, no. 5, pp. 3038–3049, 2016.

[78] A. Mohammadi, M. Tavakoli, and H. Marquez, "Disturbance observer-based control of non-linear haptic teleoperation systems," *IET Control Theory & Applications*, vol. 5, no. 18, pp. 2063–2074, 2011.

[79] A. Isidori, *Nonlinear Control Systems: An Introduction*. Springer, 1985.

[80] J. Yang, S. Li, C. Sun, and L. Guo, "Nonlinear-disturbance-observer-based robust flight control for airbreathing hypersonic vehicles," *IEEE Transactions on Aerospace and Electronic Systems*, vol. 49, no. 2, pp. 1263–1275, 2013.

[81] H. K. Khalil, *Nonlinear Systems*. Prentice hall Upper Saddle River, NJ, 2002, vol. 3.

[82] L. Sonneveldt, E. van Oort, Q. Chu, and J. Mulder, "Immersion and invariance based nonlinear adaptive flight control," in *AIAA Guidance, Navigation, and Control Conference*, 2010, p. 7690.

[83] D. Karagiannis and A. Astolfi, "Observer design for a class of nonlinear systems using dynamic scaling with application to adaptive control," in *47th IEEE Conference on Decision and Control (CDC)*, 2008, pp. 2314–2319.

[84] G. B. Folland, *Real Analysis: Modern Techniques and Their Applications*. John Wiley & Sons, 1999, vol. 40.

[85] D. Swaroop, J. K. Hedrick, P. P. Yip, and J. C. Gerdes, "Dynamic surface control for a class of nonlinear systems," *IEEE Transactions on Automatic Control*, vol. 45, no. 10, pp. 1893–1899, 2000.

[86] J. A. Farrell, M. Polycarpou, M. Sharma, and W. Dong, "Command filtered backstepping," *IEEE Transactions on Automatic Control*, vol. 54, no. 6, pp. 1391–1395, 2009.

[87] J. Yang, W.-H. Chen, S. Li, and X. Chen, "Static disturbance-to-output decoupling for nonlinear systems with arbitrary disturbance relative degree," *International Journal of Robust and Nonlinear Control*, vol. 23, no. 5, pp. 562–577, 2013.

[88] Q. Nguyen and K. Sreenath, "Exponential control barrier functions for enforcing high relative-degree safety-critical constraints," in *American Control Conference (ACC)*, 2016, pp. 322–328.

[89] T. Sun, H. Pei, Y. Pan, H. Zhou, and C. Zhang, "Neural network-based sliding mode adaptive control for robot manipulators," *Neurocomputing*, vol. 74, no. 14-15, pp. 2377–2384, 2011.

[90] Ø. N. Stamnes, O. M. Aamo, and G.-O. Kaasa, "A constructive speed observer design for general Euler-Lagrange systems," *Automatica*, vol. 47, no. 10, pp. 2233–2238, 2011.

[91] S. Wang, B. Lyu, S. Wen, K. Shi, S. Zhu, and T. Huang, "Robust adaptive safety-critical control for unknown systems with finite-time elementwise parameter estimation," *IEEE Transactions on Systems, Man, and Cybernetics: Systems*, 2022.

[92] H. Xu and P. A. Ioannou, "Robust adaptive control for a class of MIMO nonlinear systems with guaranteed error bounds," *IEEE Transactions on Automatic Control*, vol. 48, no. 5, pp. 728–742, 2003.

[93] Y. Wang and X. Xu, "Adaptive safety-critical control for a class of nonlinear systems with parametric uncertainties: A control barrier function approach," *Systems & Control Letters*, vol. 188, p. 105 798, 2024.

[94] X. Xu, "Constrained control of input–output linearizable systems using control sharing barrier functions," *Automatica*, vol. 87, pp. 195–201, 2018.

[95] X. Tan, W. S. Cortez, and D. V. Dimarogonas, "High-order barrier functions: Robustness, safety, and performance-critical control," *IEEE Transactions on Automatic Control*, vol. 67, no. 6, pp. 3021–3028, 2021.

[96] R. A. Horn and C. R. Johnson, *Matrix Analysis*. Cambridge University Press, 2012.

[97] C. K. Verginis, F. Djeumou, and U. Topcu, "Safety-constrained learning and control using scarce data and reciprocal barriers," *arXiv preprint arXiv:2105.06526*, 2021.

[98] G. R. Wood and B. Zhang, "Estimation of the Lipschitz constant of a function," *Journal of Global Optimization*, vol. 8, no. 1, pp. 91–103, 1996.

[99] M. Fazlyab, A. Robey, H. Hassani, M. Morari, and G. Pappas, "Efficient and accurate estimation of Lipschitz constants for deep neural networks," *Advances In Neural Information Processing Systems*, vol. 32, 2019.

[100] Y. Wang and X. Xu, "Safe control of Euler-Lagrange systems with limited model information," in *62th IEEE Conference on Decision and Control (CDC)*, 2023, pp. 5722–5728.

[101] Y. Wang and X. Xu, "Proxy control barrier functions: Integrating barrier-based and lyapunov-based safety-critical control design," *Automatica*, vol. 178, p. 112 364, 2025.

[102] J. Du, A. Abraham, S. Yu, and J. Zhao, "Adaptive dynamic surface control with Nussbaum gain for course-keeping of ships," *Engineering Applications of Artificial Intelligence*, vol. 27, pp. 236–240, 2014.

[103] T. I. Fossen, *Guidance and Control of Ocean Vehicles*. New York, NY, USA: Wiley, 1994.

[104] Y.-J. Liu and S. Tong, "Barrier Lyapunov functions for Nussbaum gain adaptive control of full state constrained nonlinear systems," *Automatica*, vol. 76, pp. 143–152, 2017.

[105] S. Kolathaya and A. D. Ames, "Input-to-state safety with control barrier functions," *IEEE Control Systems Letters*, vol. 3, no. 1, pp. 108–113, 2018.

[106] X. Jin, "Adaptive fixed-time control for MIMO nonlinear systems with asymmetric output constraints using universal barrier functions," *IEEE Transactions on Automatic Control*, vol. 64, no. 7, pp. 3046–3053, 2018.

[107] M. H. Cohen, P. Ong, G. Bahati, and A. D. Ames, "Characterizing smooth safety filters via the implicit function theorem," *IEEE Control Systems Letters*, vol. 7, pp. 3890–3895, 2023.

[108] P. Ong and J. Cortés, "Universal formula for smooth safe stabilization," in *58th IEEE Conference on Decision and Control (CDC)*, 2019, pp. 2373–2378.

[109] M. H. Cohen, T. G. Molnar, and A. D. Ames, "Safety-critical control for autonomous systems: Control barrier functions via reduced-order models," *Annual Reviews in Control*, vol. 57, p. 100 947, 2024.

[110] A. J. Taylor, P. Ong, T. G. Molnar, and A. D. Ames, "Safe backstepping with control barrier functions," in *61st IEEE Conference on Decision and Control (CDC)*, 2022, pp. 5775–5782.

[111] J. Breeden and D. Panagou, "High relative degree control barrier functions under input constraints," in *60th IEEE Conference on Decision and Control (CDC)*, 2021, pp. 6119–6124.

[112] C. Wen, J. Zhou, Z. Liu, and H. Su, "Robust adaptive control of uncertain nonlinear systems in the presence of input saturation and external disturbance," *IEEE Transactions on Automatic Control*, vol. 56, no. 7, pp. 1672–1678, 2011.

[113] X. Xu, J. W. Grizzle, P. Tabuada, and A. D. Ames, "Correctness guarantees for the composition of lane keeping and adaptive cruise control," *IEEE Transactions on Automation Science and Engineering*, vol. 15, no. 3, pp. 1216–1229, 2018.

[114] E. Daş and J. W. Burdick, "Robust control barrier functions using uncertainty estimation with application to mobile robots," *IEEE Transactions on Automatic Control*, vol. 70, no. 7, pp. 4766–4773, 2025.

[115] J. Yu, P. Shi, and L. Zhao, "Finite-time command filtered backstepping control for a class of nonlinear systems," *Automatica*, vol. 92, pp. 173–180, 2018.

[116] K. Hashimoto, "A review on vision-based control of robot manipulators," *Advanced Robotics*, vol. 17, no. 10, 2003.

[117] Y. Zhao, L. Gong, Y. Huang, and C. Liu, "A review of key techniques of vision-based control for harvesting robot," *Computers and Electronics in Agriculture*, vol. 127, pp. 311–323, 2016.

[118] A. Beyeler, J.-C. Zufferey, and D. Floreano, "Vision-based control of near-obstacle flight," *Autonomous Robots*, vol. 27, no. 3, pp. 201–219, 2009.

[119] F. Codevilla, M. Müller, A. López, V. Koltun, and A. Dosovitskiy, "End-to-end driving via conditional imitation learning," in *IEEE International Conference on Robotics and Automation (ICRA)*, 2018, pp. 4693–4700.

[120] E. S. Jones and S. Soatto, "Visual-inertial navigation, mapping and localization: A scalable real-time causal approach," *The International Journal of Robotics Research*, vol. 30, no. 4, pp. 407–430, 2011.

[121] A. K. Das, R. Fierro, V. Kumar, J. P. Ostrowski, J. Spletzer, and C. J. Taylor, "A vision-based formation control framework," *IEEE Transactions on Robotics and Automation*, vol. 18, no. 5, pp. 813–825, 2002.

[122] S. Dean, N. Matni, B. Recht, and V. Ye, "Robust guarantees for perception-based control," in *Learning for Dynamics and Control*, PMLR, 2020, pp. 350–360.

[123] N. Rahimi, S. Talebi, A. Deole, M. Mesbahi, S. Bandyopadhyay, and A. Rahmani, "Robust controller synthesis for vision-based spacecraft guidance and control," in *AIAA SCITECH Forum*, 2022, p. 2213.

[124] C. Hsieh, Y. Li, D. Sun, K. Joshi, S. Misailovic, and S. Mitra, "Verifying controllers with vision-based perception using safe approximate abstractions," *IEEE Transactions on Computer-Aided Design of Integrated Circuits and Systems*, vol. 41, no. 11, pp. 4205–4216, 2022.

[125] S. Hutchinson, G. D. Hager, and P. I. Corke, "A tutorial on visual servo control," *IEEE Transactions on Robotics and Automation*, vol. 12, no. 5, pp. 651–670, 2002.

[126] F. Chaumette and S. Hutchinson, "Visual servo control. I. basic approaches," *IEEE Robotics & Automation Magazine*, vol. 13, no. 4, pp. 82–90, 2006.

[127] F. Chaumette and S. Hutchinson, "Visual servo control. II. advanced approaches [tutorial]," *IEEE Robotics & Automation Magazine*, vol. 14, no. 1, pp. 109–118, 2007.

[128] P. Geng, M. Luo, T. Li, H. Wang, Y. Qin, and J. Han, "Duality-based optimization of occlusion avoidance for active optical navigation system in robotic orthopedic surgeries," *IEEE Transactions on Automation Science and Engineering*, vol. 22, pp. 15 215–15 226, 2025.

[129] D. Nicolis, M. Palumbo, A. M. Zanchettin, and P. Rocco, "Occlusion-free visual servoing for the shared autonomy teleoperation of dual-arm robots," *IEEE Robotics and Automation Letters*, vol. 3, no. 2, pp. 796–803, 2018.

[130] B. Penin, P. R. Giordano, and F. Chaumette, "Vision-based reactive planning for aggressive target tracking while avoiding collisions and occlusions," *IEEE Robotics and Automation Letters*, vol. 3, no. 4, pp. 3725–3732, 2018.

[131] Y. Zhang, Y. Yang, and W. Luo, "Occlusion-free image-based visual servoing using probabilistic control barrier certificates," *IFAC-PapersOnLine*, vol. 56, no. 2, pp. 4381–4387, 2023.

[132] S. Wei, B. Dai, R. Khorrambakht, P. Krishnamurthy, and F. Khorrami, "Diffocclusion: Differentiable optimization based control barrier functions for occlusion-free visual servoing," *IEEE Robotics and Automation Letters*, vol. 9, no. 4, pp. 3235–3242, 2024.

[133] M. Luo, Y. Qin, and J. Han, "Online occlusion-free optimization scheme for active optical navigation system in robotic orthopedic surgeries," *Control Engineering Practice*, vol. 148, p. 105 948, 2024.

[134] K. He et al., "Visibility maximization controller for robotic manipulation," *IEEE Robotics and Automation Letters*, vol. 7, no. 3, pp. 8479–8486, 2022.

[135] A. De Luca, G. Oriolo, and P. Robuffo Giordano, "Feature depth observation for image-based visual servoing: Theory and experiments," *The International Journal of Robotics Research*, vol. 27, no. 10, pp. 1093–1116, 2008.

[136] S. P. Boyd and L. Vandenberghe, *Convex Optimization*. Cambridge University Press, 2004.

[137] B. Grünbaum, V. Klee, M. A. Perles, and G. C. Shephard, *Convex Polytopes*. Springer, 1967, vol. 16.

[138] M. W. Spong, S. Hutchinson, and M. Vidyasagar, *Robot Modeling and Control*. Wiley: New York, 2006.

[139] X. Zhang, A. Liniger, and F. Borrelli, "Optimization-based collision avoidance," *IEEE Transactions on Control Systems Technology*, vol. 29, no. 3, pp. 972–983, 2020.

[140] B. Amos and J. Z. Kolter, "Optnet: Differentiable optimization as a layer in neural networks," in *International Conference on Machine Learning*, PMLR, 2017, pp. 136–145.

[141] P. Glotfelter, J. Cortés, and M. Egerstedt, "A nonsmooth approach to controller synthesis for boolean specifications," *IEEE Transactions on Automatic Control*, vol. 66, no. 11, pp. 5160–5174, 2020.

[142] A. Thirugnanam, J. Zeng, and K. Sreenath, "Duality-based convex optimization for real-time obstacle avoidance between polytopes with control barrier functions," in *American Control Conference (ACC)*, 2022, pp. 2239–2246.

[143] J. Nocedal and S. J. Wright, *Numerical Optimization*. Springer, 2006.

[144] W. S. Cortez, D. Oetomo, C. Manzie, and P. Choong, "Control barrier functions for mechanical systems: Theory and application to robotic grasping," *IEEE Transactions on Control Systems Technology*, vol. 29, no. 2, pp. 530–545, 2019.

[145] J. Breeden, K. Garg, and D. Panagou, "Control barrier functions in sampled-data systems," *IEEE Control Systems Letters*, vol. 6, pp. 367–372, 2021.

[146] Y. Zhang, S. Walters, and X. Xu, "Control barrier function meets interval analysis: Safety-critical control with measurement and actuation uncertainties," in *American Control Conference (ACC)*, 2022, pp. 3814–3819.

[147] J. A. Andersson, J. Gillis, G. Horn, J. B. Rawlings, and M. Diehl, "CasADi: A software framework for nonlinear optimization and optimal control," *Mathematical Programming Computation*, vol. 11, no. 1, pp. 1–36, 2019.

[148] B. Stellato, G. Banjac, P. Goulart, A. Bemporad, and S. Boyd, "OSQP: An operator splitting solver for quadratic programs," *Mathematical Programming Computation*, vol. 12, no. 4, pp. 637–672, 2020.

[149] R. Han et al., "RDA: An accelerated collision free motion planner for autonomous navigation in cluttered environments," *IEEE Robotics and Automation Letters*, vol. 8, no. 3, pp. 1715–1722, 2023.

[150] D. Morton and M. Pavone, "Safe, task-consistent manipulation with operational space control barrier functions," in *IEEE/RSJ International Conference on Intelligent Robots and Systems (IROS)*, 2025, pp. 187–194.